MANCHESTER 1824
The University of Manchester

The University of Manchester Research

Encapsulation methods for phase change materials – A critical review

DOI:
10.1016/j.ijheatmasstransfer.2022.123458

Document Version
Final published version

Link to publication record in Manchester Research Explorer

Citation for published version (APA):
Huang, Y., Stonehouse, A., & Abeykoon, C. (2023). Encapsulation methods for phase change materials – A critical review. *International Journal of Heat and Mass Transfer*, *200*, 123458. Article 123458. Advance online publication. https://doi.org/10.1016/j.ijheatmasstransfer.2022.123458

Published in:
International Journal of Heat and Mass Transfer

Citing this paper
Please note that where the full-text provided on Manchester Research Explorer is the Author Accepted Manuscript or Proof version this may differ from the final Published version. If citing, it is advised that you check and use the publisher's definitive version.

General rights
Copyright and moral rights for the publications made accessible in the Research Explorer are retained by the authors and/or other copyright owners and it is a condition of accessing publications that users recognise and abide by the legal requirements associated with these rights.

Takedown policy
If you believe that this document breaches copyright please refer to the University of Manchester's Takedown Procedures [http://man.ac.uk/04Y6Bo] or contact uml.scholarlycommunications@manchester.ac.uk providing relevant details, so we can investigate your claim.

OPEN ACCESS

Download date:27. Sept. 2023

International Journal of Heat and Mass Transfer 200 (2023) 123458

Contents lists available at ScienceDirect

International Journal of Heat and Mass Transfer

journal homepage: www.elsevier.com/locate/hmt

Review

Encapsulation methods for phase change materials – A critical review

Yongcai Huang, Alex Stonehouse, Chamil Abeykoon*

Department of Materials, Faculty of Science and Engineering, North West Composites Centre and Aerospace Research Institute, University of Manchester, Manchester M13 9PL, UK

ARTICLE INFO

Article history:
Received 24 June 2022
Revised 10 September 2022
Accepted 16 September 2022
Available online 26 October 2022

Keywords:
Thermal energy storage
Phase change materials
Thermal properties
Encapsulation methods
Bifunctional microcapsules
Multi-layered shell

ABSTRACT

Currently, non-renewable resources are heavily consumed, leading to increased global warming resulting from the production of carbon dioxide etc., phase change materials (PCMs) are regarded as a solution to mitigate these global crises attributed to their promising thermal energy storage capability. In this critical review, the thermal properties of different encapsulation methods of PCMs are summarised and compared. Encapsulation ensures that PCMs are used safely and efficiently, therefore the method needs to be thoroughly investigated and improved before their practical implementation. The applicable thermal properties for different encapsulation techniques and encapsulation materials such as particle diameter, enthalpy, encapsulation efficiency and thermal cycling times are reviewed. Future researchers are advised to measure and report thermal conductivities, displaying them in a convenient manner; many studies ignore this parameter, hindering research progression. Evaluation criteria for mechanical properties should be developed to enable comparisons between studies. It is suggested that eutectic and metallic PCMs, sol-gel encapsulation methods, complex coacervation methods, and spray drying are the areas that can be further investigated for better microcapsule performance, higher microcapsule yield, and improved synthesis conditions. In the future, bifunctional microcapsules, copolymer encapsulation, and doped high-performance materials are highly promising developments when compared with current monofunctional capsules with pure polymer shells.

© 2022 The Authors. Published by Elsevier Ltd.
This is an open access article under the CC BY-NC-ND license (http://creativecommons.org/licenses/by-nc-nd/4.0/)

Abbreviations: AMA, allyl methacrylate; APS, (3-aminopropyl)-trimethoxysilane; BA, behenic acid; CaAlg, calcium alginate; CA, capric acid; CDA, cellulose diacetate; CHI or CH, chitosan; CLPS, crosslinked polystyrene; CNCs, cellulose nanocrystals; CNFs, carbon nanofibers; CO, coconut oil; CTAB, hexadecyl trimethyl ammonium bromide; CTMAC, cetyltrimethylammonium chloride; DA, decanoic acid; DETA, diethylenetriamine; DMA, dimethylacetamide; DMI, diisocyanate; DSC, differential scanning calorimeter; DTMAB, dodecyltrimethylammonium bromide; DTMAC, dodecyltrimethyl-ammonium chloride; DTMS, decyltrimethoxysilane; DVB, divinylbenzene; EC, ethylcellulose; EDX, energy dispersive X-Ray spectroscopy; EGDMA, ethylene glycol dimethacrylate; EPS, [3-(2,3-epoxypropoxy)-propyl]-trimethoxysilane; ES, n-Eicosane; FT-IR, Fourier transform infrared spectroscopy; GB, type-B gelatine; GLA, glutaraldehyde; Gly, glycerol; GMA, glycidyl methacrylate; GO, graphene oxide; HCHO, formaldehyde; HCl, hydrochloride; hCNCs, hairy Cellulose nanocrystals; HD, n-hexadecane; HDPE, high-density polyethene; HEA, 2-hydroxyethyl acrylate; HEMA, hydroxyethyl methacrylate; HMDA, hexamethylene diamine; IPDI, isophorone diisocyanate; LA, lauric acid; LDPE, low-density polyethylene; LHS, latent heat storage; LO, linseed oil; MA, myristic acid; MAPTMS, γ-methacryloxypropyltrimethoxysilane; MF, melamine-formaldehyde; MMA, methyl methacrylate; MPS, [3-(methacryloyloxy)-propyl]-trimethoxysilane; MS, modified nano-SiO_2; MTES, methyl triethoxysilane; ND, n-nonadecane; NRL, natural rubber latex; OA, oleic acid; OD, n-octadecane; P(MMA-co-HEMA), poly (methyl methacrylate-co-2-hydroxyethyl methacrylate); P(MMA-co-MA), poly(methyl methacrylate-co-methyl acrylate); P(St-co-BA-co-DVB), poly(styrene-co-n-butyl-acrylate-co-divinylbenzene); P(St-co-MMA), poly(styrene-co-methyl methacrylate); PA, palmitic acid; PBA, poly(butyl acrylate); PCL-diol, Polycaprolactone diol; PCMs, phase change materials; PECA, poly(ethyl-2-cyanoacrylate); PEG, polyethylene glycol; PETRA, pentaerythritol tetraacrylate; PEVA, poly(ethylene vinyl acetate); PLA, polylactic acid; PMMA, poly (methyl methacrylate); PNC-HEMA, hexa(methacryloylethylenedioxy) cyclotriphosphazene; POA, poly (octadecyl acrylate); poly(BA-co-MMA), poly(butyl acrylate-co-methyl methacrylate); poly(MeS-co-DVB), poly(4-methylstyrene-co-divinylbenzene); poly(SMA-co-HEMA), poly(stearyl methacrylate-co-hydroxyethyl methacrylate); PPFS, poly(2,3,4,5,6-pentafluorostyrene); PPG2000, polypropylene glycol 2000; PS, polystyrene; PTMG, poly(tetrahydrofuran); PU or PUA, polyurea; PUU, poly(urea-urethane); PVA, polyvinyl alcohol; PVC, polyvinyl chloride; PVP, polyvinylpyrrolidone; PW, paraffin wax; RSC, core-shell ratio; SA, stearic acid; SDBS, sodium dodecyl benzene sulfonate; SDS, sodium dodecyl sulfate; SEM, scanning electron microscope; SF, silk fibroin; SMA, stearyl methacrylate; St, styrene; TDA, 1-tetradecanol; TDI, toluene-2,4-diisocyanate; TEOS, tetraethoxysilane; TO, thyme oil; TTCS, triethoxyoctylsilane; UF, urea-formaldehyde; UV, ultraviolet; VETS, vinyl triethoxysilane.

* Corresponding author.
E-mail address: chamil.abeykoon@manchester.ac.uk (C. Abeykoon).

https://doi.org/10.1016/j.ijheatmasstransfer.2022.123458
0017-9310/© 2022 The Authors. Published by Elsevier Ltd. This is an open access article under the CC BY-NC-ND license (http://creativecommons.org/licenses/by-nc-nd/4.0/)

1. Introduction

Human development is inseparable from the development of energy. Energy plays the most significant role throughout history. However, people in the past overwhelmingly relied on burning natural resources like coal, oil and natural resources, which cannot be regenerated sustainably. Amongst them, coal currently dominates the energy market in Asia [1,2]. Fig. 1 shows the global energy consumption, with the traditional energy resources accounting for 84.7%, and the remaining small portion is from renewable resources [3]. When a large amount of traditional resource consumption occurs, global warming becomes a serious problem [4]. This has led to an increase in global temperature by 0.8°C during the past century [5]. According to present research, increasing numbers of people are focusing on the reduction of carbon dioxide emissions [6].

It is important to find alternatives to traditional, polluting resources. Many people require thermal energy to survive throughout the world, therefore, conserving it is of great importance [7,8]. Thermal energy storage is divided into a few categories: sensible and latent heat, sorption and chemical reactions [9]. However, latent heat is more practical than others because of the large amount of energy stored in a small volume, and it is also more useful because it can be released at a constant temperature [10]. First, the definition of latent heat (Eq. (1)) is the thermal energy released or absorbed during the phase transition of materials [11].

$$Q = \int_{T_i}^{T_m} mC_p dT + ma_m \Delta H_m + \int_{T_m}^{T_f} mC_p dT \quad (1)$$

Where Q is the quantity of heat stored (J), T_i is the initial temperature (°C), T_f is the final temperature (°C), m is the mass of heat storage medium (kg), C_p is the specific heat (J/kg), a_m is the fraction melted, and ΔH_m is the heat of melting per unit mass.

The materials that could provide a large amount of latent heat at phase transition are regarded as phase change materials (PCMs) [12–14]. Currently, there are methods that exist to increase the latent heat capacity of organic phase change materials [15]; this involves increasing the degree of PCM crystallization with the addition of nanoparticles. Fig. 2 conveys that the number of publications issued has exponentially increased over the last 51 years (1970 to 2021) as interest in PCMs for thermal storage began a rapid increase from the year 2000 to 2010. So far, 2020 is the year with the largest number of publications issued on thermal energy storage and PCMs, reaching 1825 and 2827, respectively (data from Scopus). According to this trend, the number of publications in 2021 is expected to far exceed the previous year. Along with the increasing attention, the applications of these materials penetrate

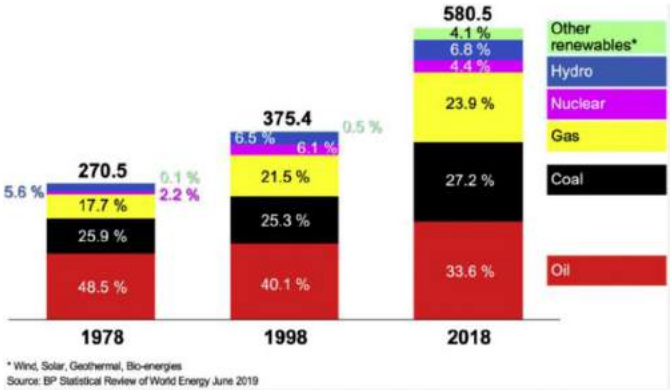

Fig. 1. The global energy consumption [3].

all aspects of people's life including thermal batteries [16], food preservation [17], solar heat systems [18], cooling systems [19], building constructions [19,20], refrigeration systems [21], textiles [22], air-conditioning [23] etc., due to their wide range of melting point and various other useful properties such as high thermal energy provided, tunable speed of energy exchange, good durability [24].

While investigating the number of patents issued over years regarding the PCMs, a similar increasing tendency, similar to publications, can be observed in Fig. 3. From 1954 to 1982 there are less than 30 patents in total; some of the years even have no patents issued, such as in 1973 and 1975. However, the number of them increases sharply until recent years with the highest of 3962 patents filed in 2020. It is notable that the year of 2002 witnesses a double increase in patents issued compared with the previous year. The number of patents issued at the patent office varies (Table 1), with the most for the United States Patent & Trademark Office (34,263)

Table 1
The number of patents issued about PCMs at different patent offices (data from Scopus, CNKI, inPASS).

Patent office	The number of patents issued
United States Patent & Trademark Office	34,263
China Patent Office	16,976
Japan Patent Office	12,010
Indian Patent Office	6808
World Intellectual Property Organization	3926
European Patent Office	3551
United Kingdom Intellectual Property Office	398

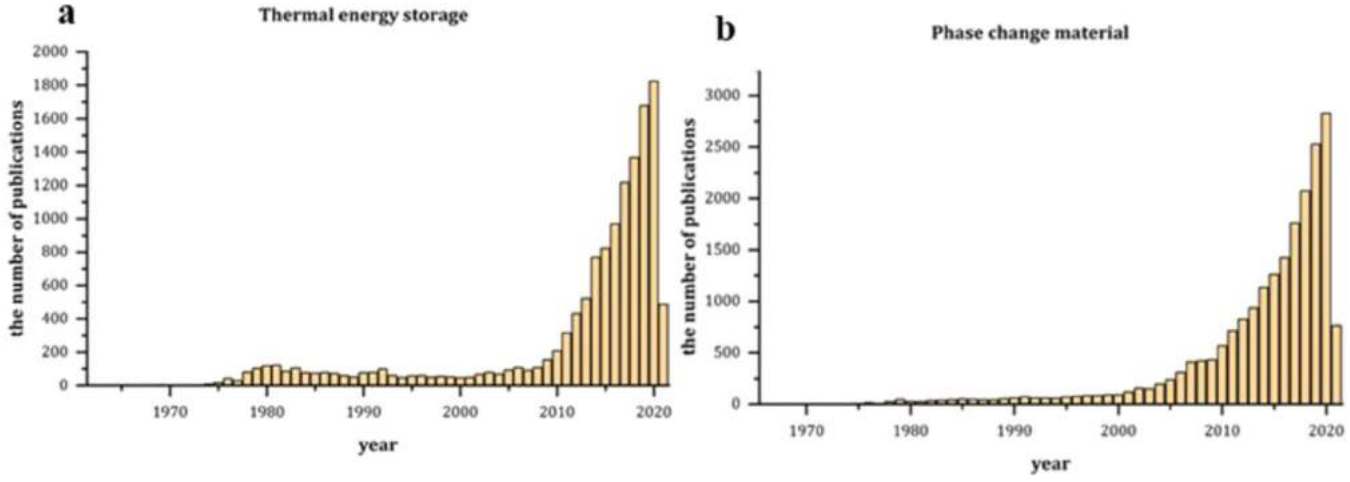

Fig. 2. The number of academic publications involving from 1970–2021: (a) thermal energy storage and (b) phase change material over years (data from Scopus).

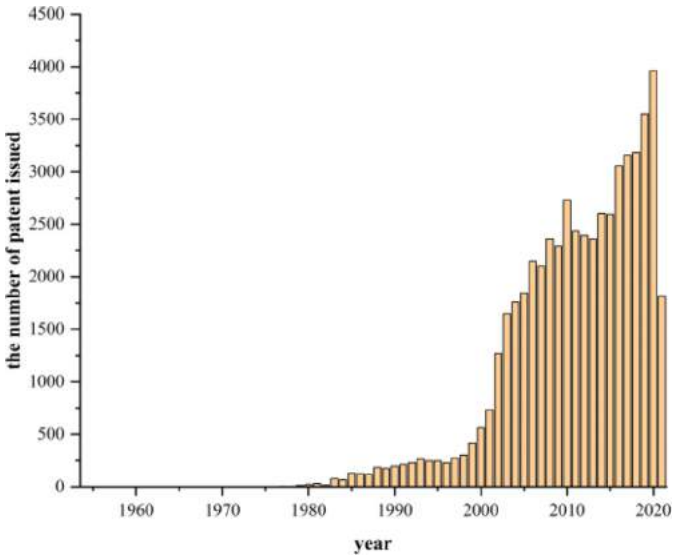

Fig. 3. The number of patents issued about PCMs over years (data from Scopus).

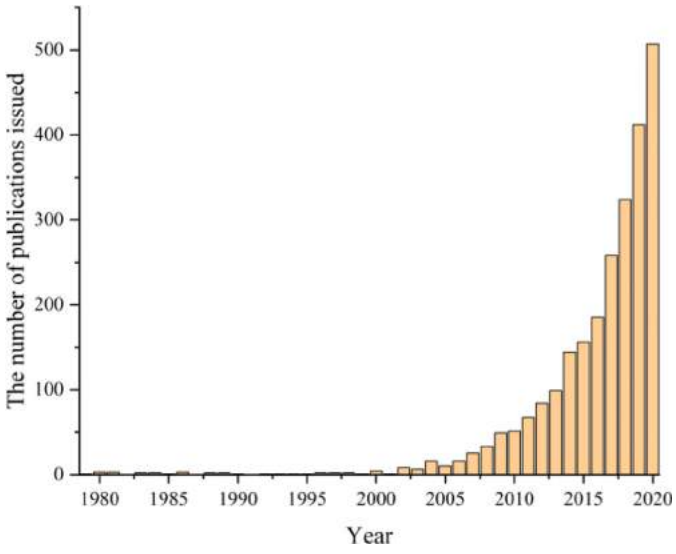

Fig. 4. The number of publications issued about PCMs encapsulation the last few decades (data from Scopus).

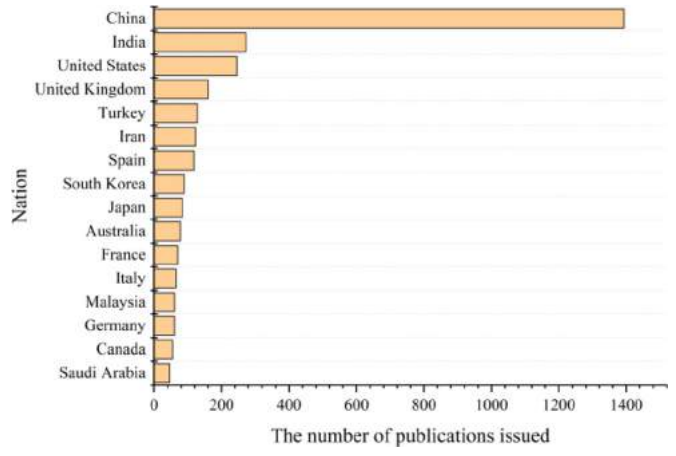

Fig. 5. The number of publications reported on PCMs encapsulation methods by different countries (data from Scopus).

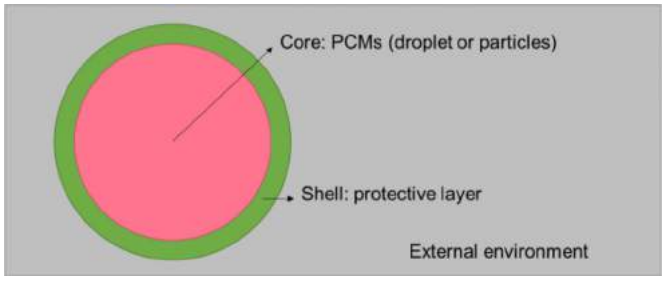

Fig. 6. The schematic of the structure of a PCM capsule.

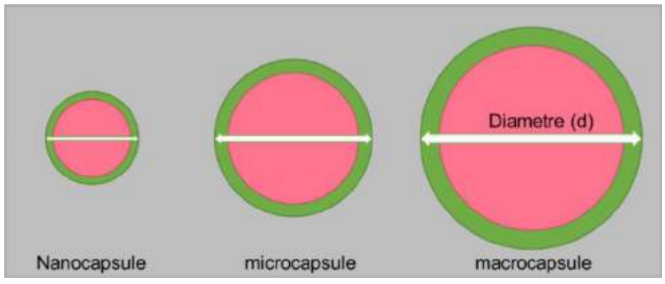

Fig. 7. Three capsules of different scale diameter.

and the least for United Kingdom Intellectual Property Office (398).

However, most PCMs may not be used directly because of toxicity, leakage (liquid or gas state), low thermal conductivity etc. [25–27], which means these shortcomings hinder the final application [28]. One of the most effective methods to address the leakage issues and enhance their shortcomings is the encapsulation techniques, for which the valuable PCMs are wrapped or sealed by tough and property-enhancing materials [29]. For instance, through encapsulation, a polystyrene (PS) shell can strongly fix the shape of PCMs and provide high resistance to external forces. Zhu et al. [30] validated this mechanical improvement by introducing PS into silica to make a hybrid shell, and the load withstood improved from 14.7 μN to 39.9 μN. Therefore, it is this flexibility of material choice that allows researchers to prepare different shells, attaining different property enhancements. This concept is derived from nature-like creatures' cells or eggshells. The encapsulated PCMs are composed of core (PCMs) and shell (polymer or organic materials). These shell materials are usually divided into organic, inorganic, and hybrid shells. The selection of shell materials essentially depends on their compatibility, which is mainly affected by the interfacial properties and intermolecular forces between the core and shell [31,32], and the desired improvement of properties such as mechanical strength and thermal conductivity. As shown in Fig. 4, there is a rising trend since 2000, meaning that the development of encapsulation technique is required to achieve better performance from PCMs. All over the world, China has published the highest number of studies on PCMs encapsulation methods with five times more the amount of studies presented by India, the second largest publisher (Fig. 5). The shapes formed for encapsulations are usually spherical (irregular shapes are also possible) due to surface tension, and the size varies from nanometre to millimetre (Fig. 6).

The first encapsulation technique was invented by Barett K in 1955 [33]. After that, this innovative technique is widely used in various fields including chemistry and medicine. The idea of this technique is to form a capsule with different scale diameters as shown in Fig. 7, like nano-encapsulation (0nm<d<1000 nm), micro-encapsulation (d<1 cm) and macro-encapsulation(d>1 cm) [34], for which the PCM cores are surrounded or wrapped by a

Table 2
The advantages and disadvantages of the encapsulation techniques [38–40].

Advantages	Disadvantages
Protection from light, heat, moisture, and high oxygen concentration that might lead to decomposition of PCMs	Micro and nanoencapsulation are complicated to conduct, and macro encapsulation has lower structure stability and fracture resistance
Prevent evaporation of volatile compounds that harm the environment and users' health	Needs standard selection procedure of PCMs and shell materials
Cover unpleasant odours	Low thermal conductivity due to polymer used as the shell
Control the speeds of internal materials release	

protective layer. The key factors that determine a successful encapsulation are a completed shell formation, no leakage, and no incorporation of impurities that have negative effects on PCMs properties [35]. Also, it is worth knowing the encapsulation ratio (Eq. (2)) or encapsulation efficiency (Eq. (3)) because they are the important parameters to evaluate the effectiveness of encapsulation [36,37]. If the values obtained are higher, a higher proportion of PCM is successfully wrapped by the shell.

$$\eta = \frac{\Delta H_{(m)microcapsule}}{\Delta H_{(m)bulk\ PCM}} \times 100\% \tag{2}$$

$$E = \frac{\Delta H_{(m)microcapsule} + \Delta H_{(s)microcapsule}}{\Delta H_{(m)bulk\ PCM} + \Delta H_{(s)bulk\ PCM}} \times 100\% \tag{3}$$

Where, "m" and "s" mean melting and solidification.

The advantages and disadvantages of encapsulation techniques are further summarized in Table 2 below. As shown in Fig. 8, the encapsulation methods can be divided into three categories based on only the chemical reactions (usually polymerisation or polycondensation to form the shell), mechanical processes, or the combination of the mechanical and chemical procedures.

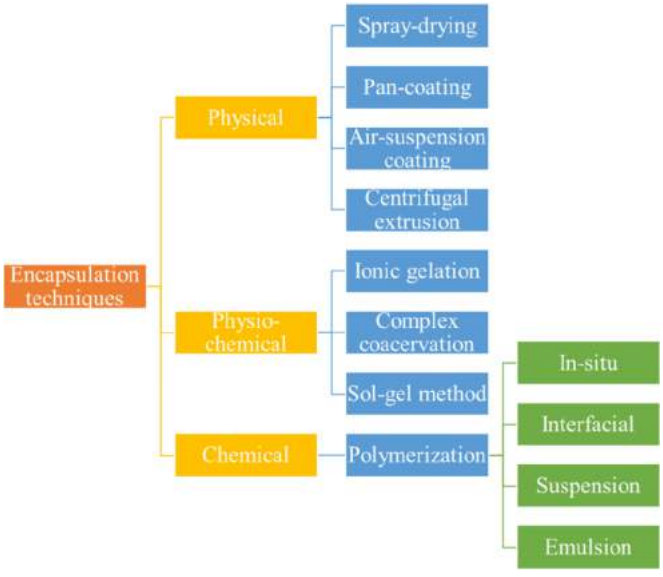

Fig. 8. Encapsulation methods.

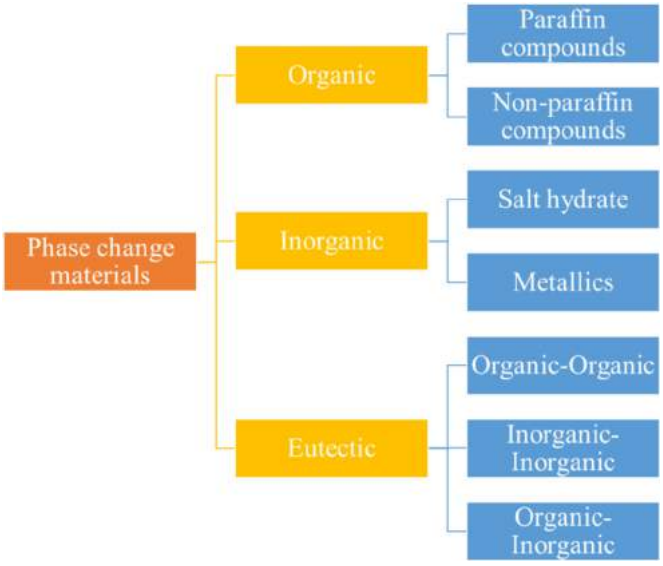

Fig. 9. General classification of PCMs.

2. Classification of PCMs

Different classifications of PCMs have been identified for improved performance, presented in Fig. 9. Initially, there are three major categories to which the PCM materials can be classified: organic, inorganic ones, and eutectic PCMs [41].

The organic phase change materials can be classified further into two sub-categories that have shown reasonable success in the way the PCMs can be used. These include the paraffin and non-paraffin compounds [41]. Amongst the inorganic materials, however, there have been identified salt hydrates and metallics as the key PCMs that may be exploited and harnessed for use [42]. Moreover, the eutectic materials may have a further three levels of classification denoted as the organic- organic eutectic materials, the inorganic-inorganic eutectic materials, and the mix of the organic and the inorganic eutectic materials [43]. Some of these materials are naturally occurring while others must be created from a mixture of compounds, through purification. Techniques should be developed that release useful amounts of energy for commercial processes [44], over suitable temperature ranges, and that use safe measures.

2.1. Organic PCMs

2.1.1. Paraffin used as PCMs

Paraffins are alkanes with the chemical formula, (C_nH_{2n+2}) [45]. The presence of the chemical compound (CH_2)$_n$ is the repeating unit in the structure of different paraffins make them ideal materials that can store and release energy as applicable in the PCMs category. These kinds of chemicals have stable physical properties and have varying meting point temperature ranges [46]. These are the key attributes that make them preferred for use in areas where there is a need for Latent Heat Storage (LHS) as in the case of PCMs [47]. Accordingly, the melting point temperatures have been widely associated with the number of carbon atoms in the chemical structure of the kinds of paraffin, with the relationship between temperature and the carbon atoms being directly related. The more carbon atoms in the paraffin chain, the higher the melting point [48]. Paraffins can also be separated

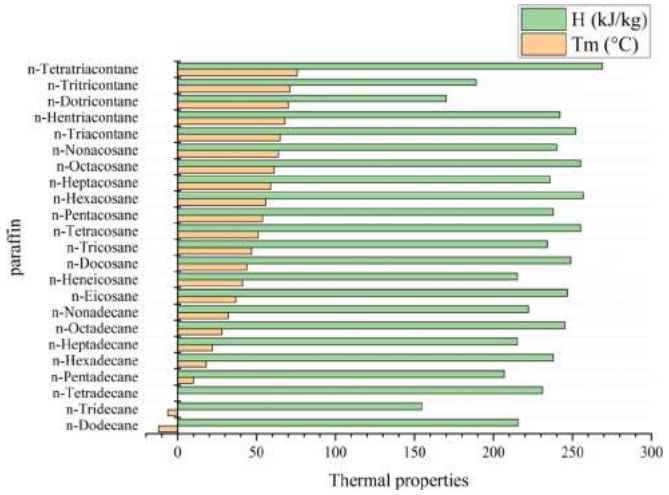

Fig. 10. The thermal and physical properties of paraffin [55,56].

from petroleum by-products made in oil refineries, but this kind of source may not meet sustainability requirements [48–52]. Notably, PCMs should be as sustainable as possible. The thermal and physical properties of high enthalpy paraffin are summarized in Fig. 10. It shows that Amongst these common paraffins, only enthalpies of n-Tetradecane, n-Dotricontane and n-Tritricontane are below 200 kJ/kg. Also, the major advantage of the organic PCMs is the fact that they show no change in performance or structure (e.g., phase separation) over numerous phase change cycles [53,54].

2.1.2. Non-paraffin compounds used as PCMs

Non-paraffinic organic PCMs include examples of ether, fatty acid, alcohol, and glycol as thermal energy storage materials [57]. In comparison to paraffin, the oxygen atoms are incorporated in the molecule. $C_mH_nO_2$ is the chemical formula used to indicate the specific non-paraffin PCMs. The key distinguishing feature of the non-paraffin organic PCMs is that they normally have a high latent heat capacity. Unfortunately, much like paraffin they are generally flammable, but they show less resistance to oxidation [57]. Also, these materials in the category of non-paraffin organic PCMs have low thermal conductivity and low combustion temperatures [58]. These are the negative attributes that have been defied by their use in the development of reliable and commercialize PCMs [52,58–60]. In addition, they have varying toxicity that increases the cost of handling them [45] as extra care would be needed to handle such materials. The most important non-paraffinic PCMs are sugar alcohols and a select category of fatty acids [61]. A key advantage these non-paraffinic PCMs have is that they can be combined with other non-paraffin PCMs to have a higher latent heat fusion, which will be discussed later in details in Section 2.3. Non-paraffin PCMs can retain properties such as high deformation stability, phase separation resistance after cycling, and also crystallization without supercooling; these are retained especially when the non-paraffin PCM is mixed with another non-paraffin PCMs [42,62,63]. This kind of arrangement would give the best PCMs for use, but it deters people based on the cost of the items. It is an expensive mixture compared with the individual costs of either the paraffin materials or the fatty acid PCMs, due to the cost of exploring a suitable combination and concentration [57]; this is not true if a mixture with predetermined properties can be made. Fig. 11 summarizes some non-paraffin compounds with their melting point and high heat of fusion (above 200 kJ/kg).

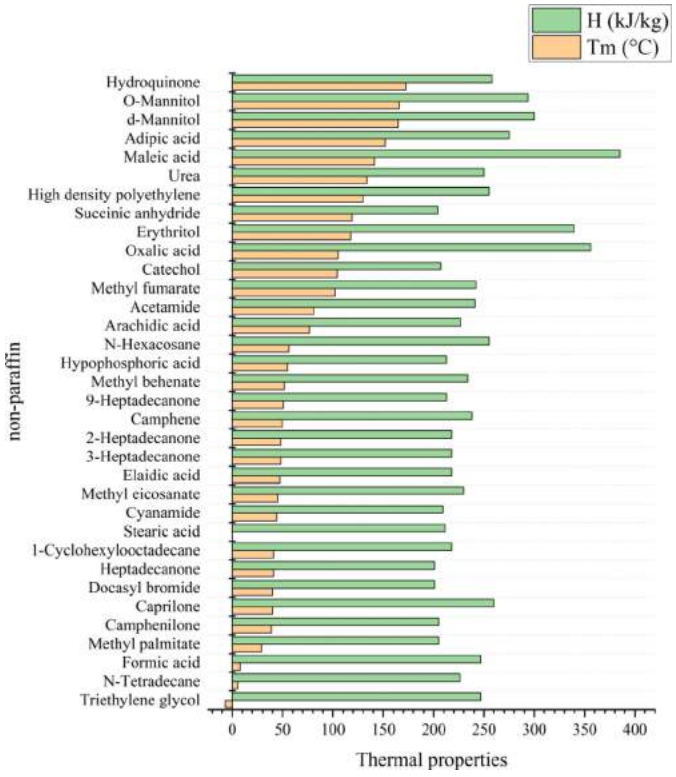

Fig. 11. The thermal and physical properties of non-paraffin compounds [55,64,65].

2.2. Inorganic PCMs

2.2.1. Inorganic compounds used as PCMs

Inorganic compounds have been used in the past, especially water with its excellent latent heat (more than 300 kJ/kg) compared to other organic PCMs. However, the nature of contamination and toxicity for some substances hinders the development of them as PCMs. Similar to the combination of non-paraffin PCMs themselves, inorganic compounds can also be combined with each other to achieve congruent melting and solidification behaviors without separation [66]. For instance, the combination of Na_2CO_3 and NaCl can be obtained, not only for keeping high levels of thermal energy (283.3 J/g), but also empowering the special property of exceptional thermal and chemical stability in CO_2-rich environments at high temperatures of around 700°C [67]. Fig. 12 summarized some inorganic compounds with their melting point and high heat of fusion (above 200 kJ/kg).

2.2.2. Salt hydrates used as PCMs

Salts hydrates are the result of an anhydrous salt forming a solid crystalline structure in the presence of water [52,68]. It means that some salts do not have water in their state (anhydrous), but when water is added to them, they absorb water in the process of ionization in specific molar ratios [69]. The salts, therefore, realize a general change in the ionic structure of the salt [70]. Many kinds and types of salt hydrates can form. Unfortunately, not many can release desired energy as there are only a few thermodynamically stable PCMs that can be used [71]. When anhydrous salts are hydrated, and in the process release energy, the energy can be harvested for sustainable energy that can also be commercialized in the long run [72].

Accordingly [73], the commonly used salts for PCMs include sodium sulfate decahydrate ($Na_2SO_4{\cdot}10H_2O$), calcium chloride hexahydrate ($CaCl_2{\cdot}6H_2O$), and sodium hydrogen phosphate dodecahydrate ($Na_2HPO_4{\cdot}12H_2O$). Other hydrated salts in this category

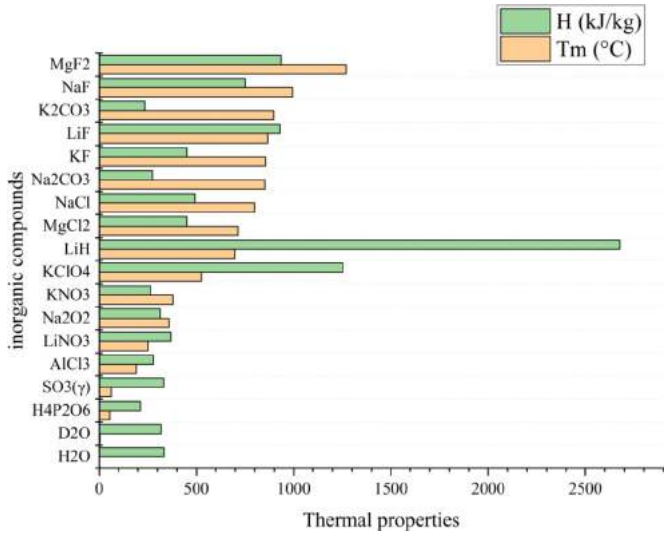

Fig. 12. The thermal and physical properties of inorganic compounds [55,64].

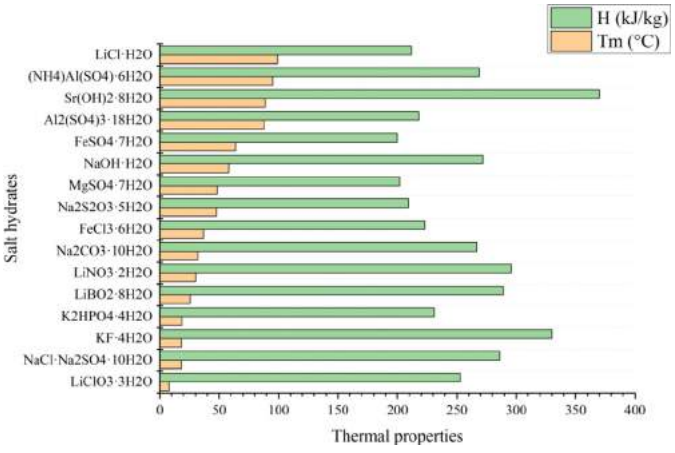

Fig. 13. The thermal and physical properties of salt hydrates [55,65].

that may also play significant roles in creating PCMs include iron (III) chloride hexahydrate ($FeCl_3{\cdot}6H_2O$) and zinc nitrate hexahydrate ($ZnNO_3{\cdot}6H_2O$) [73]. The quality of these salts for use in various categories depends on the key features like the melting point temperatures and their ability to undergo supercooling [68]. The most commonly used salt hydrate is Sodium sulfate decahydrate ($Na_2SO_4{\cdot}10H_2O$) [73]. Its use is majorly preferred ahead of the other hydrated salts because it has a melting point temperature of 32.4°C which is higher than the other salts [74–76]. However, it has various disadvantages based on its inconsistent temperatures for its melting and inconsistent supercooling points [77]. By better understanding their phase transition point, they can be applied efficiently [78]. Fig. 13 summarized some salt hydrates with their melting point and relatively high latent heat of fusion (above 200 kJ/kg).

2.2.3. Metallics used as PCMs

Some of the PCMs are metallic, and this makes them non-organic PCMs, but inorganic are in the same category as the salt hydrates [79]. These materials have different levels or kinds of properties. The use of metallic PCMs like other materials used for a similar purpose can transport heat away from a critical device meaning that they can buffer the temperature of a device during periods of transient high-power operation [80]. They then can store that heat using the latent heat of fusion. They absorb

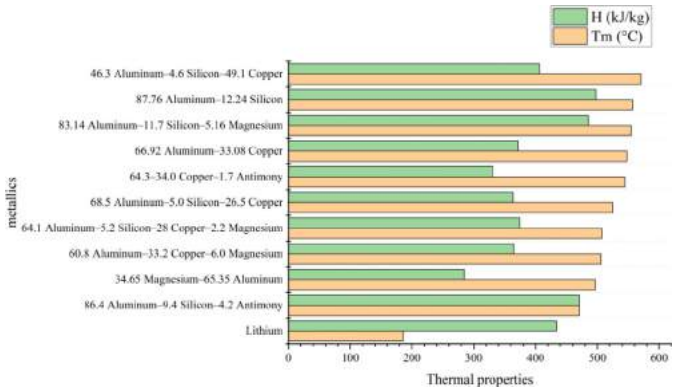

Fig. 14. The thermal and physical properties of metallics (the number before each material's name denotes the weight fraction) [55,84].

energy from the desired material, and later release the thermal energy to other desired materials [72]. These are attributes that make such metals, and in some cases, with their alloys to be useful PCMs, because of excellent thermal conductivity. For example, the thermal conductivity of Cu is measured to be 180.4 W/mK at 1600°C [81]. Thus, the use of metallic PCMs may offer additional advantages over salt hydrates and organic PCMs (thermal conductivity less than 1 W/mK) especially in areas of heat dissipation [80]. Most of the metallic PCMs have found greater applicability in the manufacture of electric vehicles, a use that does not fit organic PCMs and even the salt compounds, because metallic PCMs can not only meet the needs of higher thermal conductivity but also good mechanical properties (Young's modulus of Al up to 70 GPa) [82]. Notably, the electric vehicles would demand a high amount of thermal energy absorbed, which can only be achieved by the implementation of the metallic PCMs, and not any other material [83].

The costs associated with the material may vary depending on the manufacturing costs and the economic conditions under which it has been produced [68,85]. The search for cost-effective PCMs, including in the metal category, continues; it is the primary focus that will influence the frontier of the development of the PCMs [80]. Metallic PCMs are more expensive than salts; their cost of extraction and even implementation into suitable conditions are higher than the other organic PCMs and the salt compounds [80]. Fig. 14 presents some metallic PCMs with their melting points and high heats of fusion (above 200 kJ/kg).

2.3. Eutectics

In addition to the organic and inorganic PCMs, there are eutectic PCMs [86]. Therefore, it is useful to understand that this category of PCMs is normally made by mixing different types of PCMs from either category. In some cases, two organic PCMs may be combined to develop better properties, such as latent heat and supercooling values. In that case, the new PCM would fall in the category of organic-organic PCMs [87]. In other cases, two inorganic PCMs may also be combined to make inorganic-inorganic PCMs [88]. Again, these kinds of mixtures of two inorganic PCMs are likely to create a set that has better attributes compared to the initial individual inorganic materials. Moreover, an organic and an inorganic PCM may be combined to make up a set of organic-inorganic PCMs [17]. These kinds of mixed PCMs are normally called eutectics [89]. Their attributes, advantages, disadvantages, and uses are derived from the constituents [90]. However, the mixture is always controlled to increase the positive attributes of the resulting PCM for greater usability and reliability, relative to the application the PCM will be used in

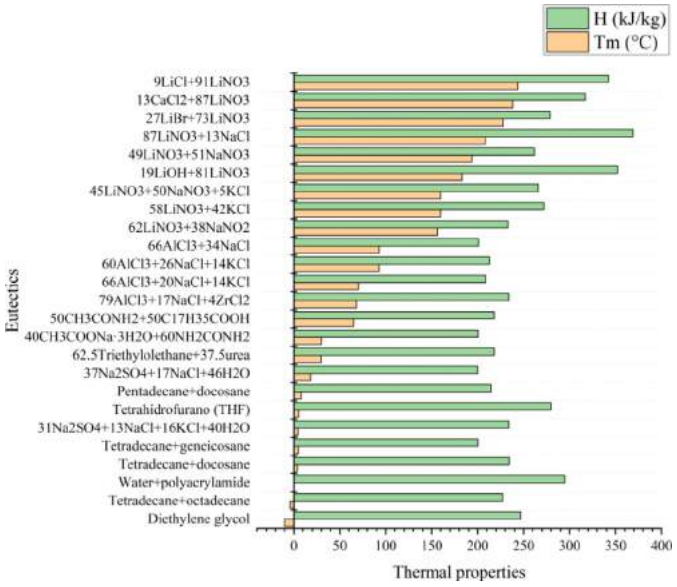

Fig. 15. The thermal and physical properties of eutectics (the number before the materials denotes the weight fraction) [55,65,95].

[17]. Again, in the manufacturing of the eutectic, it is important to realize that the suitable combinations that would give viable solutions economically, would considerably be pursued for commercialization.

The most distinguishing feature of most eutectics is that they remain unaffected by cyclic heating and cooling, hence, they have a stable phase change. The materials in this category are therefore useful in making low-temperature refrigerators [91]. Over the years, refrigerator cooling devices were not only bulky, but they also made the refrigerators delicate and prone to failure [92]. However, the infusion of eutectics into the thermal component makes the facility much more sleek, efficient and reliable in its areas of use and application [93]. Such kinds of eutectic materials remain significantly importance in daily applications, even though many people may not realize their usage in such areas. Freezers and refrigerators are some of the common areas of application of eutectic PCMs [94]. Fig. 15 summarizes some eutectics with their melting points and high heats of fusion (above 200 kJ/kg).

2.4. Comparison of various PCMs

PCMs are a large family containing different categories of materials. Some of the advantages and disadvantages have been discussed in previous sections, and Table 3 summarizes more comprehensive information from the perspective of organic, inorganic, and eutectic PCMs.

Fig. 16 is the 95% confidence ellipse summarizing a large proportion of PCMs (more than 350 PCMs) with their melting points and latent heats [55,56,64,65,84,95,101–106]. Inorganic compounds and metallic PCMs are widely distributed and have higher melting points and latent heats compared to other types, however, both properties are not continuous according to the previous section. Paraffin PCMs have higher latent heat overall than non-paraffin and salt hydrates, while there is narrow application temperature for paraffin and non-paraffin PCMs compared to salt hydrates. Therefore, this is where the advantages of eutectics are reflected, with continuous and wide-distributed properties.

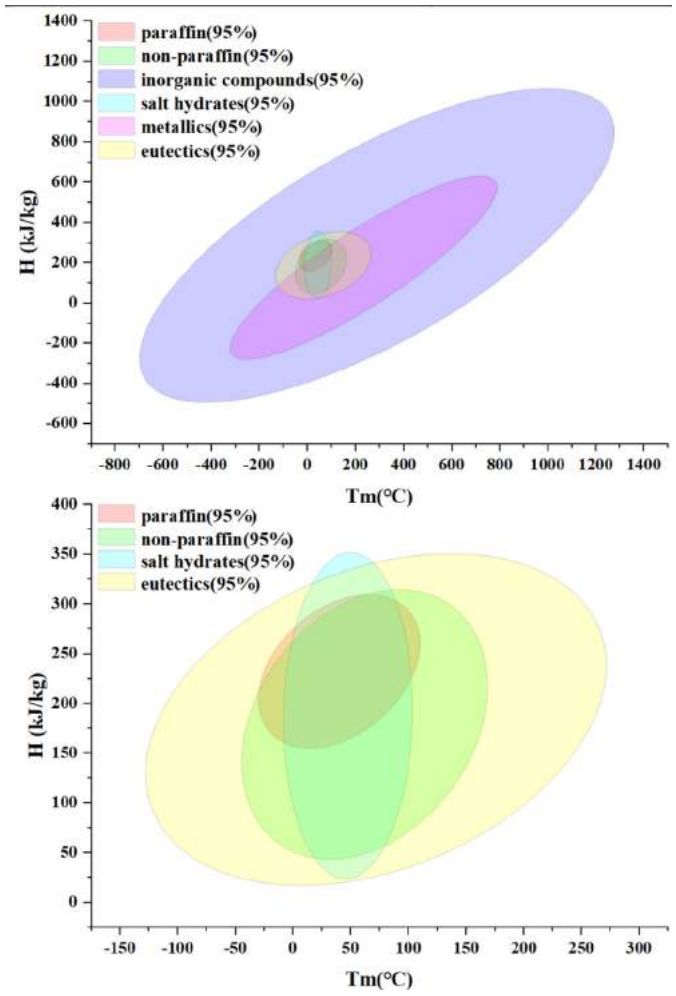

Fig. 16. The melting point and heat of fusion for different kinds of PCMs [55,56,64,65,84,95,101–106].

3. Encapsulation techniques

3.1. Encapsulation shell materials

The properties of capsules are not only determined based on the PCMs, but also the shell materials used as well, so it is really important to select suitable shell materials to meet the requirements in various applications. Like the PCMs themselves, shell materials also share similar classifications, which are organic, inorganic, organic-inorganic hybrid shell materials [107,108]. The common shell materials and their advantages and disadvantages are summarized below in Table 4.

3.2. Physical encapsulation methods

3.2.1. Spray drying

It is useful to note that the most used physical methods for encapsulating PCMs are spray-drying. Fig. 17 is drawn according to

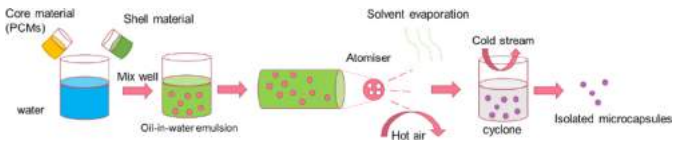

Fig. 17. The process of spray drying.

Table 3
The advantages and disadvantages of different categories of PCMs.

Advantages	Disadvantages
Organic [96–99]	
• No supercooling while undergoing phase change • Homogeneous and continuous phase change meaning no phase segregation • High compatibility with encapsulation materials • Congruent melting • Corrosion resistance • Most have no toxicity • Small volume change • Good chemical stability • Adjustable and gradually increasing melting point • Low vapour pressure while undergoing phase change • Good reliability after thermal cycling • Excellent freezing and melting behaviour • Self-nucleation • Fast nucleate rate • Recyclable • Long freeze-melting cycle	• Poor thermal conductivity (1-tetradecanol: only 0.32 W/mK for example [100]) • High cost • High flammability especially for non-paraffin PCMs • High volatility • Low phase change enthalpy (most below 400 J/g) • Paraffins are less compatible with plastic containers • Should not be exposed to oxidizing agents (especially for non-paraffin PCMs) • Not eco-friendly (due to PEG and paraffin)
Inorganic [96–99]	
• Large phase change enthalpy • Superior thermal conductivity (usually more than 1 W/mK, up to 180 for Cu [97]) • Cheap (metallics excluded) • Low flammability • Sharp phase change • High latent heat of fusion per unit volume • Recyclable • Small volume changes on melting • Compatible with plastic	• Problematic supercooling • Corrosion • Phase segregation • Low thermal stability • Slight toxicity • Low reliability, dehydration, after thermal cycling • Decomposition • Less compatible with encapsulation materials compared with organic PCMs • Incongruent melting • Poor nucleating behaviour • Too heavy for metallic PCMs
Eutectic [96,99]	
• Sharp melting temperature • No phase segregation • High volumetric thermal storage density • Adjustable melting point and latent heat due to different kinds and dosage combination	• Supercooling exists • Unpleasant and strong odours • Insufficient combinations have been studied • High cost

a previous research articles description and shows the process of spray drying [96,112]. The process of spray-drying can include the use of preparing an oil-water emulsion containing PCMs and shell materials. The choice of the materials to be used, again, depends on how the two may react. Then, the next process involves spraying the prepared oil-water emulsion in a drying chamber using an atomizer. The later stage is drying the sprayed droplets. Therefore, it would be useful to carry out the process by drying gas streams at a suitable temperature. Finally, the process of the encapsulation solutions would involve separating the solid particles by cyclone.

Hawlader et al. [113] firstly applied the spray drying method by using paraffin wax as the core (with a melting point of 60–62°C) and gelatine/Arabic as the shell. By comparing different mi-

Table 4
The advantages and disadvantages of different types of shell materials [96,109–111].

Common shell materials	Advantages	Disadvantages
Organic shell		
• Melamine-formaldehyde (MF) resin • Urea-formaldehyde (UF) resin • Poly(urea-urethane) (PUU) • Polyurea (PU) • Acrylic resins	• Good structure stability • Superb durability after many thermal cycles • Excellent UV stability, non-toxicity, easily handle, exceptional mechanical strength and chemical resistance (for outstanding acrylic resins)	• Poor chemical and thermal stabilities • Low thermal conductivity • Toxicity • Flammability • Poor thermal stability
Inorganic shell		
• Silica • Titania • Calcium carbonate • Zinc oxide • Alumina	• Better utilization than organic shell • Exceptional thermal stability • High thermal conductivity • Easy to surface modification with different functional groups	• Low long-term stability • Brittle • Easy to fracture leading to the leakage
Organic and inorganic hybrid shell		
• Silver nanoparticles in organic shell • Iron nanoparticles in organic shell • Silicon nitride in organic shell	• Outstanding thermal conductivity • Mechanical strength • Chemical stability	• Inorganic additives are easy to detach from the surface

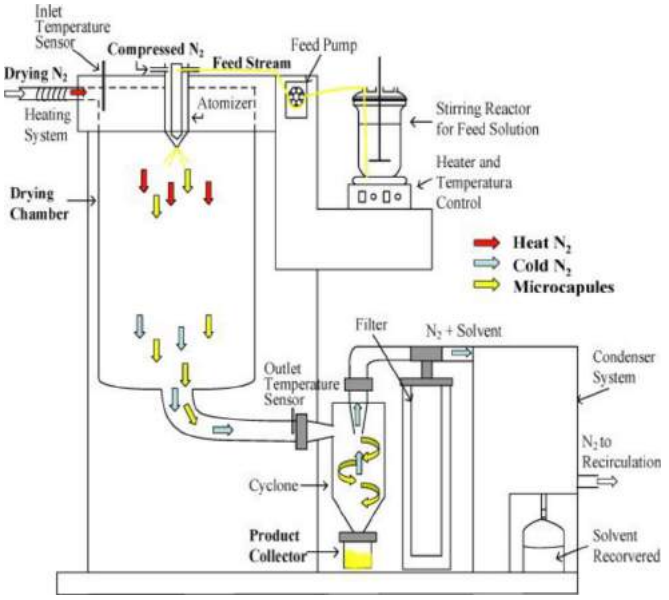

Fig. 18. The spray drying device [115].

crocapsules produced from the 2:1, 1:1, 1:2 core-shell ratio, they concluded that with the core-to-shell mass ratio increase, the encapsulation efficiency decreases, and the storage capacity increases. The spray drying technique can result in capsules with uniform size and spherical shape without any dents or edges.

Wu et al. [114] achieved heat transfer enhancement by using this method. The microcapsules with spherical shapes are obtained by encapsulating paraffin in polystyrene (PS). They found that the spray method gives an average heat transfer coefficient increase of 70% when there is 28% of paraffin nanoparticle volume fraction in slurry, compared to the water.

Borreguero et al. [115] introduced a study of carbon nanofibers (CNFs) incorporating a Low-density polyethene (LDPE)/Poly(ethylene vinyl acetate) (PEVA) shell. The core material, in this case, is commercially used paraffin named Rubitherm®RT27.

The spray drying is conducted by the device shown in Fig. 18 in which core and shell materials are mixed to form an oil-in-water emulsion in the stirring reactor, followed by pumping them into the drying chamber along with hot air (nitrogen). The microcapsules are collected in the product collector after solvents are carried with nitrogen by the cyclone. They found that the latent heat of the microcapsules is comparable to that of using suspension polymerisation to form a styrene shell. Suspension polymerisation will be discussed in Section 1.1.1. Besides, after the incorporation of CNFs, the thermal conductivity and mechanical properties are largely enhanced without a significant reduction in heat storage capacity (98.14 to 95.64 J/g). However, there is an agglomeration problem occurring in the drying chamber as shown in Fig. 19 b. According to a test carried out with 3000 thermal cycles (to simulate the 30-years of continuous operation), the resulting microcapsules are more stable than that by using only PS as the shell.

Li et al. [116] adopted acetone/dimethylacetamide (DMA) as the mixed solvent and cellulose diacetate (CDA) as the shell to encapsulate the n-octadecane by spray method. The optimal CDA concentration and acetone/DMA was found to be 6 wt.% and 1:1, respectively. Fig. 20 shows that the mixed solvent ratio of 5:5 provides a narrowed size distribution and a more regular spherical shape. Furthermore, they applied the crosslinking agent, glutaraldehyde (GLA), to improve the compactness of the shell and protection of the core. However, the crosslinking process results in a lowering in enthalpy of microcapsules due to oil phase permeation.

Methaapanon et al. [117] encapsulated the n-octadecane and methyl palmitate as core materials in silica as the shell, the fabrication process is shown in Fig. 21. They found that the increase in surfactant to core ratio results in a lowering number of droplets and smaller emulsion droplets, which is unfavourable due to worse coverage and lower surface area, leading to a lower encapsulation efficiency (see Fig. 22). The emulsion time before spray drying and core-shell ratio are also key parameters. As shown in Fig. 23, the morphology exhibits the normal spherical shape when the core-shell mass ratio is 0.25 to 0.5, but a thinner shell. As the gel time increase, the thickness of the shell is increased, preventing leakage due to the longer polycondensation reaction of silica to form the network. Herein, the shell is porous acting as multicore container for PCMs. Conclusively, the most suitable core-shell ratio was found to be 0.25 due to the highest encapsulation efficiency and good morphology.

A summary of the previous works used spray drying for encapsulation is provided in Table 5.

3.2.2. Solvent evaporation

Solvent evaporation is another physical microencapsulation method; this is applied in cases where the materials used as PCMs are resistant to heat. In other words, they are used in cases where there is high heat, used to evaporate the low boiling-point solvent, instead of affecting the PCMs we need, thus leading to deposition of shell materials on the surface of the PCMs. For the solvent evaporation mechanism, an aqueous phase with a suitable emulsifier and oil phase containing polymer are used as a shell material; the core materials and low boiling point solvent (that could dissolve

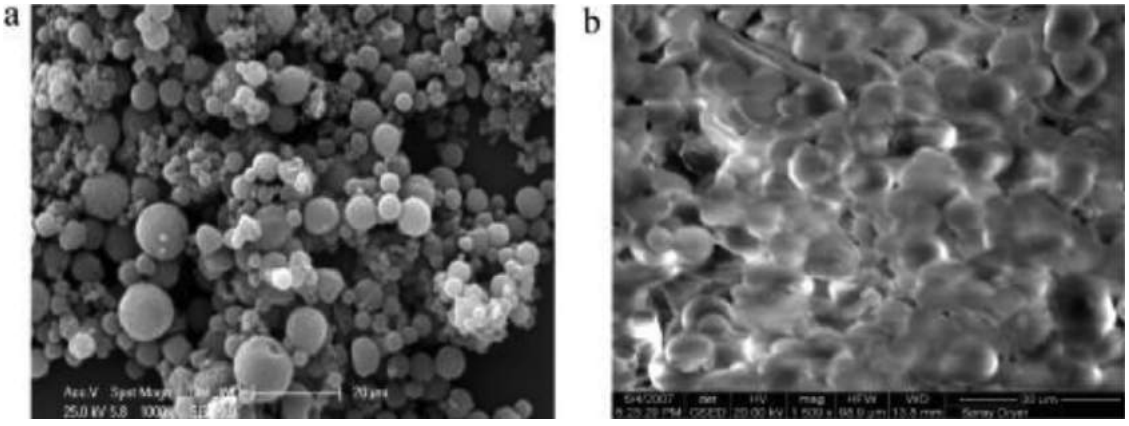

Fig. 19. The SEM images of microcapsules collected in (a) product collector and (b) drying chamber [115].

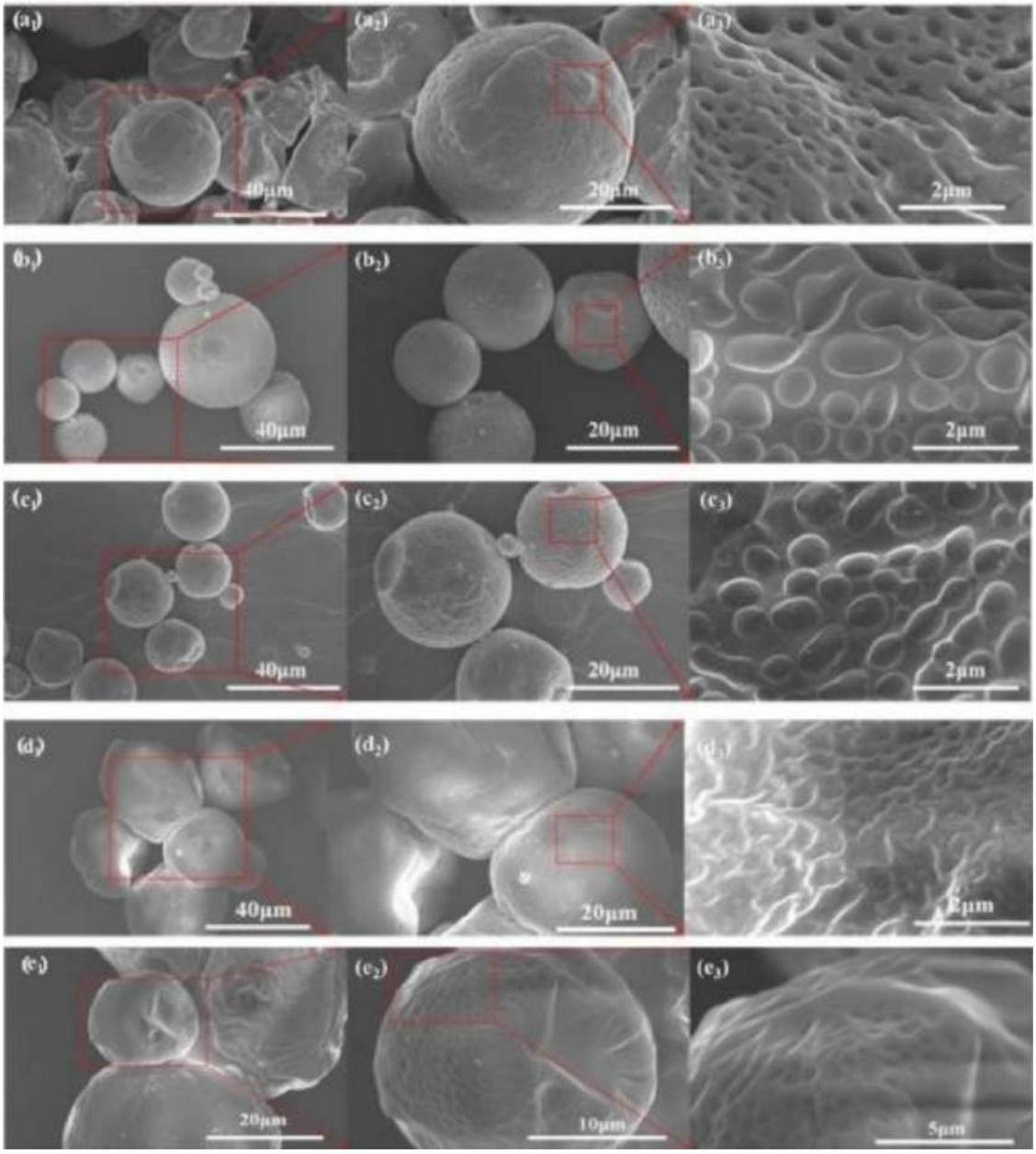

Fig. 20. The SEM images of microcapsules produced by different acetone/ DMAratio, (a) 9:1, (b) 7:3, (c) 5:5, (d) 3:7, (e) 1:9 [116].

Table 5
The properties of the encapsulated capsules using spray drying.

Refs.	Core material	Shell material	Average diameter (μm)	Thermal cycling (cycles)	Encapsulation efficiency (%)	heat of fusion (J/g)	Other properties
[113]	Paraffin wax	Gelatine and acacia	<1	-	91.98	216	• Narrow particle size distribution with spherical shape and smooth surface. • The ideal core-shell ratio is 2: 1
[114]	Paraffin	PS	0.1	5000	-	220.3	• Spherical shaped microcapsules
[115]	Rubitherm®RT27 (paraffin)	LDPE-PEVA (containing CNFs)	3.9	3000	63	98.1	• Core content: 49.32 wt.% • Good mechanical properties • Good thermal stability
[117]	N-octadecane methyl palmitate	Silica	11.5	-	-	-	• Spherical shape with porous shell

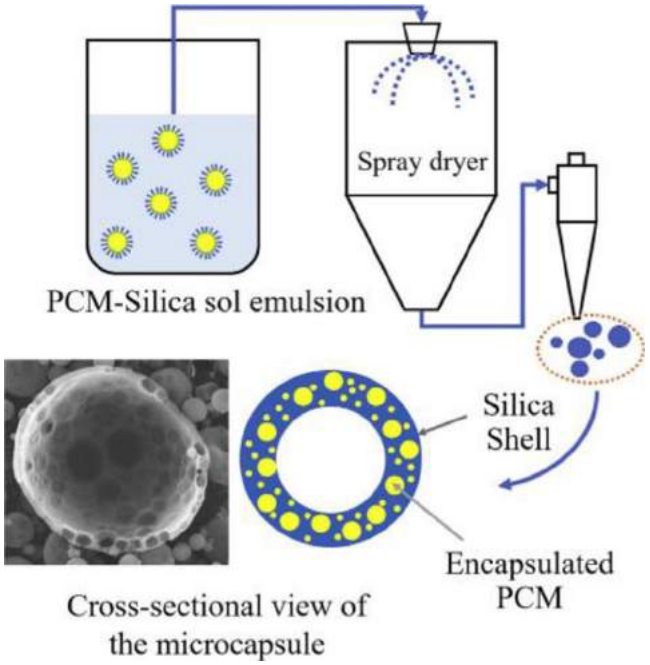

Fig. 21. The fabrication process of microcapsule [117].

the polymer) are prepared first. The two phases are then mixed to form the emulsion. With the help of heating and reduction of pressure, evaporation of the low boiling point solvent is accelerated, and phase separation of the polymer occurs. Once the solvent is evaporated entirely, the polymer migrates to the surface of core materials in the water system to form microcapsules, due to surface tension interactions, and the emulsion is transformed into a suspension. Lastly, the microcapsules are washed and dried. The whole process and mechanism are depicted in Fig. 24 below based on previous research descriptions [118].

Es-haghi et al. [119] successfully modified ethylcellulose (EC) as the shell material by three kinds of coupling agents, (3-aminopropyl)-trimethoxysilane (APS), [3-(methacryloyloxy)-propyl]-trimethoxysilane (MPS), and [3-(2,3-epoxypropoxy)-propyl]-trimethoxysilane (EPS), before encapsulating linseed oil (LO) by the solvent evaporation method. The highest modification efficiency is obtained by using MPS, where the chemical interaction of Si-O-EC is confirmed. The morphologies of unmodified and modified microcapsules were compared; Fig. 25 shows that the external surface is not dependant on shell molecular weight because the content of core materials and procedure remain unchanged. However, if EC is modified, the internal morphology is different due to the higher molecular weight of the shell, leading to structural complexity. The internal morphology of unmodified microcapsules has a smooth membrane. Nevertheless, the internal morphology turns into the matrix (b), and a combination of matrix and multi-nuclear (c and d). Thus, the modification of shell material (EC) does have a great influence on internal morphology and the promising application of self-healing coatings.

Fashandi and Leung [120] developed the encapsulation of a palmitic acid (PA) core in polylactic acid (PLA) by using the solvent evaporation method. They further investigate the effects of core content, solvent content, surfactant type and content, and oil-aqueous phase ratio on properties of resultant microcapsules. They found that higher PA content gives rise to a higher core content and average diameter of microcapsules due to an increase in viscosity of the oil phase. For the emulsifiers Polyvinyl alco-

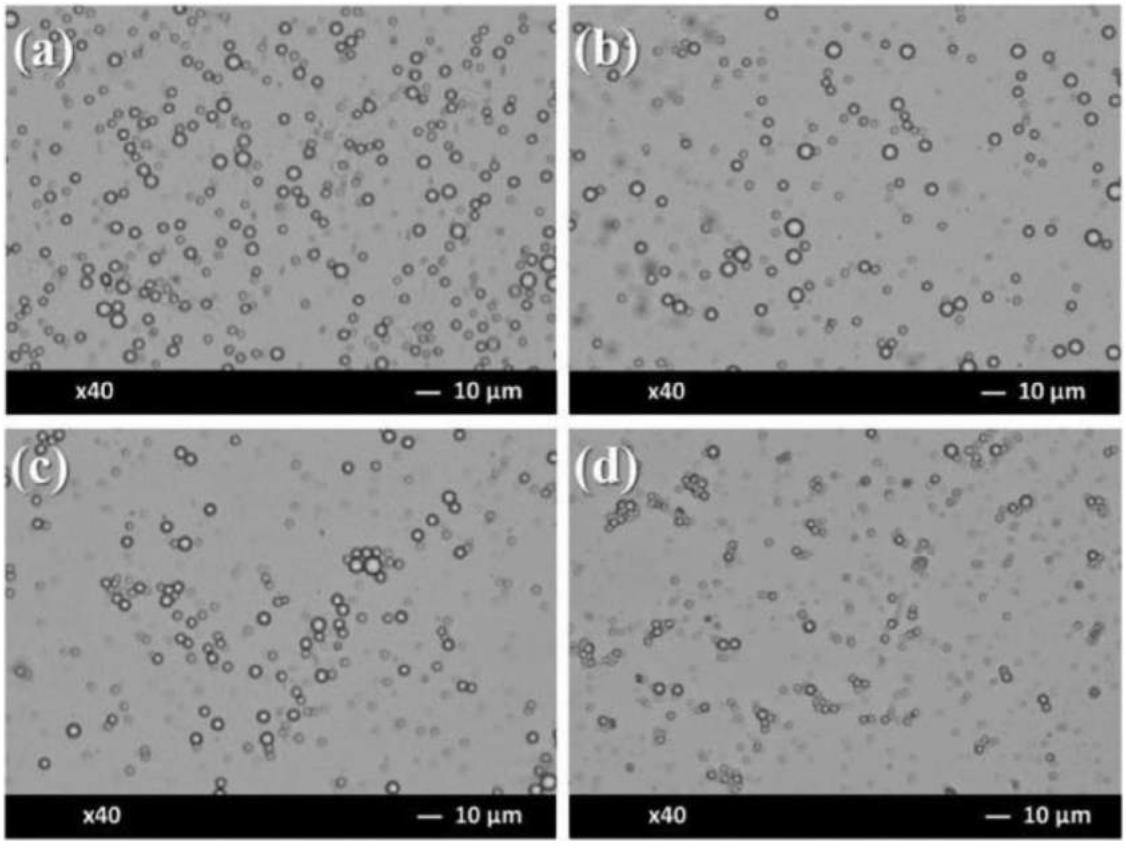

Fig. 22. The size and distribution of emulsion droplets based on different surfactant-core ratio, (a) 0.05, (b) 0.1, (c) 0.5, (d) 1 [117].

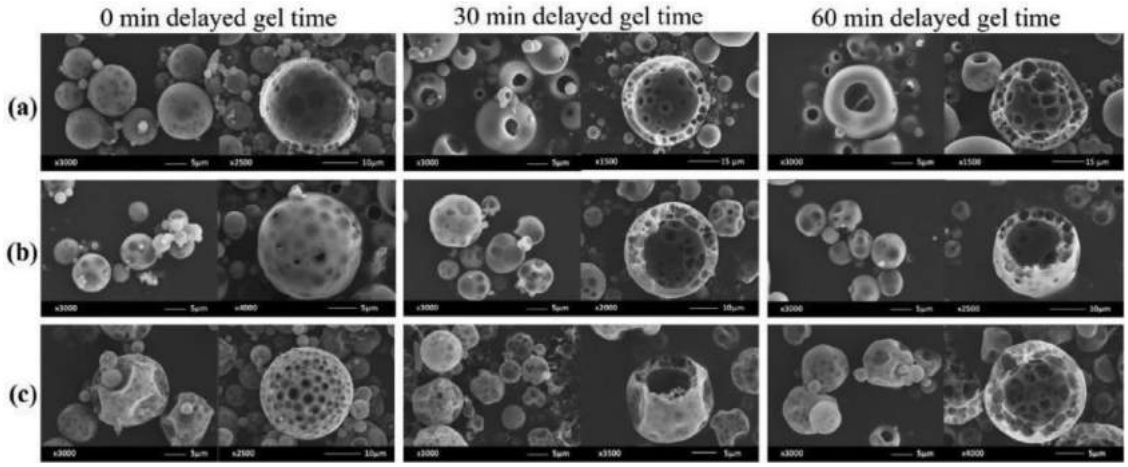

Fig. 23. SEM images of microcapsules based on different core-shell ratio (a) 0.25, (b) 0.5, (c) 1 [117].

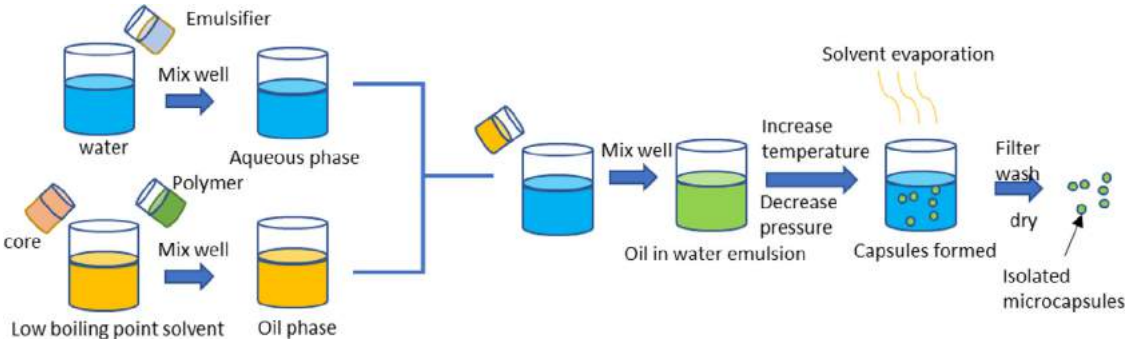

Fig. 24. The process and mechanism of solvent evaporation technique.

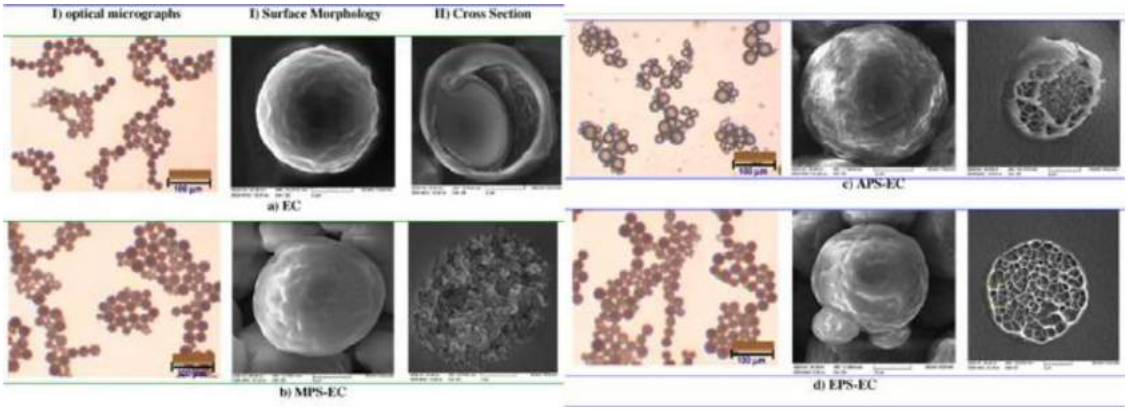

Fig. 25. The external (I) and internal (II) morphology of unmodified (a) and modified (b–d) microcapsules [119].

hol (PVA) and sodium dodecyl sulfate (SDS), an increase in the content of both leads to smaller particle size due to a resulting lower surface energy. Nevertheless, once the content is beyond the critical micelle concentration, a larger particle is obtained. Furthermore, they suggested SDS is not a suitable surfactant to generate this kind of microcapsule, due to the core dissolution in the aqueous phase, leading to a lower encapsulation efficiency.

According to the research by Lin et al. [121], myristic acid (MA) is sealed by EC to form spherical microcapsules. By preparing different microcapsules with different core-shell ratios, they found the 2:1 core-shell ratio is the most suitable. They also pointed out the reason why the freezing point is smaller than the melting point is that the EC hinders the solidification of the core material.

Khan et al. [122] explored a novel shell material, poly (methyl methacrylate-co-2-hydroxyethyl methacrylate) [poly (MMA-co-HEMA)], to encapsulate paraffin wax as core material (see Fig. 26). The optimum ratio of MMA-HEMA is 75:25, obtained in previous research [123]. They further found that the obtained microcapsules can be excellently dispersed in natural rubber latex (NRL) due to the mechanism that polymer chains from microcapsules tend to self-assembly towards rubber, leading to strong adhesion (see Fig. 27). This results in the enhancement of mechanical strength, and the optimal microcapsule incorporation content of 20% can be seen for the largest strength (see Fig. 28).

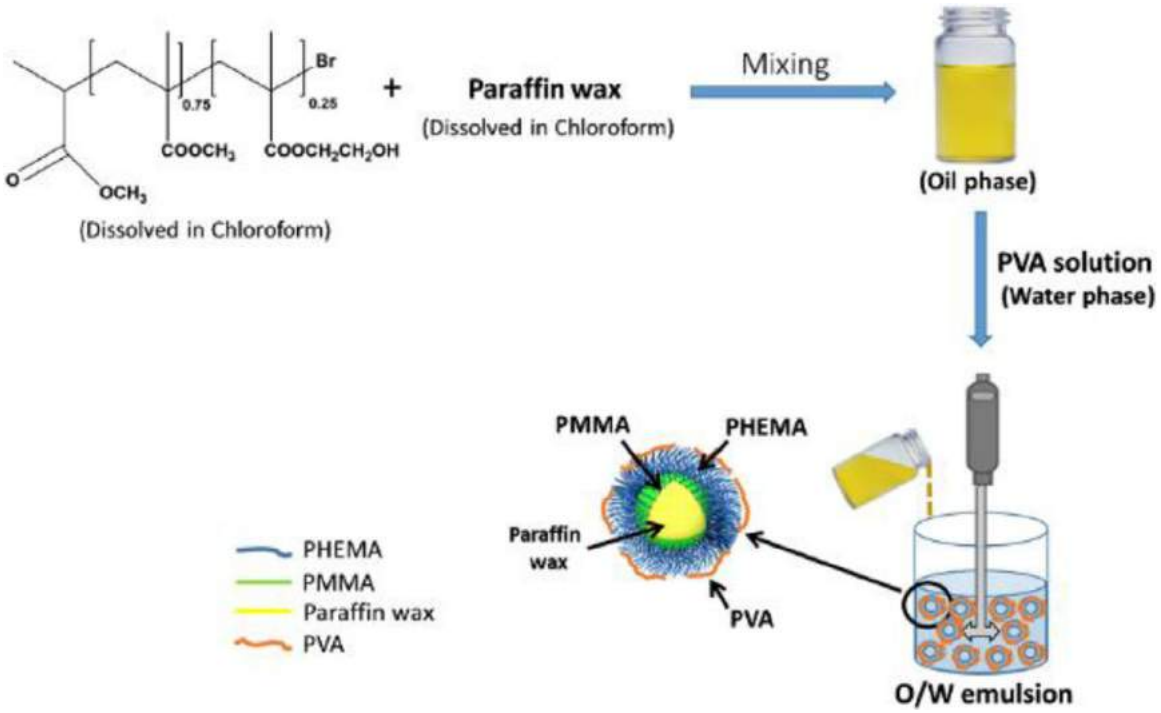

Fig. 26. The fabrication process of microcapsules [122].

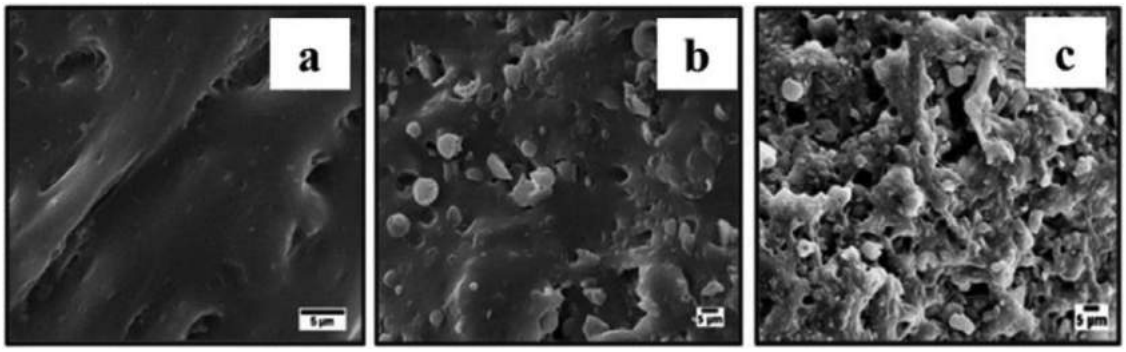

Fig. 27. The SEM images of cryofractured natural rubber loaded with different content of microcapsules; (a) 0 wt.%, (b) 20 wt.% (c) 50 wt.% [122].

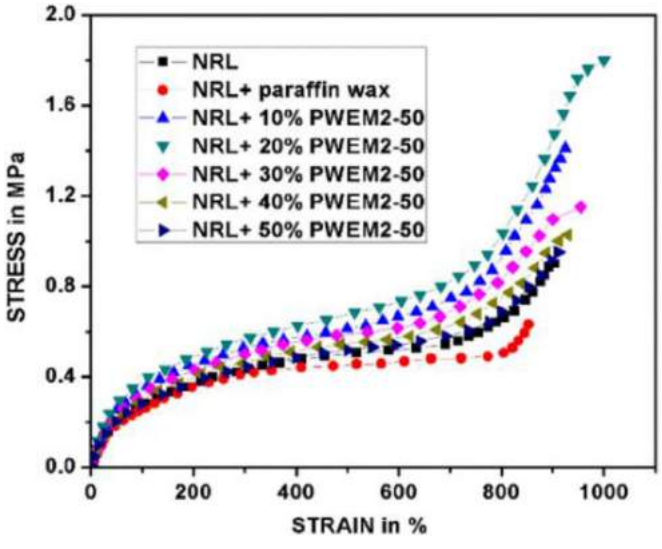

Fig. 28. The stress-strain curves of NRL loaded with different content of capslues.

Wang et al. [124] successfully incorporated cellulose nanocrystals (CNCs) in poly (methyl methacrylate) (PMMA) as the shell to encapsulate the n-eicosane by Pickering emulsion assisted solvent evaporation method. Pickering emulsion results in outstanding stability and more specific information can be found in this previous

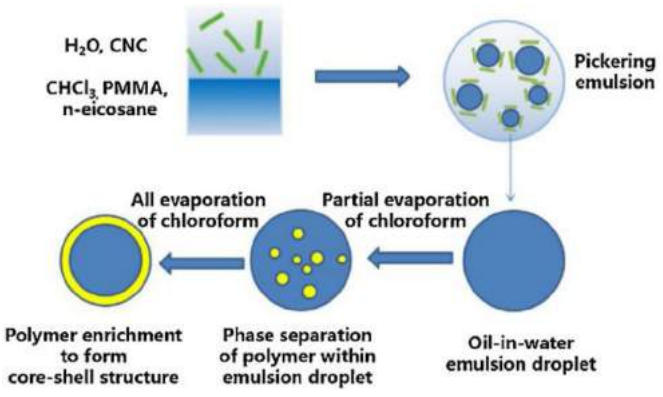

Fig. 29. The fabrication process of microcapsules [124].

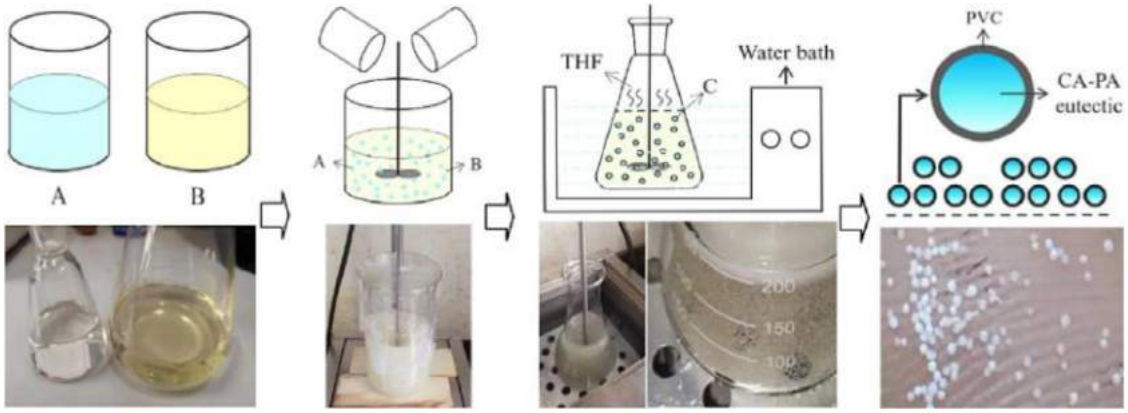

Fig. 30. The preparation process of microcapsules [126].

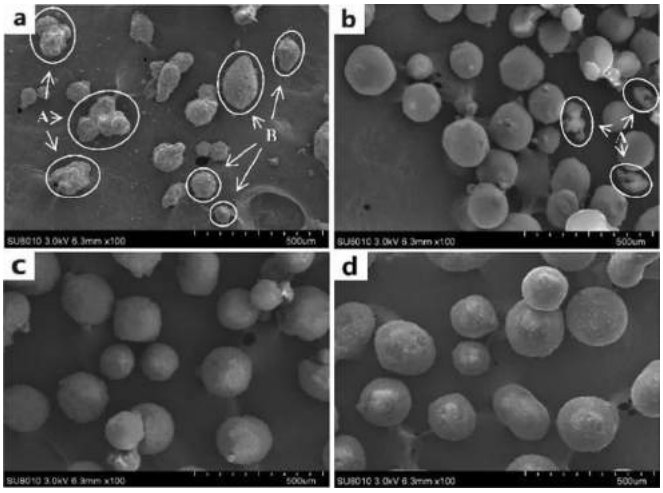

Fig. 31. The morphology of microcapsules made from different core-shell ratio; (a) 2:0.5, (b) 2:1, (c) 2: 1.5, (d) 2:2 [126].

research [125]. The preparation method is depicted in Fig. 29. They found that the optimal core-shell ratio of 2:1 provides ideal thermal properties and morphologies.

Xing et al. [126] focused on the encapsulation of eutectic PCMs. They used Polyvinyl chloride (PVC) to encapsulate the mixture of CA and PA (see Fig. 30). The most suitable core-shell ratio was found to be 2:1; this can be deduced by the morphology study in Fig. 31. The shape is distorted in Fig. 31 a due to the insufficiency of PVC. Despite the small amount of irregular shaped microcapsules, the mean size distribution is narrow in Fig. 31 b. If the shell content increases, the shell thickness increases, leading to bigger particles and lower energy transition efficiency (c and d in Fig. 31).

Table 6 shows previous progress by using solvent evaporation for encapsulation.

3.2.3. Centrifugal extrusion

Southwest Research Institute (SwRI) first employed the centrifugal extrusion method [127] the whole process is illustrated in Fig. 32 below. To interpret, the liquid phase with core materials flows through an inner tube, and the shell material flows through an outer and annular tube that is around the inner tube. Due to immiscibility between the core and shell, vibration and rotation are needed to transfer them to orifice together. Then, spherical drops are formed by a surface tensile force. Finally, with the help of heating or chemical reaction, depending on the shell materials used, these drops are solidified in a bath [112,128]. It is a feasible and simple technique to use, although the capsule diameter range is large (1–5000 μm) [129], and there is no study of PCM preparation by using this method.

3.2.4. Pan coating

The pan coating technique is widely applied to make small solid particles with coating materials (shells), or tablets in the pharmaceutical industry. As in Fig. 33 below, the core material is surrounded by the solid coating; this can be achieved via spraying the coating or mix core and coating material from the start of the process. The former one gives lower energy and take less time [130]. Followed by the heating and cooling down, the coating material seals the core material and then solidifies to form capsules with improved properties. It is worth noting that the melting point of the core material must be higher than that of the coating, otherwise the core material will lose its shape and melt, preventing encapsulation. Due to the melting point restriction and the fact that this method cannot prepare capsules in the micro and nano range, there are few studys involving this method.

Wang et al. [131] applied the pan coating method to prepare macrocapsules with a wall thickness of about 30–50 μm, con-

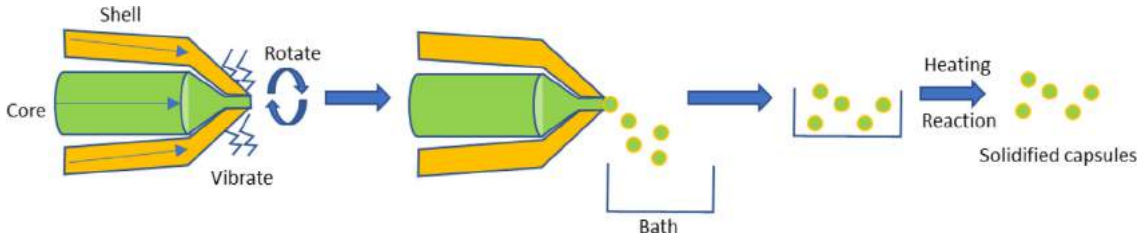

Fig. 32. The process of centrifugal extrusion.

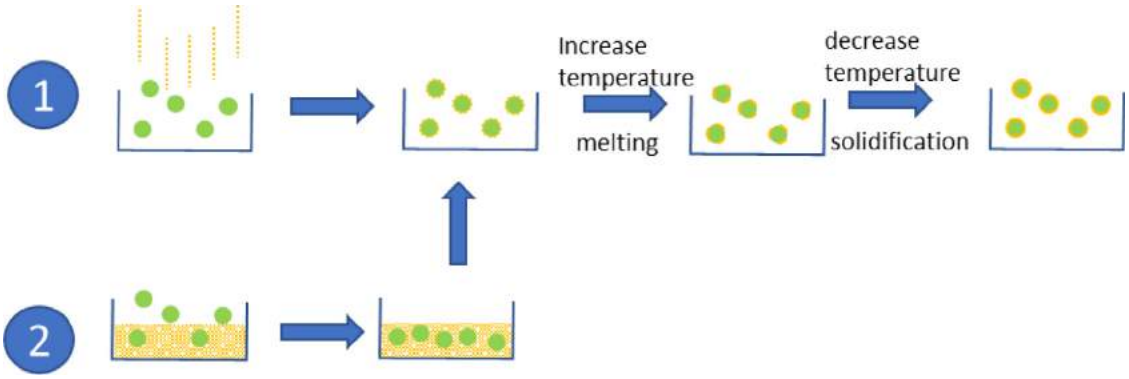

Fig. 33. The process of pan coating.

Table 6
The properties of encapsulated capsules using solvent evaporation.

Refs.	Core material	Shell material	Average diameter (μm)	Thermal cycling (cycles)	Encapsulation efficiency (%)	Heat of fusion (J/g)	Other properties of microcapsules
[119]	LO	Silane-treated and untreated EC	5–35	-	97.6	-	• The Core-shell ratio is 7:3 • Shell thickness: 0.5–2.0 • Spherical shape with a rough surface • Internal morphology is tunable
[120]	PA	PLA	90–100	50	-	70.1	• Core content: 41.9 wt.% • Melting temperature: 62.1°C
[121]	MA	EC	3–5	100	62	122.61	• Melting and freezing point: 53.32 and 44.44°C • Spherical shape • The Core-shell ratio is 2:1 • Maximum operating temperature: 80°C
[122]	Paraffin wax	poly (MMA-co-HEMA)	5	500	92.34	61.8	• Thermal conductivity: 0.49 W/mK • thermal storage capability: 99.85%
[124]	N-eicosane	PMMA	5–10	100	58.2	150.8	• Regular spherical shape • The Core-shell ratio is 2:1
[126]	Eutectic of CA and PA	PVC	159.3	500	57	92.1	• Spherical shape • Melting and freezing point: 17.1 and 18.8 • The Core-shell ratio is 2:1

sisting of a 1:1 n-octadecane (OD) and high-density polyethene (HDPE) core material, and calcium alginate (CaAlg) as the shell material, seen in Fig. 34 below. They found that by using chromic acid, the hydrophilicity and permeability of PCMs can be modified, in addition to the roughness, with pores of 3 μm. Besides, the release kinetic of OD in petroleum solvent is dominated by both quasi-Fickian diffusion and anomalous transport.

3.2.5. Air suspension coating

Compared to the pan-coating technique mentioned above, air suspension coating is more flexible and gives better control of the shell thickness and closure by increasing the number of times the core material passes through the coating zone to obtain better coating coverage [127]. Fig. 35 below shows the process where solid particles (core material) are suspended in a coating chamber with the help of a recirculating air stream. As the solid particles move through the chamber, a coating material dissolved in water or organic solvent is sprayed onto the moving particles. After multiple circulations depending on the thickness of coating expected, particles get dried and coated, which can be accelerated by increasing the temperature of the air stream. Although this process is widely used in the food, cosmetic and pharmaceutical industry, encapsulation of PCMs is not well-received [132].

3.3. Chemical encapsulation methods

3.3.1. In-situ polymerization

The principle of *in-situ* polymerization is that the polymerization of monomers occurs on the surface of the core material. Fig. 36 below shows the process. Initially, the oil-in-water emulsion is prepared by mixing the oil phase-containing core material and aqueous phase consisting of the suitable emulsifier and water-soluble shell material (monomers or pre-polymers). Then, by initiating polymerization (usually pH adjustment), monomers are continuously consumed to form the water-insoluble shell. Finally, microcapsules are filtered, washed, and dried.

Graham et al. [133] employed this technique to encapsulate magnesium nitrate hexahydrate ($Mg(NO_3)_2{\cdot}6H_2O$) with poly(ethyl-2-cyanoacrylate) (PECA) to solve corrosion and incongruent melting problems. The two methods that can obtain nanocapsules are

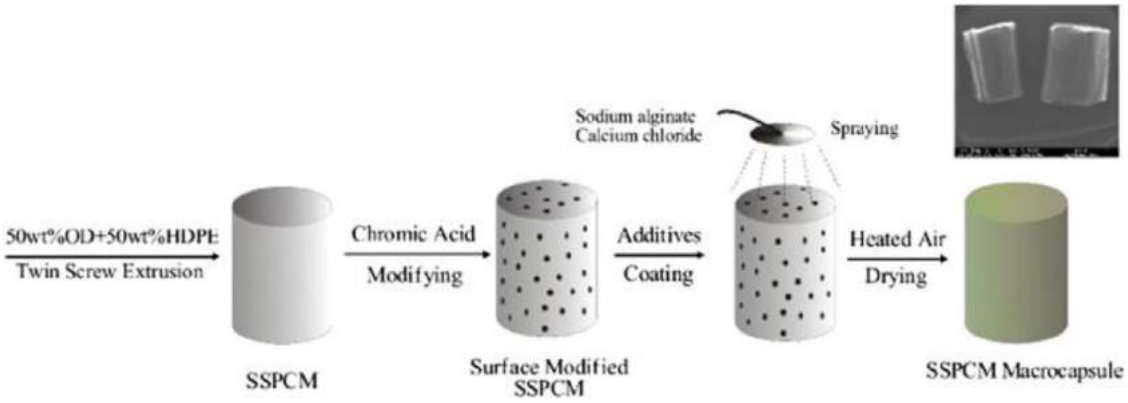

Fig. 34. Macro-capsules preparation by using the pan coating method [131].

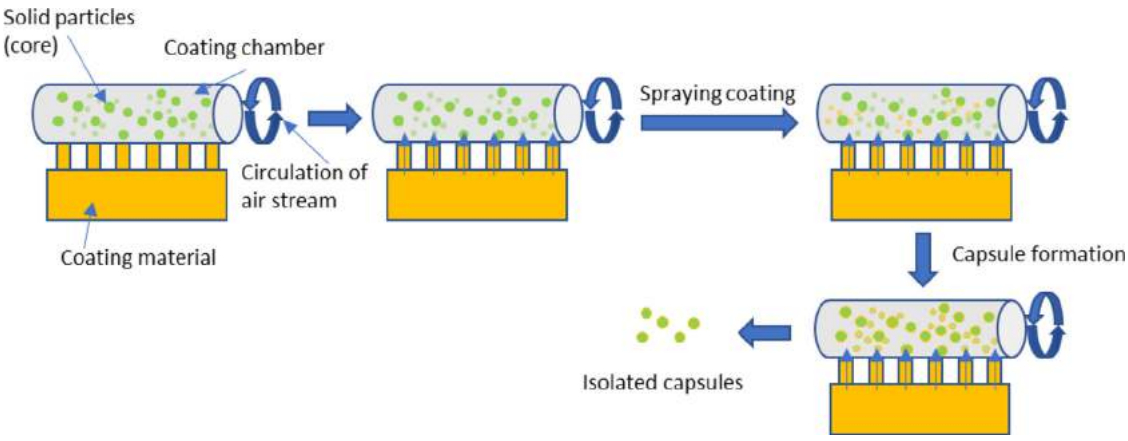

Fig. 35. The process of air suspension technique .

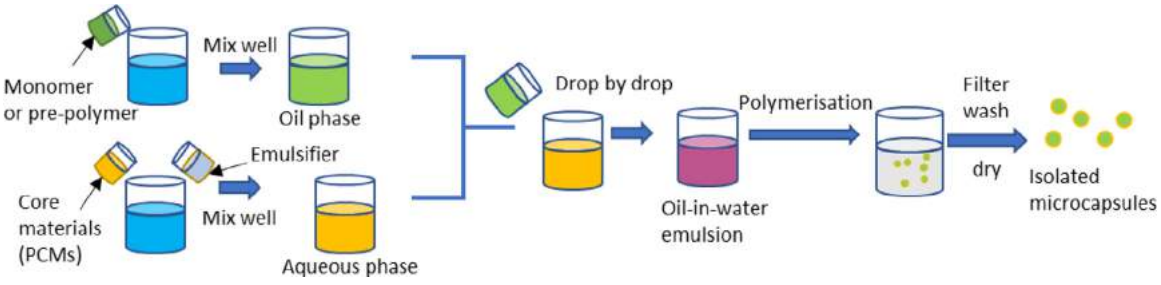

Fig. 36. The process of *in-situ* polymerization for PCMs encapsulation.

shown in Fig. 37 below. A difference from common *in-situ* polymerization is that they utilized sonication to prepare miniemulsion; this special emulsion requires less amount of emulsifier, less time and avoids the presence of two melting points. By investigating the obtained nanocapsules that had a diameter of 100–200 nm, they proved that they had a high thermal stability with only 3% latent heat reduction of the nanocapsules after conducting more than 100 thermal cycles. In comparison, bulk magnesium nitrate hexahydrate decomposition occurs after 5 cycles.

Fig. 38 displays the evidence of higher stability, where the optimal formula of NanoPCM3 containing 5 wt% surfactants, 20 wt% $Mg(NO_3)_2{\cdot}6H_2O$ and 200 µL; this exhibits a slightly changed curve after 100 cycles.

Qiao and Mao [134] successfully obtained encapsulated paraffin by urea-formaldehyde (UF) using in- situ polymerization with a special particle diameter of about 45 µm. Besides, they enhanced the thermal conductivity with the addition of graphene oxide (GO) via two different methods, inside incorporation (paraffin/GO@UF composite) and outside coating (paraffin@UF/GO composite). The two processes and mechanisms are depicted in Fig. 39 below. Paraffin@UF/GO composites are obtained by the formation of capsules first, and coverage second with the help of interaction between cationic and anionic surfactants, hexadecyl trimethyl ammonium bromide (CTAB) and sodium dodecyl benzene sulfonate (SDBS). Whereas the paraffin/GO@UF composite derives from the interaction between GO and paraffin, and then polymerization. They found that thermal conductivity increases with the content of GO. At the 10 wt% of GO, however, paraffin@UF/GO composite contributes more for enhancement of thermal conductivity from 0.2236 (UFP capsules) to 1.067 W/(m·K) compared to the other

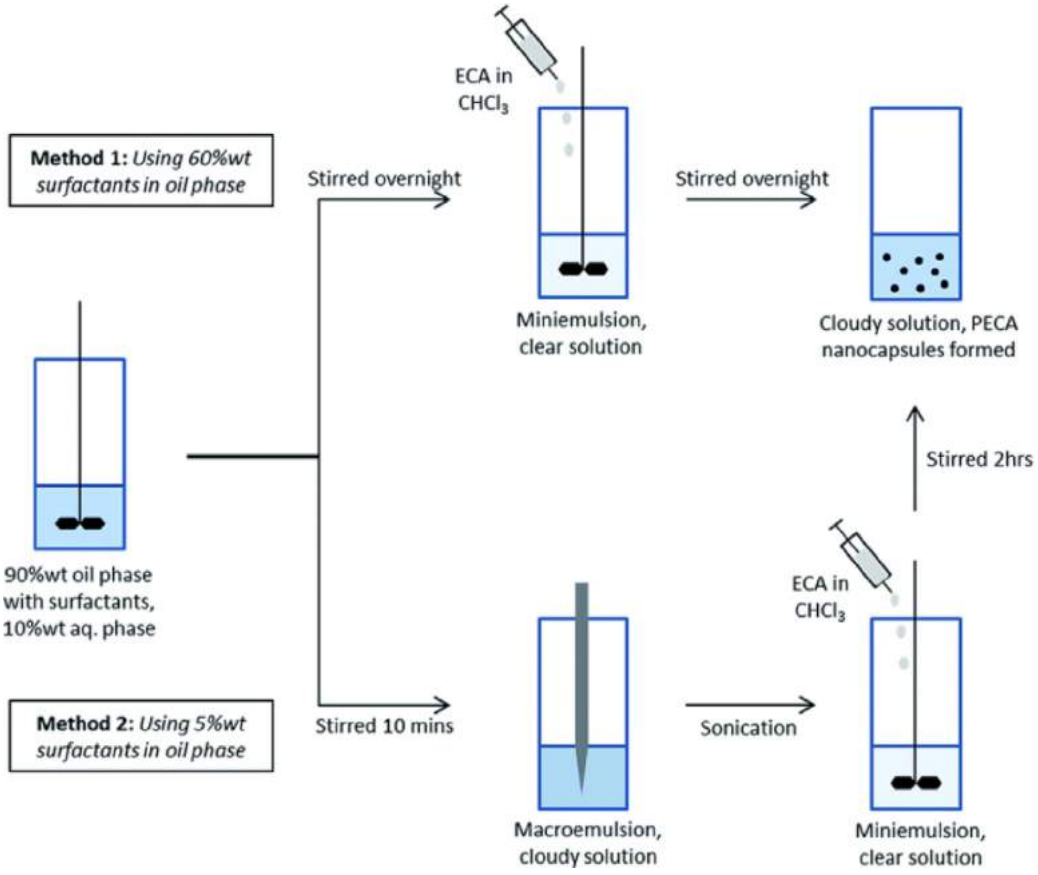

Fig. 37. Two methods to prepare nanocapsules [133].

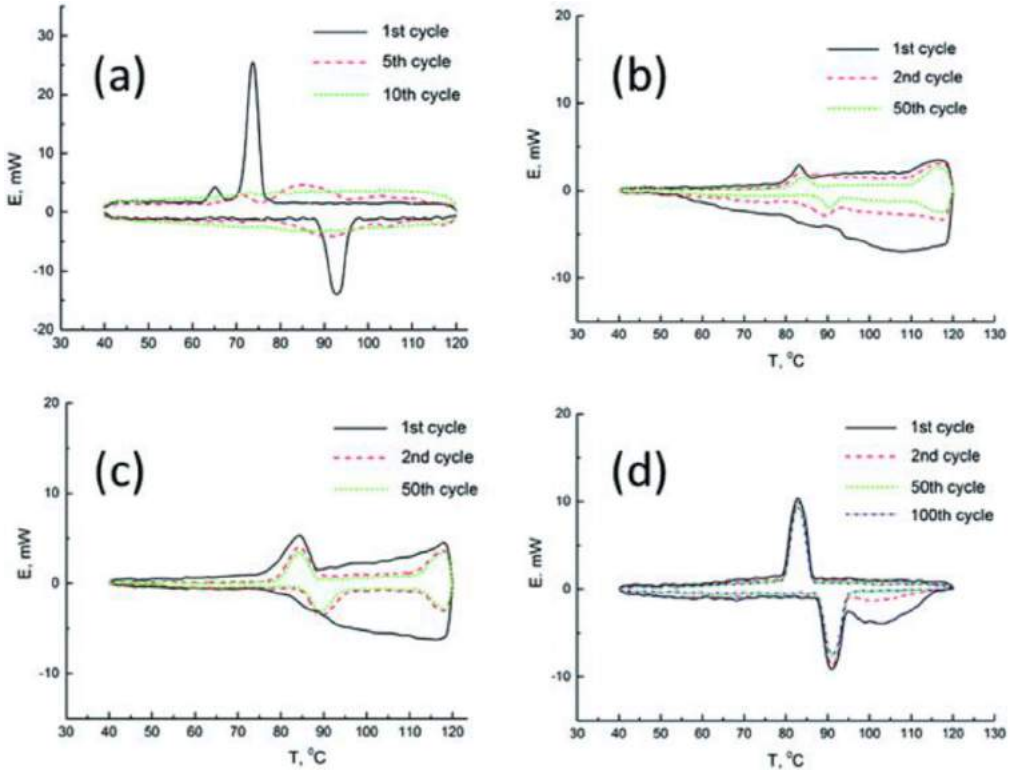

Fig. 38. The DSC curves of (a) bulk PCM, (b) NanoPCM1, (c) NanoPCM2 and (d) NanoPCM3 (optimal) [133].

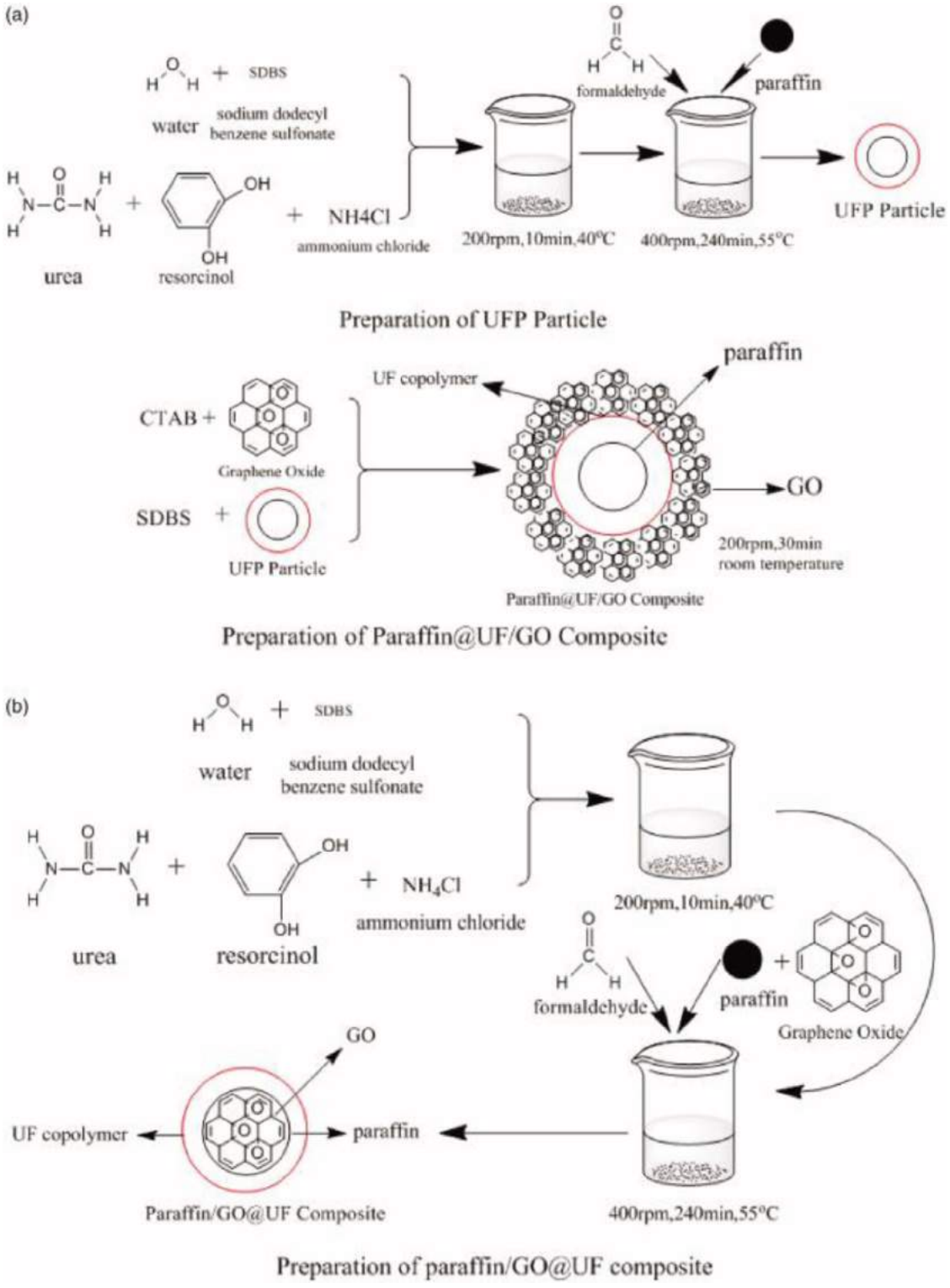

Fig. 39. The process to prepare two different microcapsule composites [134].

with a slight increase to 0.2517 W/(m·K), seen Fig. 40 below. In the future, it is highly possible that we can entirely exchange polymer shells for graphene shells, instead of using graphene as an enhancement material. Morales-Narváez et al. [135] have summarized synthesis, applications and future trends of graphene-encapsulated materials, like graphene oxide, pristine graphene, polycrystalline graphene etc. However, this field is on the early development and need to tackle bottlenecks so that graphene can reach its full potential especially on PCMs encapsulation.

Pethurajan and Sivan [136] used the *in-situ* polymerization methods to prepare paraffin wax/ UF microcapsules, integrated with different metal oxide nanoparticles to enhance the properties; the process is displayed below in Fig. 41. By using different characterization methods, like Scanning Electron Microscope (SEM), Fourier Transform Infrared spectroscopy (FT-IR), spectrum and Differential Scanning Calorimeter (DSC) thermograms, different properties are investigated. The results show that the average particle size of microcapsules with a spherical shape is 65 μm,

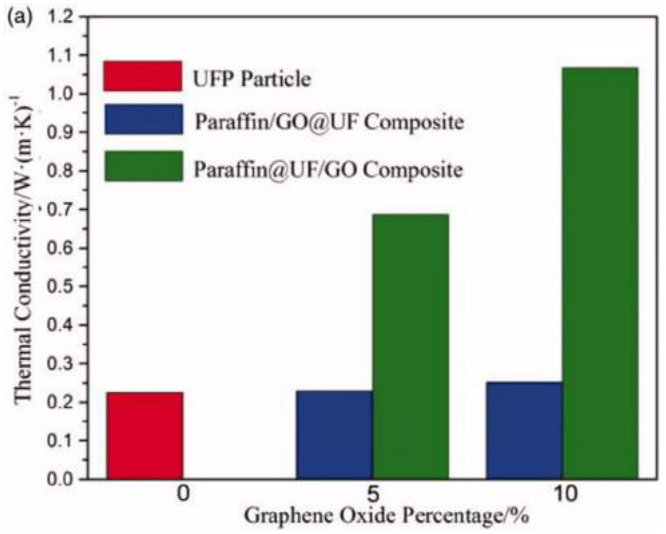

Fig. 40. The thermal conductivity of UFP, paraffin/GO@UF composite and paraffin@UF/GO composite with their different GO contents [134].

and there is no chemical interaction between each component. Although the addition of alumina, copper oxide, titanium oxide slightly reduces the latent heat of paraffin wax by 9%, 11.9%, 5.4%, the conductivity has largely increased by 21%, 49%, 59.38%, respectively. Amongst these three metal fillers, copper oxide accelerates the thermal cycle most.

According to the study by Rakkappan et al. [137] issued in 2021, the low-cost 1-Decanol is encapsulated by a urea-formaldehyde (UF) shell. The mechanism and process are illustrated in Fig. 42 below. Like the synthesis from Graham et al. [133], they also use ultrasonication to accelerate the emulsion process (step 1–2). On top of that, they included the addition of GnP and CuO nanoparticles to facilitate the thermal properties. By using the *in-situ* polymerization, they initially prepared the capsules with an encapsulation efficiency of 59.56%, melting and freezing enthalpy of 120.12 J/g and 118.92 J/g at the optimal amount of 10 g. Additionally, after two nanoparticles are incorporated, the resultant capsules maintain their average particle size within the nanoscale (Fig. 43 below). For the addition of GnP and CuO, their optimal weight fraction is 6% and 10%, resulting in an encapsulation efficiency of 56.14% and 54.52%, and a thermal conductivity increase of about 2.19 and 1.98 times, respectively. The thermal reliability of the modified nanocapsules is exceptional, even after one thousand cycles. Impressively, the charging and discharging time of modified capsules is on average 30% faster than capsules with no addition of nanoparticles.

Graham et al. [138] used ultrasonic treatment with *in-situ* polymerization to prepare the poly(ethyl-2cyanoacrylate)-encapsulated $Mg(NO_3)_2{\cdot}6H_2O$, $Na_2SO_4{\cdot}10H_2O$ eutectic mixture. DSC demonstrated that, with the aid of special confinement and protection

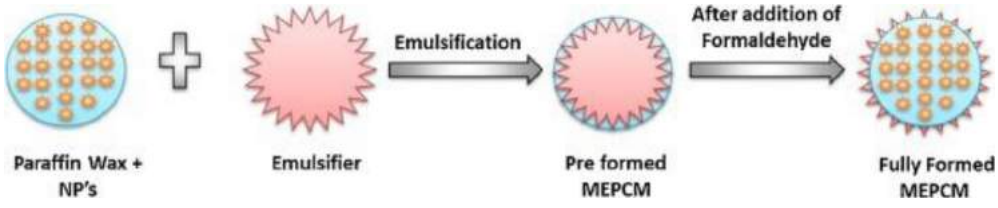

Fig. 41. Encapsulation process by using *in-situ* polymerization [136].

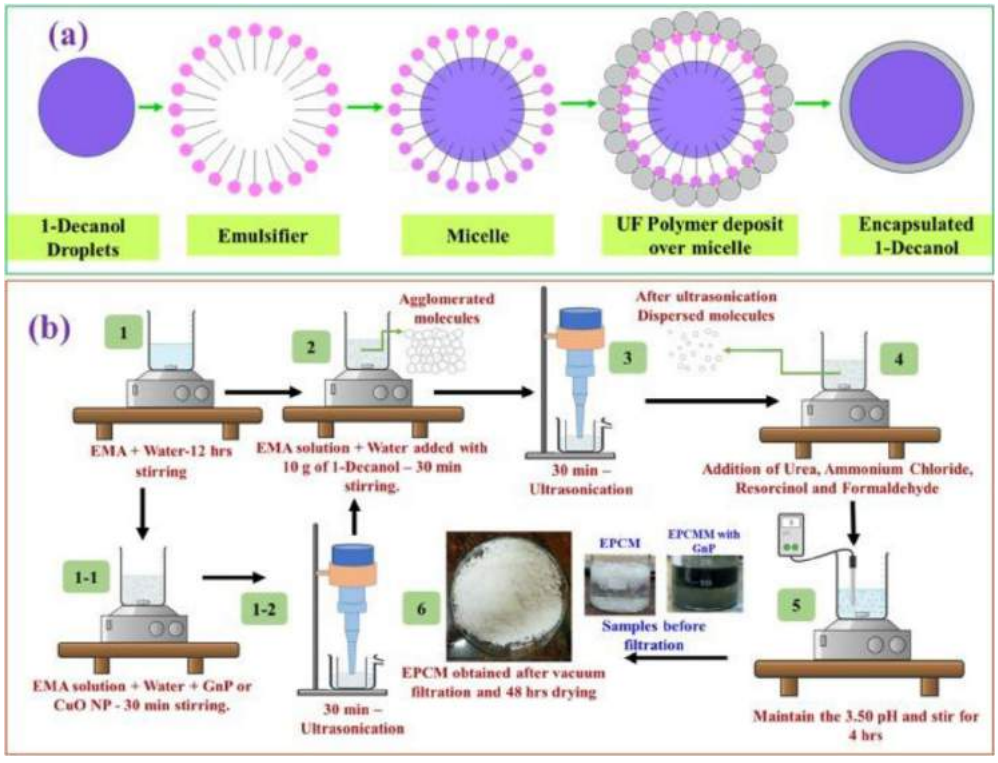

Fig. 42. (a) The mechanism and (b) process to prepare modified capsules by using *in-situ* polymerization [137].

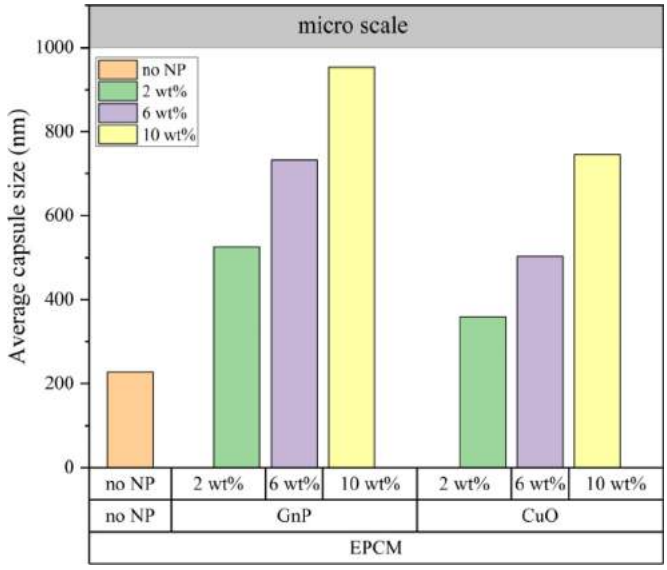

Fig. 43. The average capsules size of encapsulated1-Decanol with and without different kinds and contents of nanofillers [137].

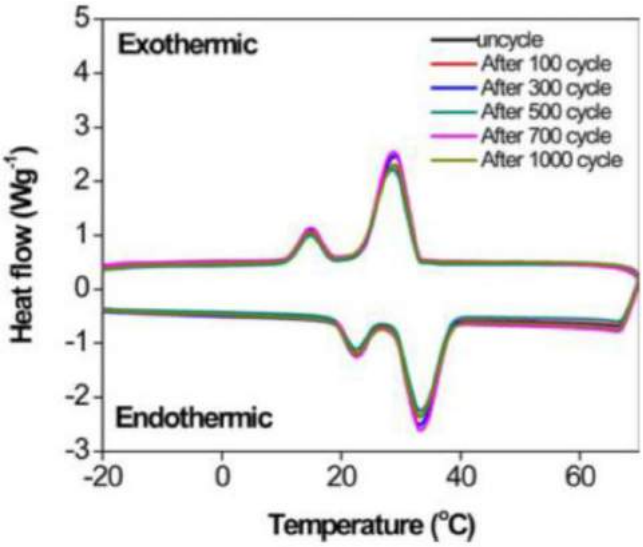

Fig. 44. The thermal stability of n-Nonadecane encapsulated St/MMA [139].

of the shell, its high stability and reliability after above one hundred phase transition cycles is ensured. They stated that there is the potential to design microcapsules with different phase transition points by changing the ratio of the crystallohydrate mixture using this method.

According to the research from Khadiran et al. [139], an n-Nonadecane encapsulated copolymer of styrene (St) and methylmethacrylate (MMA) was successfully achieved by one-step miniemulsion *in-situ* polymerization. The ratio of the two copolymer components is crucial to prepare well-performed capsules. When the ratio is 4:1 (St: MMA), a spherical shape with an average diameter of 160 nm is formed. With the highest encapsulation efficiency of 45.8%, the melting point and freezing points are 33.1°C and 30.2°C along with excellent latent heat of 76.9 J/g and 82.0 J/g, respectively. Besides, the thermal properties after 1000-cycles are comparable to uncycled capsules (see Fig. 44).

Huang et al. [140] endowed the n-Octadecane/MF microcapsules with light-thermal energy conversion properties by the incorporation of ZnO. The incorporation of 7 wt% ZnO largely enhanced the mechanical properties of the microcapsules, with them fracturing at a force of 1470 N (see Fig. 45). Amongst different amounts of ZnO (from 0 wt% to 9 wt%), 7 wt% dosage exhibits

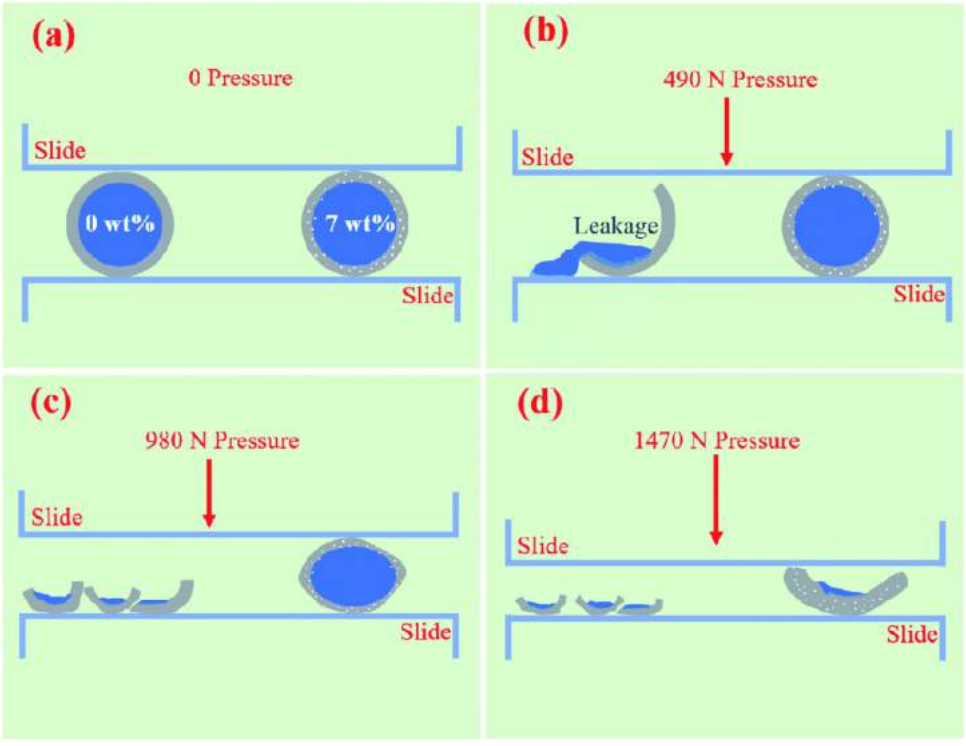

Fig. 45. The mechanical property test of ZnO reinforced microcapsules [140].

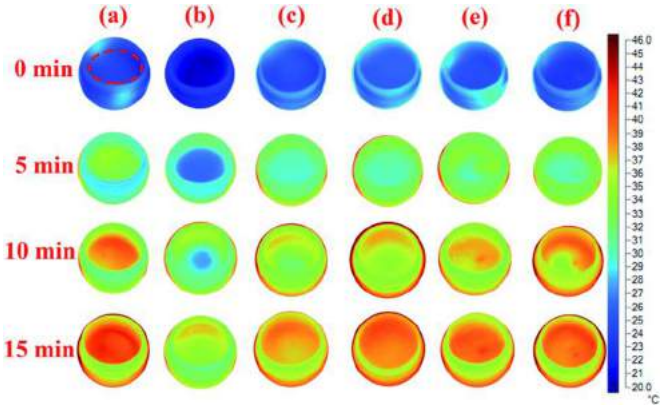

Fig. 46. The infrared images of microcapsules with different amounts of ZnO; (a) nano-ZnO powder; (b) 0 wt%; (c) 3 wt%; (d) 5 wt%; (e) 7 wt%; (f) 9 wt% [140].

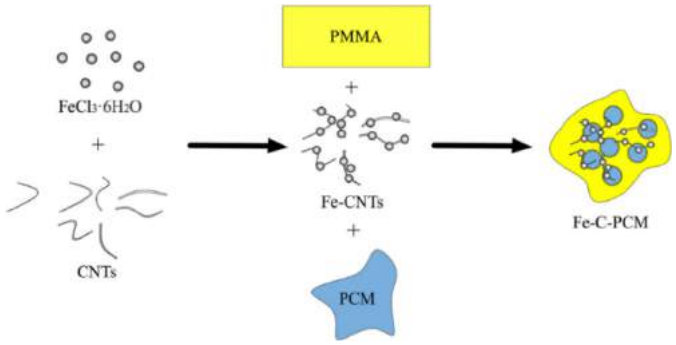

Fig. 47. Formation of Fe_3O_4-CNTs-PCMs [141].

excellent light-thermal energy conversion properties, having the highest rate of temperature increase after illumination for 10 min (see Fig. 46).

The drawbacks of low thermal conductivity, undesirable thermal stability and flammability for organic shells and PCMs are well-received, and have been discussed before. Recently, Cheng et al. [141] utilized the integration of carbon nanotubes (CNTs) and Fe_3O_4 particles to produce encapsulated PCMs with good thermal behaviour and flame retardance using *in-situ* polymerization, and the process of synthesis is shown in Fig. 47. In their research, the morphology is investigated (Fig. 48), where Fe_3O_4 particles are located around microcapsules and connected by CNTs. Through chromatic aberration method, the heating process is visualized (Fig. 49), where Fe_3O_4 particles and CNTs integrated microcapsules undergo smallest temperature change after 200 s. Their research largely promoted the insulation application.

Previous works using in-situ polymerization method for encapsulation are integrated into Table 7.

3.3.2. Interfacial polymerization

Interfacial polymerization techniques involve two different hydrophilic and hydrophobic monomers dissolving in the aqueous phase and oil phase (core), respectively. Due to the stabilization of the emulsifier, the oil phase including hydrophobic monomers is dispersed in the aqueous phase. Polymerization is initiated by change in temperature and pH during the process of adding hydrophilic monomers. Eventually, microcapsules are obtained by filtering, washing, and drying. The mechanism and process are shown in Fig. 50 below.

The first study about interfacial polymerization was written by Cho et al. [142] synthesizing microcapsules with a smooth spherical particle diameter of 1 μm that consisted of octadecane (core) and PU (shell). In this case, the hydrophilic and hydrophobic monomers are diethylenetriamine (DETA) and toluene-2,4-diisocyanate (TDI), respectively. According to the results, they found that the shell material is formed in two ways, the reaction of TDI and DETA, and then the additional reaction of TDI and amines from the hydrolysis of TDI at the interface. The phase transition temperature is in the range of 29–30°C, which is in the range of bulk octadecane, the encapsulation efficiency is inversely propor-

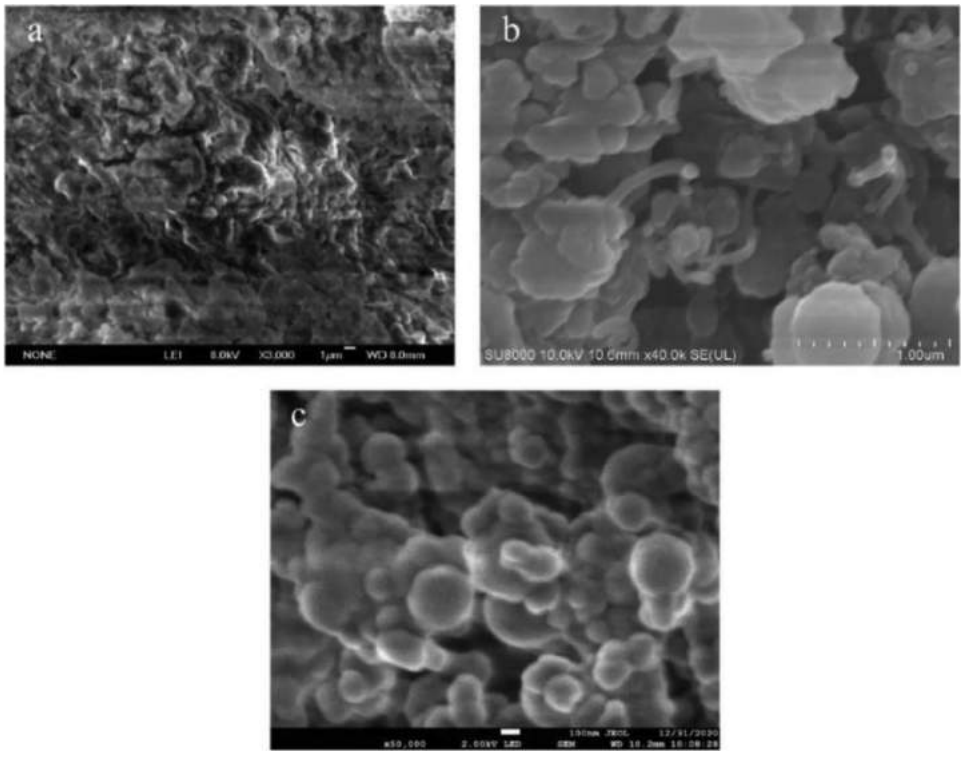

Fig. 48. SEM images for morphology of a) PCMs, b) CNTs-PCM, c) Fe_3O_4-CNTs-PCMs [141].

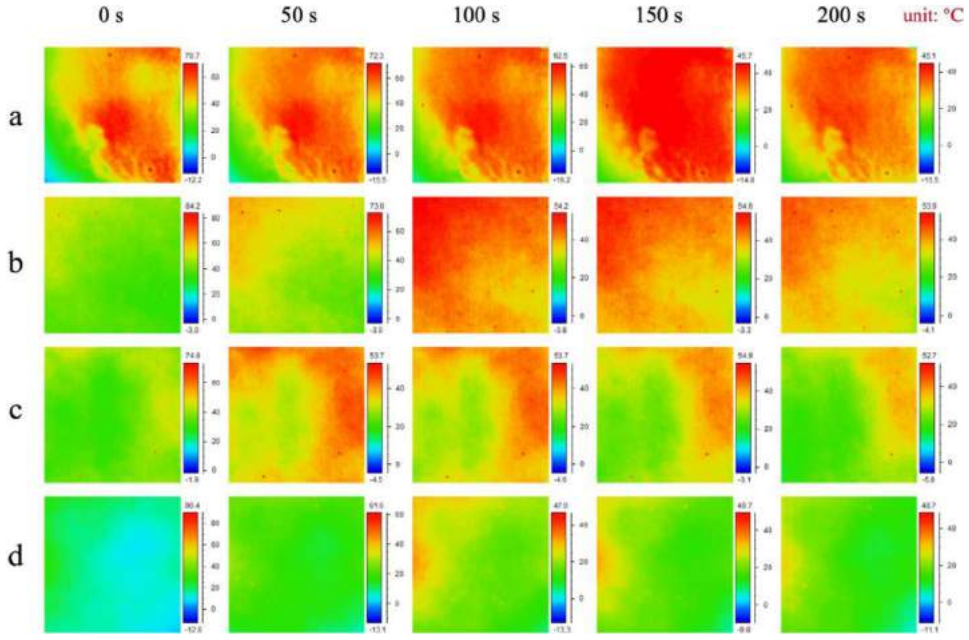

Fig. 49. Infrared images of (a) polyurethane foam, (b) PCMs, (c) CNTs-PCMs, (d) Fe_3O_4-CNTs-PCMs during heating process [141].

Table 7
The properties of encapsulated capsules using *in-situ* polymerisation.

Refs.	Core material	Shell material	Average diameter (μm)	Thermal cycling (cycles)	Encapsulation efficiency (%)	Heat of fusion (J/g)	Other properties of microcapsules
[133]	$Mg(NO_3)_2{\cdot}6H_2O$	PECA	0.1–0.2	100	52	83.20	• Melting point: 91°C
[134]	Paraffin	UF (with GO)	40–45	50	83.9	155.30	• Thermal conductivity: 1.0670 (10% GO) • good thermal stability and reliability
[136]	Paraffin wax	UF	60–65	-	52.26	110.78	• Withstand high temperature until 345°C • Thermal conductivity: 0.586 W/mK
[137]	1-Decanol	UF (with GnP and CuO)		1000	56.14	120.12	• Significant thermal conductivity enhancement
[138]	$Mg(NO_3)_2{\cdot}6H_2O$, $Na_2SO_4{\cdot}10H_2O$, Their mixture	PECA	0.1–1	100	67	126.80	
[139]	N-nonadecane	P(St-co-MMA)	0.16	1000	45.8	76.90	• Melting and freezing point: 33.1 and 30.2°C • Good chemical and thermal stability
[140]	N-Octadecane	MF	10	100	51.4	123.90	• Good light–thermal conversion properties: high photothermal storage efficiency of 75.2% • Good mechanical properties
[141]	Capric acid	PMMA	0.175	-	-	100.10	• Excellent insulation, thermal stability property • Melting point: 33.73°C

tional to the content of core material, and the maximum encapsulation efficiency of 87.2% is achieved when the weight fraction of the core material is 29.8%.

Similarly, Lan et al. [143] used the same monomers (DETA and TDI) to prepare a PU shell. However, they explored a new core material (n-eicosane) incorporated into microcapsules with an encapsulation efficiency of 75%. From thermogram analysis, the capability of withstanding high temperature is improved after encapsulation from 130°C (bulk n-eicosane) to 170°C (micro- n-eicosane).

For a detailed investigation of interfacial polymerisation, Salaün et al. [144] contributed to a large extent. The microencapsulation process is shown in Fig. 51 below. They mainly investigated the effects of different parameters, like the ratio of two kinds of monomers, stirring rate etc., on microcapsules properties like average diameter, morphology, encapsulation efficiency and core content. In this study, they synthesized xylitol/polyurea–urethane (core/shell) microcapsules. Differing from other research, the core material (xylitol) is not only used as the energy substance (PCMs) but one of the monomers forming the shell. Thus, the shell material is made from diphenyl methylene diisocyanate (DMI) and xylitol, and the reaction can be seen in Fig. 52 below. The results show the optimal encapsulation efficiency and core content are obtained when the weight ratio of core and shell is 77:23. Based on this ratio, the increase in the amount of

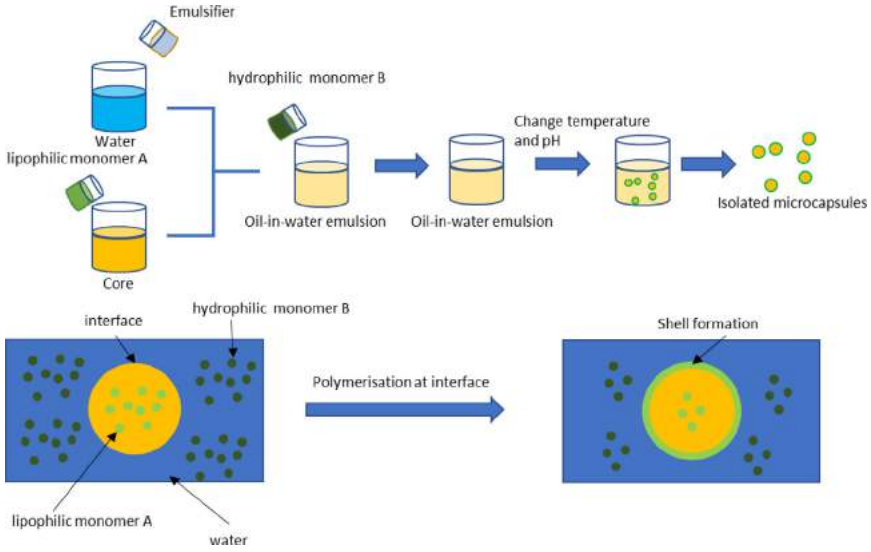

Fig. 50. The process and the mechanism of interfacial polymerization to prepare microcapsules.

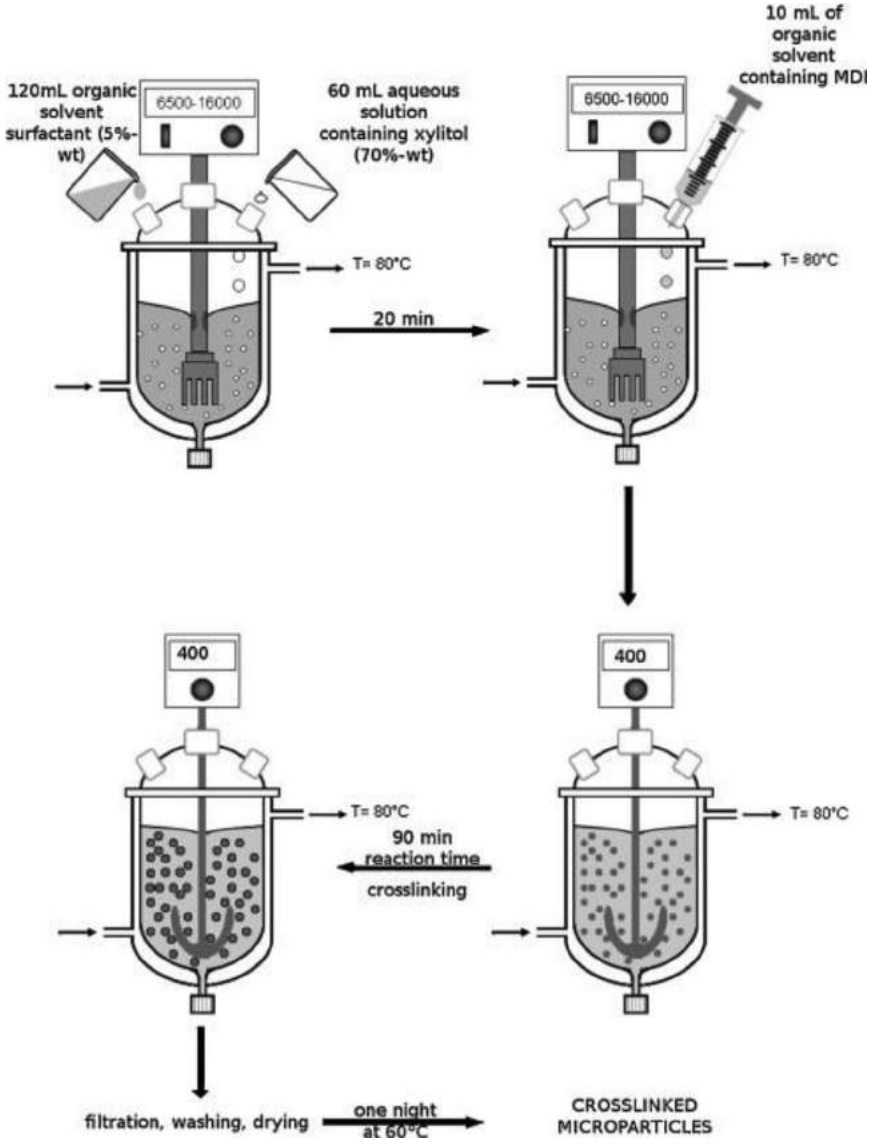

Fig. 51. The process of microcapsule preparation [144].

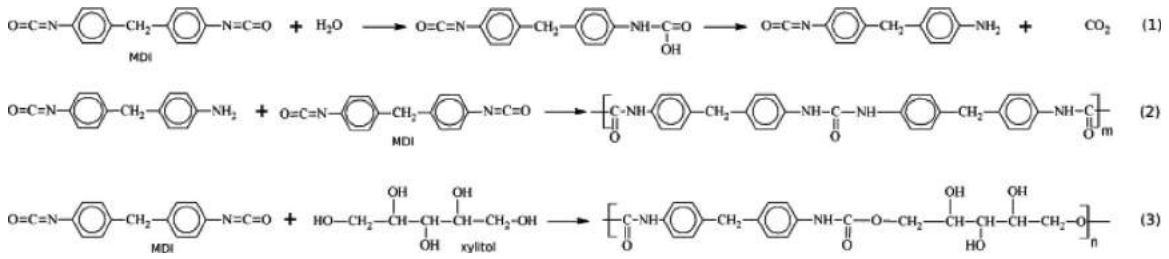

Fig. 52. The reaction of shell material formation [144].

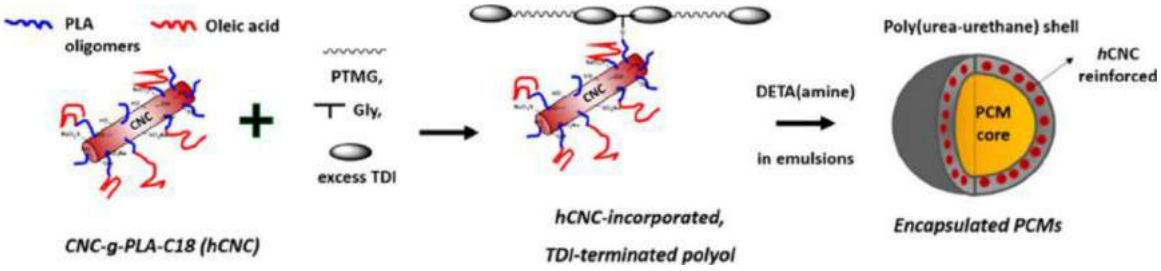

Fig. 53. The mechanism of hCNC-incorporated microcapsules [145].

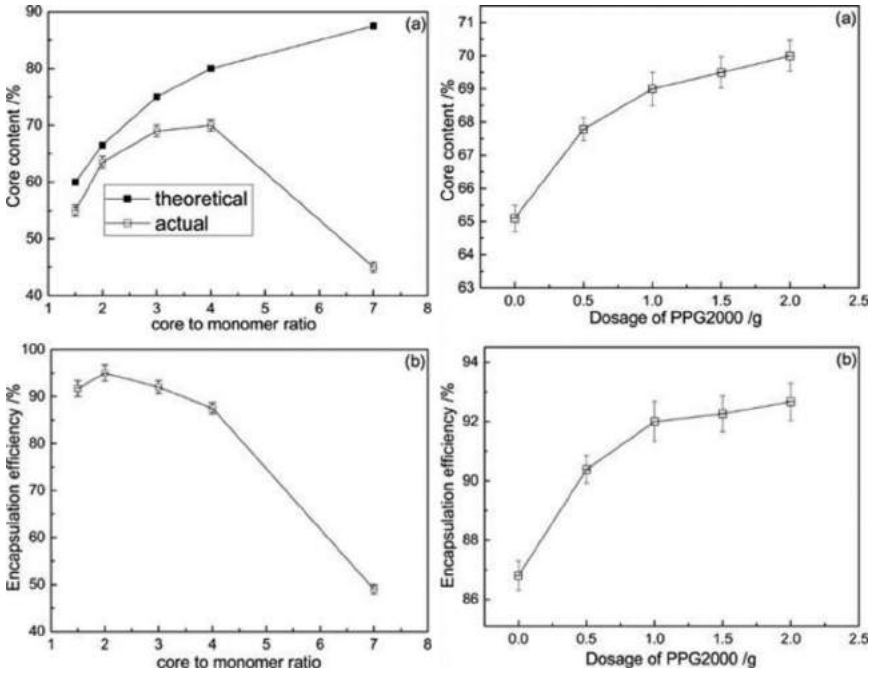

Fig. 54. The effects of the core to monomer ratio and PPG2000 dosage on encapsulation efficiency and core content [146].

MDI and decrease in stirring rate result in higher encapsulation efficiency.

Yoo et al. [145] successfully fabricated microcapsules consisting of methyl laurate as core and poly(urea–urethane) (PUU) as the shell. Besides, they modified the PU shell with CNCs as fillers. To further boost the dispersion, they came up with the surface modification by grafting poly(lactic acid) (PLA) oligomers and oleic acid (OA), and the mechanism is depicted in Fig. 53 below where TDI, DETA, Gly and PTMG are tolylene-2,4-diisocyanate (oil-soluble monomer), DETA (water-soluble monomer), glycerol and poly(tetrahydrofuran) (PTMG). In this study, they found that obtained microcapsules have good mechanical properties with the elastic modulus of 0.3–0.63 N/mm. The particle diameter and thickness have the range of 20–400 and 10–150 μm, respectively. The addition of CNCs gives rise to a denser and smoother surface while looking at the morphology. Moreover, the encapsulation efficiency and shell thickness are inversely proportional to the core-shell ratio, and the capsule diameter is proportional to the PTMG content.

Lu et al. [146] made another innovation forming a kind of double-shell to encapsulate the butyl stearate. The inner layer is a polyurethane (PU) made from TDI and polypropylene glycol 2000 (PPG2000), and the outer layer is PU synthesized by TDI and diethylenetriamine. They focused on the encapsulation efficiency and effects of monomer ratio and PPG2000 on the core content and encapsulation efficiency. When the core-monomer ratio is 3–4 and the dosage of PPG2000 is 1 g, the optimal core content and encapsulation efficiency are achieved reflected in Fig. 54 below.

Despite the formation of double-shell, the thermal properties of PCMs are not significantly affected where the phase change temperature is comparable before and after encapsulation. Astonish-

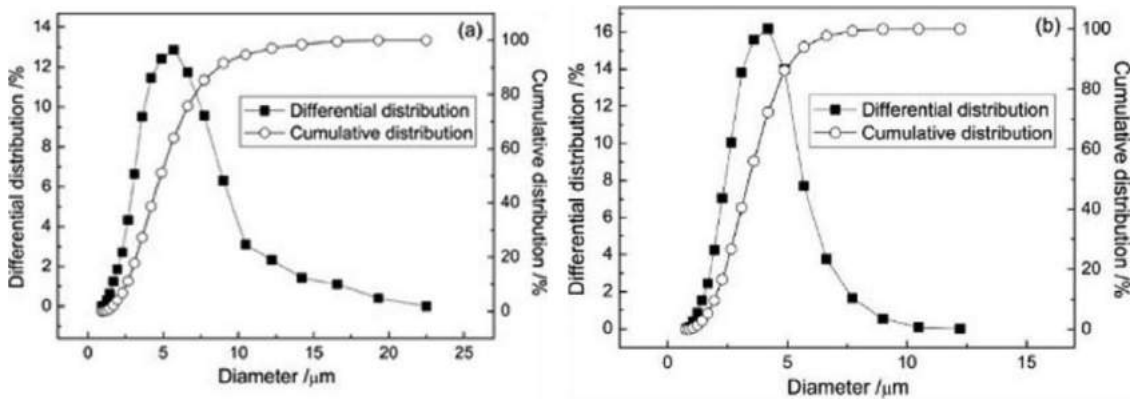

Fig. 55. Particles size with a single shell and double shell [146].

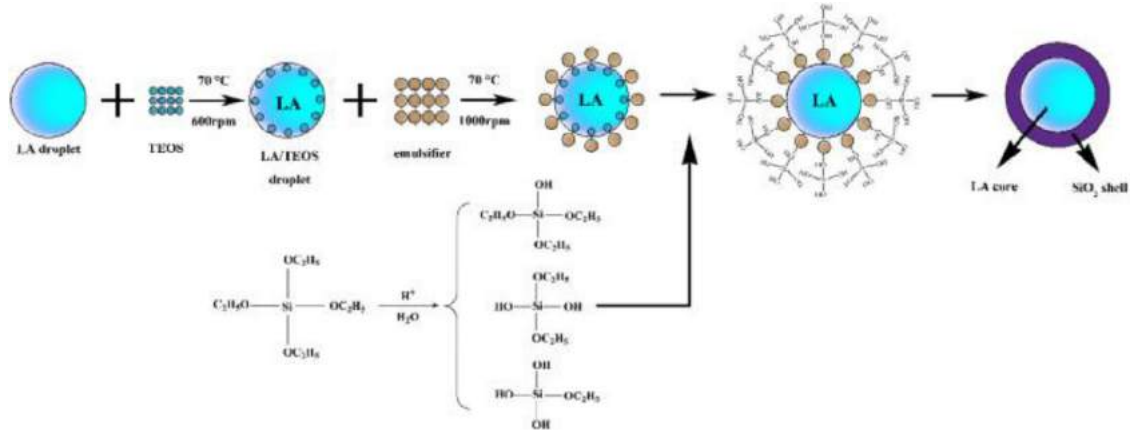

Fig. 56. The mechanism of LA@SiO_2 microcapsules using interfacial polymerization [147].

ingly, according to Fig. 55, the average particles size of the double shell (4.2 μm) is lower than the single shell (5.3 μm).

The latest research by Yang et al. [147] shows that a kind of microcapsule consisting of lauric acid (LA) as core and silica (SiO_2) as the shell was synthesized. They employed an interfacial polymerisation technique and investigated the effects of different parameters during this process on the thermal properties. The mechanism is shown in below Fig. 56 where the aqueous phase containing emulsifier and oil phase containing LA, and tetraethoxysilane (TEOS) as the precursor are prepared first. In this mechanism that differs from the above research using different monomers, they added a small amount of TEOS to form miniemulsion (LA/TEOS droplet) at a high stirring rate. After mixing the aqueous and oil phase, HCL (hydrochloride) as a catalyst is added to the system to initiate silica polymerisation occurring on the interface due to different inside and outside concentrations of TEOS. The high melting latent heat of 186.6 J/g and encapsulation efficiency of 78.6% was achieved under optimal conditions including 0.8 g Op-10 as emulsifier, 1000 rpm stirring rate and the core-shell ratio of 2:1. Besides, these spherical microcapsules exhibit exceptional thermal stability and largely prevent leakage even at 60°C for an hour.

Wang et al. [148] focused on the antibacterial properties of microencapsulated PCMs, which is promising and important in the textile and food industry. N-octadecane (OD) and thyme oil (TO), as dual-core materials, were combined and encapsulated within the PU shell. Isophorone diisocyanate (IPDI) and hexamethylene diamine (HMDA) were used as oil-soluble and water-soluble monomers, respectively. The process and chemical reaction of PU are shown in Fig. 57 below.

They found that the content of TO and OD greatly influences the properties of obtained capsules where encapsulation efficiency increases with the content of TO, and the supercooling phenomenon is effectively suppressed by 7 wt fractions of OD. For the antibacterial property, the date below (Fig. 58) demonstrates the effective dosage of microcapsules in the bacteria solution to have excellent antibacterial property. When the concentration of microcapsules in that solution is 0.5 wt.%, the inhibition rate is not satisfactory, while an increase in the concentration of 1.5 wt.% gives a jump in antibacterial capability, of more than 95%.

Cai et al. [149] developed a new interfacial polymerization method where the co-solvent cyclohexane is not necessary for the preparation of microcapsules consisting of a dodecanol dodecanoate core and PU shell. Meanwhile, the properties of microcapsules are guaranteed. The microcapsules have a spherical shape, with an average diameter of 10–40 μm, PCM-monomer ratio of 1.5:1, promising latent heat of 103.4–140.3 J/g, a thermal conductivity of 0.21 W/m K, and exceptional thermal reliability until 234.0°C. Furthermore, using interfacial polymerisation without co-solvent gives rise to not only better mechanical properties but higher latent heat (see Fig. 59). Fig. 60 below shows the morphology and latent heat of particles with and without using cyclohexane. Particles made by using the co-solvent free polymerisation method exhibit higher latent heat, mainly because many cracks form from using cyclohexane, which leads to lower mechanical properties and some extent of leakage as seen in the SEM graph below.

Recently, PCM microcapsules have been employed to solve the problem of ice coated electrical equipment made of vulcanized silicon rubber. Hu et al. [150] embedded microcapsules derived

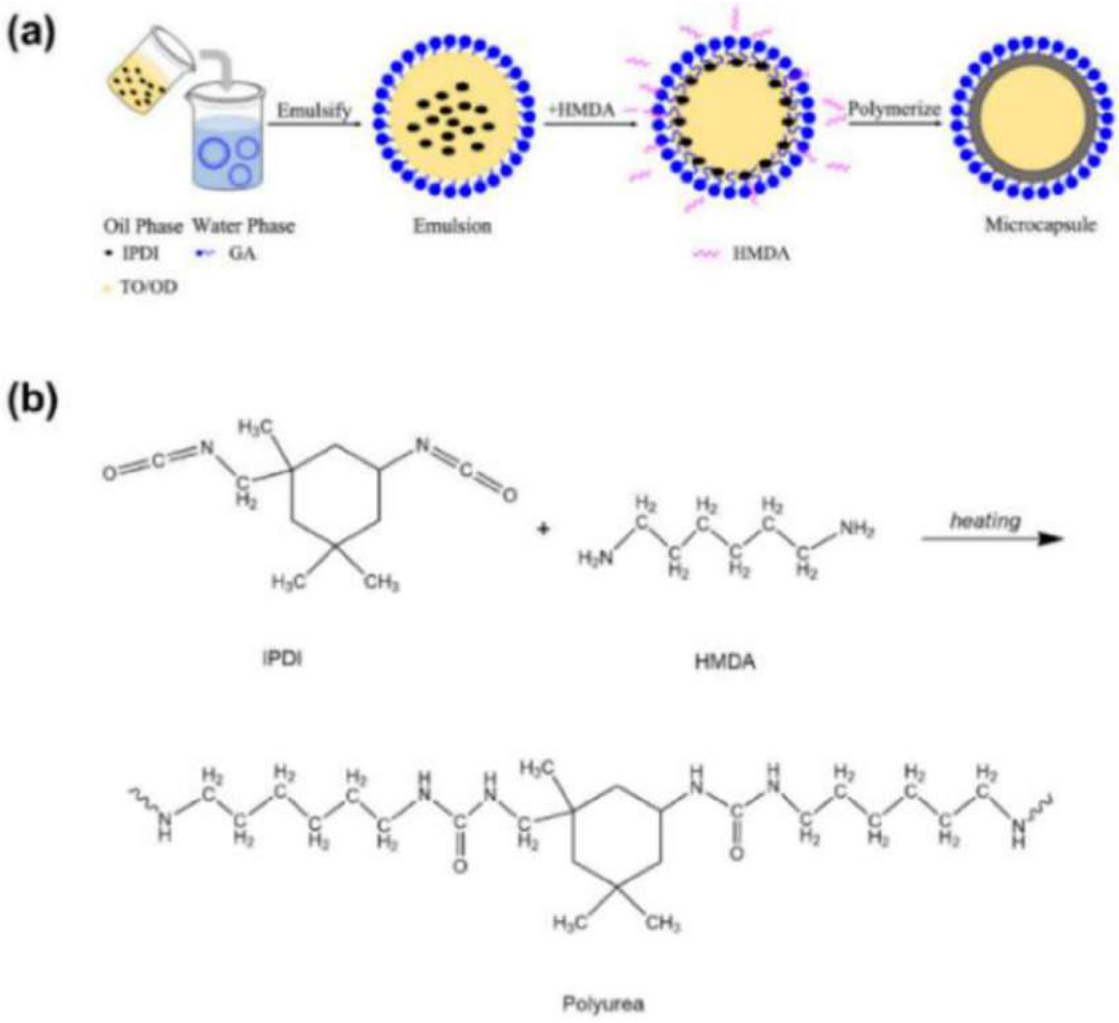

Fig. 57. The interfacial polymerisation process and chemical reaction of PU [148].

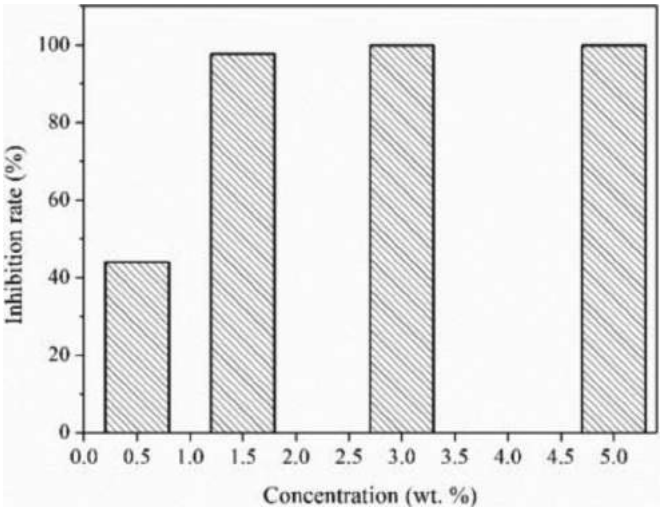

Fig. 58. The antimicrobial activities at different concentrations of microcapsules [148].

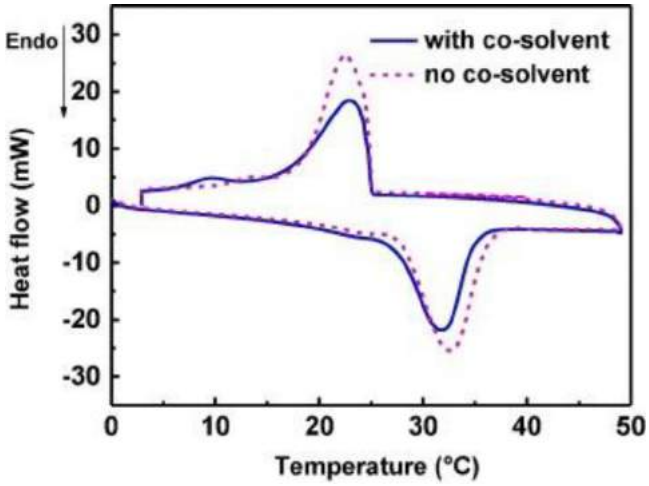

Fig. 59. The heat flow at different temperatures of particles prepared with and without cyclohexane [149].

from interfacial polymerization into silicon rubber sheets (Fig. 61), which could improve the insulation property and help to maintain around phase transition temperature of rubber when the ambient temperature decreases. In this application, the mass ratio of microcapsules and rubber is crucial, and it is proved that the ratio of 1:5 is a great one to keep rubber sheet above 0°C when the ambient temperature is -10°C. In terms of the microcapsule synthesis, the most suitable conditions are studied, with 55°C and 300r/min rotational speed being the best.

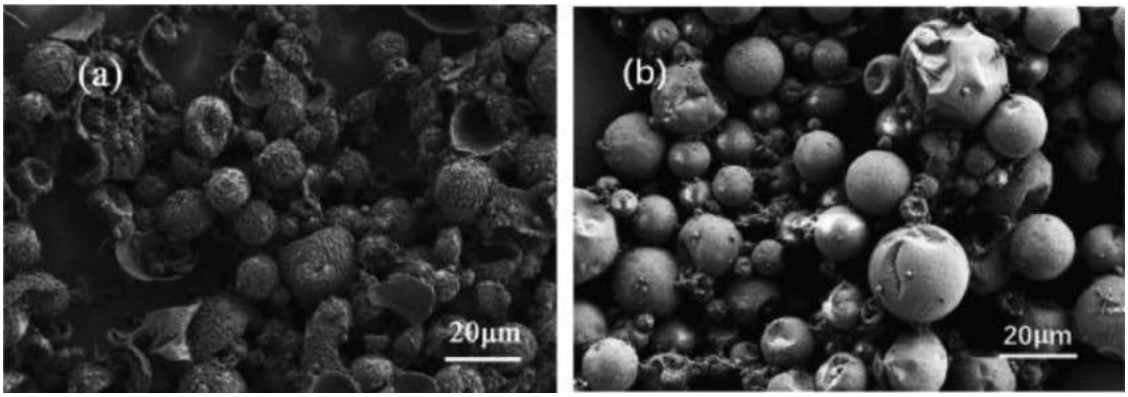

Fig. 60. The morphology of particles prepared (a) with and (b) without cyclohexane [149].

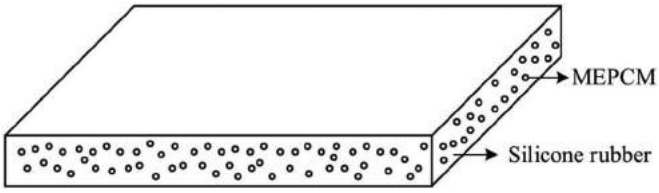

Fig. 61. Silicon rubber sheet with microcapsules mixed.

Table 8 summarizes some key works before by using interfacial polymerization for encapsulation.

3.3.3. Suspension polymerization

Suspension polymerization as a convenient, eco-friendly, cheap, and efficient method has largely drawn researchers' attention over the years [152]. The main idea is to have a water-immiscible polymerization reaction (see Fig. 62 below). Continuous phase (aqueous) mixed emulsifier and water, and discontinuous phase (oil) including core material and oil-soluble monomer are prepared first. Then, the oil-in-water emulsion is formed by mixing two phases under a high stirring rate of homogenization. After we change the temperature or pH to initiate polymerization, dispersed monomers in oil droplets react to each other on the interface. Due to concentration gradient, monomers diffuse to the interface and continuously react. The encapsulation efficiency is affected by the complicated interaction between each component, like monomers, polymers, PCMs, initiators etc. The morphology depends on the mobility, compatibility, hydrophobicity and core-shell ratio [153]. According to the early research in 1976 and 1992 [154,155], Eq. (4) of the average diameter of microcapsules is obtained:

$$\bar{d} = \frac{k(D_v R v_d \varepsilon)}{D_s N^2 \upsilon_m C_s} \tag{4}$$

Table 8
The properties of encapsulated capsules using interfacial polymerisation.

Refs.	Core material	Shell material	Average diameter (μm)	Thermal cycling (cycles)	Encapsulation efficiency (%)	Heat of fusion (J/g)	Other properties of microcapsules
[142]	Octadecane	PU	1	-	87.2	110	
[143]	N-eicosane	PU	-	-	75	63.55	• Can withstand high temperature
[144]	Polyhydric alcohol	Polyurea–urethane	11.2–21.6	-	-	196.3	
[145]	Methyl laurate	Poly(urea–urethane) (PUU) containing hCNCs	20–400	10	73	148.43	• Core content: 66 wt.% • Melting and freezing point: 6.58 and -1.64°C • Shell thickness: 10–150 μm
[146]	Butyl stearate	Polyurethane (PU)	1–5	-	95	85	• Smooth and compact surface
[147]	LA	Silica	-	300	78.6	186.6	• Good thermal stability
[148]	Eutectic of n-octadecane and thyme oil	PU	2.2	-	82	154.2	• Shell thickness: 149 nm • Melting and freezing point: 28 and 18.1°C • Antibacterial function
[149]	Dodecanol dodecanoate	PU	10–40	100	-	140.3	• Core content: 74.45 wt.% • Enhanced thermal conductivity: 0.21 W/mK • High temperature resistance until 234°C
[150]	N-tetradecane	Silica	Hundreds of nanometers	-	-	130.8	• Freezing temperature: 3.6°C • Melting temperature: 2.3°C • Good thermal insulation property
[151]	Methyl laurate	Polyurethane (PU)	1.13–144	-	75.18	136.2	• Core content: 85.28% • Core/shell ratio: 3:1

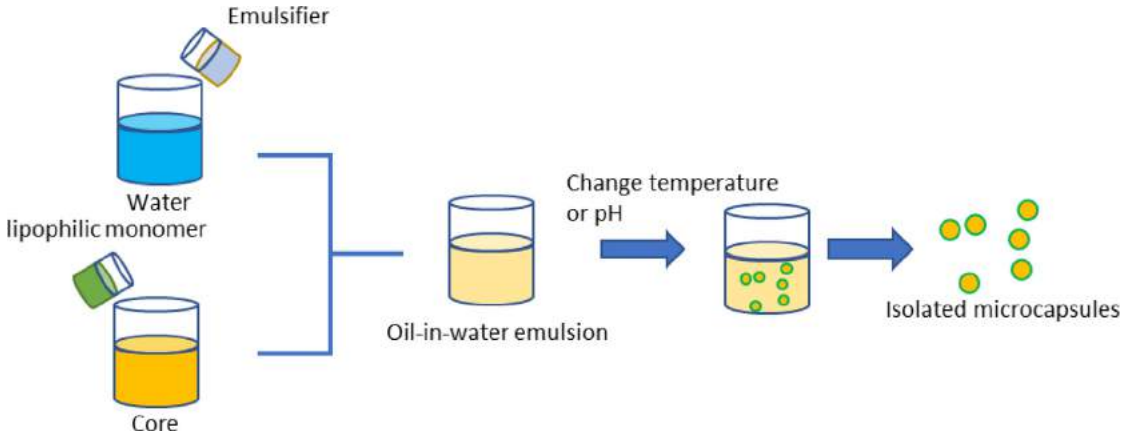

Fig. 62. The fabrication process of suspension polymerization.

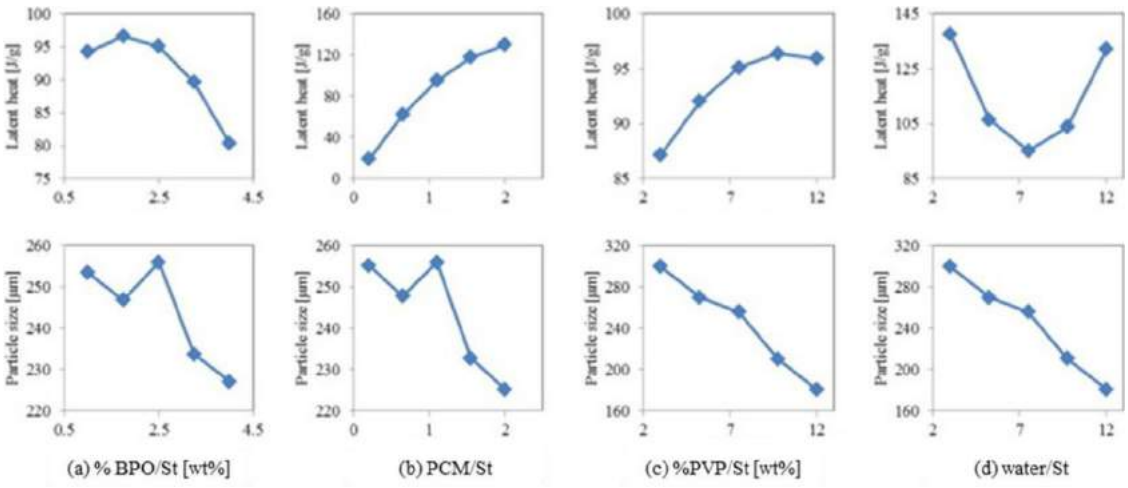

Fig. 63. Latent heat and particle size determined by initiator/monomer ratio (a), core material/monomer ratio (b), stabilizer/monomer ratio (c) and water/monomer ratio (d), where each abbreviation is benzoyl peroxide (BPO), styrene (St), paraffin wax (PCM), polyvinylpyrrolidone (PVP) [158].

Where $\bar{d}$ is average diameter, k are parameters like apparatus design, D_v is the diameter of the vessel, D_s is the diameter of the stirrer, ε is the surface tension between aqueous and oil phase, υ_m and ν_d are the viscosity of suspension medium and droplet, N is the stirring rate, R is the volume fraction of monomer phase, C_s is the concentration of stabilizer.

Sánchez et al. [156] attracted a lot of attention by using the suspension polymerization method to make encapsulation of non-polar PCMs possible with the PS shell. The non-polar PCMs they used, including tetradecane, paraffin wax PRS®, Rubitherm® RT27 etc., can be encapsulated using this method with almost core content of 50%, but polar PCMs, like PEG, cannot be encapsulated by using this method due to their hydrophilic nature. After that, they further used suspension copolymerization to prepare microcapsules containing PRS® paraffin wax as the core and copolymer of St and methyl methacrylate (MMA) as the shell. Results show that the reaction rate and particle diameter decrease with the increase of the MMA/St ratio. There is a limit of the monomer/paraffin ratio of 3.0 where encapsulation fails. Further, the optimal MMA/St mass ratio and monomers/paraffin ratio have been found at 4.0 and 3.0, respectively [157].

Enough evidence shows that PS is a feasible and well-performing shell material; Jamekhorshid et al. [158] further investigated the following different parameters during the suspension polymerization process to prepare paraffin wax/PS microcapsules: initiator/monomer ratio, core material/monomer ratio, stabilizer/monomer ratio and water/monomer ratio. Fig. 63 below shows the relationship between latent heat/particle size and the different ratios mentioned above. A clear trend can be found where the core/monomer and stabilizer/monomer ratio (PCM/St and PVP/St in Fig. 63) are proportional to the latent heat. On the other hand, stabilizer/monomer and water/monomer ratio decrease particle size. The optimal process derived from analysis of DX7 software gives the maximum latent heat and encapsulation efficiency of 148.5 J/g and 78.5%, where ratio A, B, C, D is 2.18%, 1.94, 8.84% and 11.67. N-Octadecane was encapsulated by combining silica and poly(methyl methacrylate) to form the shell in the research by Chang et al. [159]. The resultant microcapsules had an average size of 10 μm achieved the highest latent heat of 178.9 J/g and core content of 73.3% at inorganic/organic ratio of 5%. However, when they intended to further increase the amount of latent heat and core content by adding coupling agents like Vinyl triethoxysilane (VTES), methyl triethoxysilane (MTES), decyltrimethoxysilane (DTMS) and γ-methacryloxypropyltrimethoxysilane (MAPTMS), it resulted in adverse effects.

When we encapsulate PCMs using suspension polymerization, the problem of supercooling must be considered otherwise they cannot be used well in applications. Al-Shannaq et al. [160] eliminated this problem by introducing nucleating agents like Rubitherm®RT58 and 1-octadecanol. The MMA and Rubitherm®RT21 act as shell and core materials. The crystallization point of microcapsules without agents is 10 °C lower than those with adding

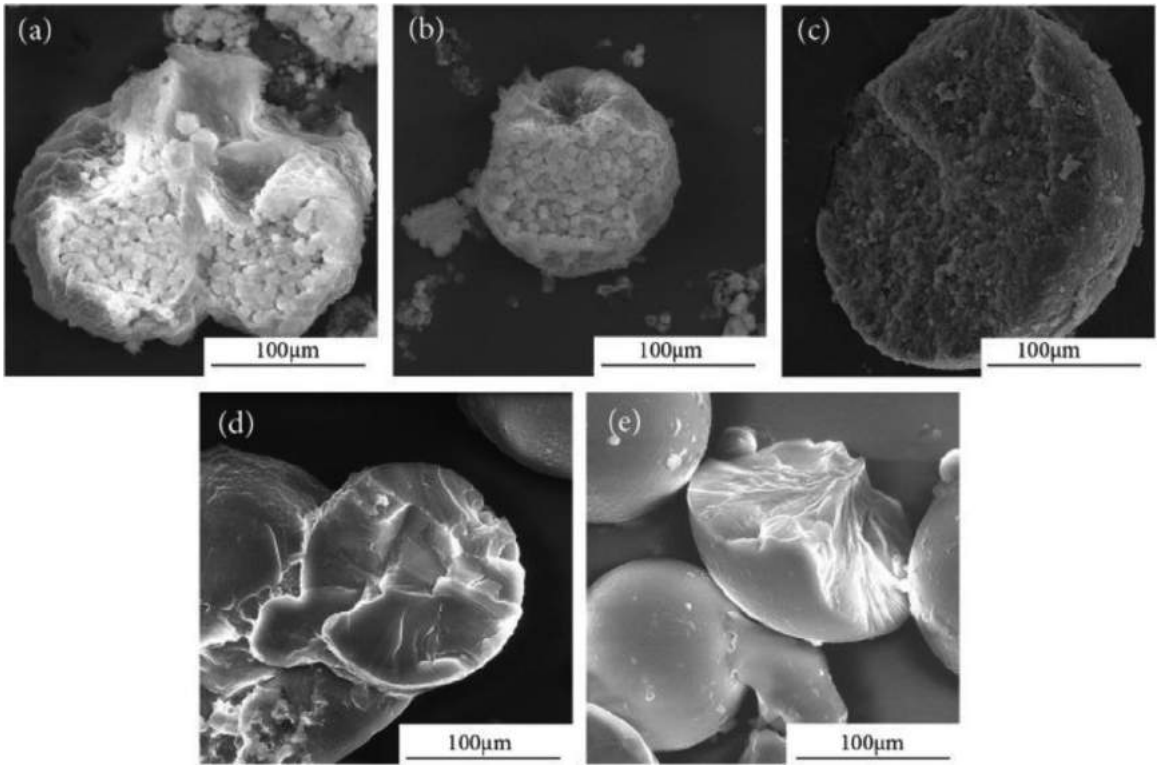

Fig. 64. The morphology of particles (a,b with no BA content) (c–e with increase in BA content) [161].

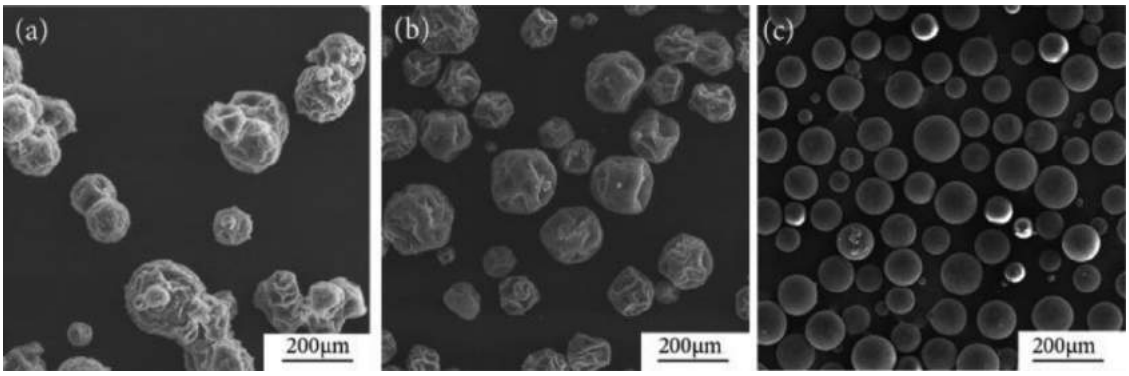

Fig. 65. The morphology of particles with PCM/MMA (a), PCM/MMA/crosslinking-agent(b), and MMA/crosslinking-agent(c) [161].

agents. Although supercooling can be solved by both, they give the unsmooth surface of particles, and 1-octadecanol has adverse effects on thermal behaviour. Another disadvantage of using 1-octadecanol is more mass loss at 50 °C. What makes these microcapsules appealing is extremely high reliability after two thousand thermal cyclings when they contain 5% RT58, meaning this nucleation agent assists sealing.

To study the thermal properties and morphology, Lashgari et al. [161] investigated the microcapsules prepared by suspension polymerization containing n-hexadecane (HD) as the core, and PMMA and poly(butyl acrylate-co-methyl methacrylate) (poly(BA-co-MMA)) as the shells. The key property, shell flexibility, has a strong relationship to encapsulation efficiency and thermal properties, thus they suggested both shell flexibility and thermal storage together, in the real application, must be considered. When the shell is just formed by PMMA, a multi-nucleus morphology can be seen. A matrix-type morphology results from the poly(BA-co-MMA) shell when BA is at high content. The morphology can be seen in Fig. 64 below, and as it shows that a transition from multi-nucleus (a) to matrix-type(e) morphology with the increase in BA content. Besides, the difference between a and b is the crosslinking agent where (b), with the crosslinking agent, maintains good shape and could largely prevent leakage during a thermal cycling test. In Fig. 65 below, as the BA content is below 25wt%, the particles obtained become wrinkled (Figs. 65 a, b and 66 a) due to shell shrinkage minimizing the surface tension between core and shell. Thus, microcapsules containing BA of 25 wt% and MMA of 75 wt% are nominated for the morphology reason. In terms of thermal properties, HD with just PMMA exhibit fierce degradation, while the incorporation of BA mitigates this issue.

Parvate et al. [162] enclosed the hexadecane with the copolymer, poly(4-methylstyrene-co-divinylbenzene) (Poly(MeS-co-DVB)), and used titanium dioxide nanopowder to enhance the properties. The suitable core-shell ratio and nanoparticles content are studied by implementing non-Pickering emulsion templated suspension polymerization; the process with mechanisms are shown in Fig. 67 below. Results show that the most suitable nanoparticle

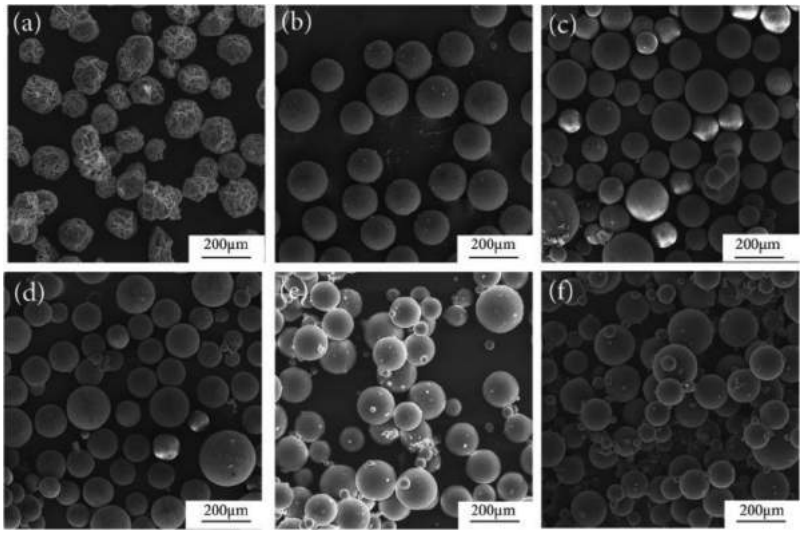

Fig. 66. The morphology of particles with the same PCM and crosslinking agents (a–e), but different BA content of 5 (a), 25 (b), 45 (c), 65 (d), 85 (e) wt%. f have the same conditions with e, but with no PCM [161].

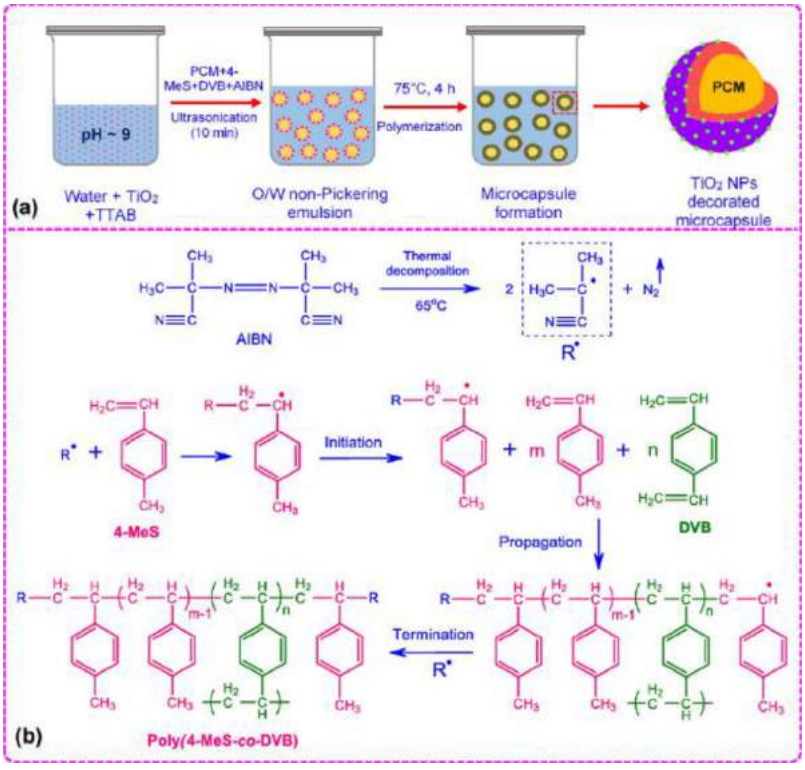

Fig. 67. The process of microcapsule preparation, and mechanism of copolymer synthesis [162].

concentration is 2.6 wt% resulting in the highest encapsulation efficiency of 76.6%, excellent reliability with good leakage-preventing properties, and exceptional photocatalytic activity due to synergistic photothermal effects that make microcapsules appealing in the biomedical and construction fields. For more morphology details (Fig. 68 below), the distribution of microcapsules is improved with the increase in nanoparticle content. The shell thickness determines how well the microcapsules prevent leakage, and the highest thickness of 3.48 μm is obtained with a core-shell ratio is 0.5:1 (see Fig. 69).

Zhang et al. [163] fabricated the nanocapsules by using n-octadecane as the core and poly(2,3,4,5,6-pentafluorostyrene) (PPFS) as the shell. The process and particle structure are depicted in Fig. 70 below. They found that the highest latent heat (171.8 J/g) and encapsulation efficiency can be obtained with a shell-core ratio of 1:2. When this ratio increases, the encapsulation efficiency and latent heat will decrease. The common problem of encapsulation is the change in thermal behaviour. Promisingly, the thermal capability of these nanocapsules is more than 99%, meaning that the process of encapsulation has little negative effect on endothermic and exothermic behaviour. Thermal conductivity is always a problem after encapsulation, authors found that the increase in encapsulation efficiency results in improvement of thermal conductivity, where the value of it is close to unencapsulated n-octadecane as the shell-core ratio is between 1:2 (NEPCM4) and 1:3 (NEPCM5) (see Fig. 71).

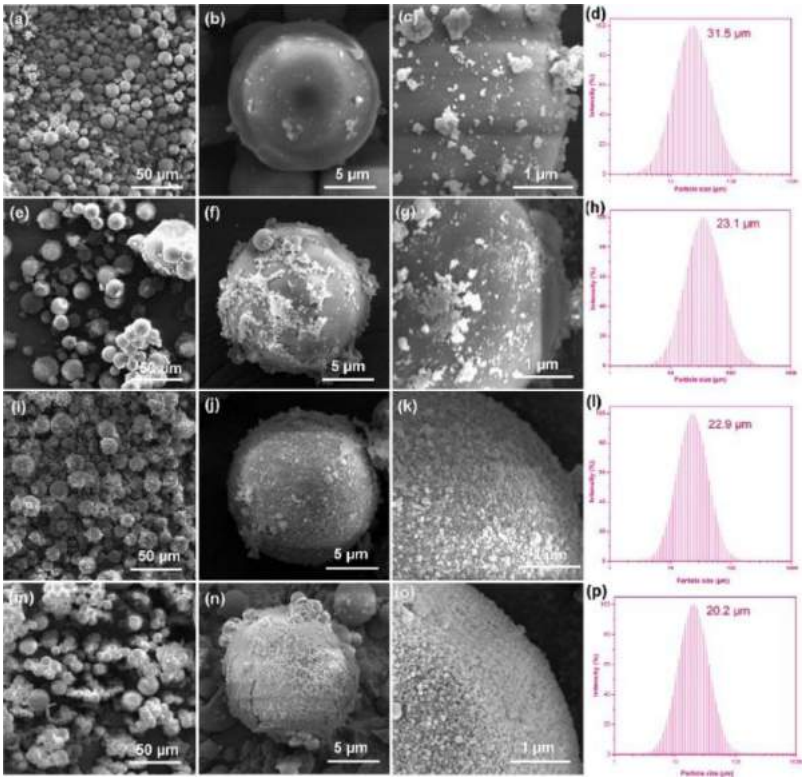

Fig. 68. The morphology and particles size with nanoparticle content of 0.8 wt % (a-d), 1.7 wt % (e-h), 2.6 wt % (i-l) and 3.5 wt% (m-p) [162].

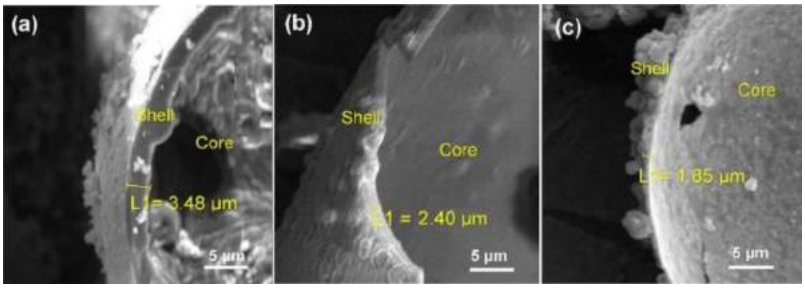

Fig. 69. The shell thickness when core-shell ratio is 0.5:1 (a), 1:1 (b), 2:1 (c) [162].

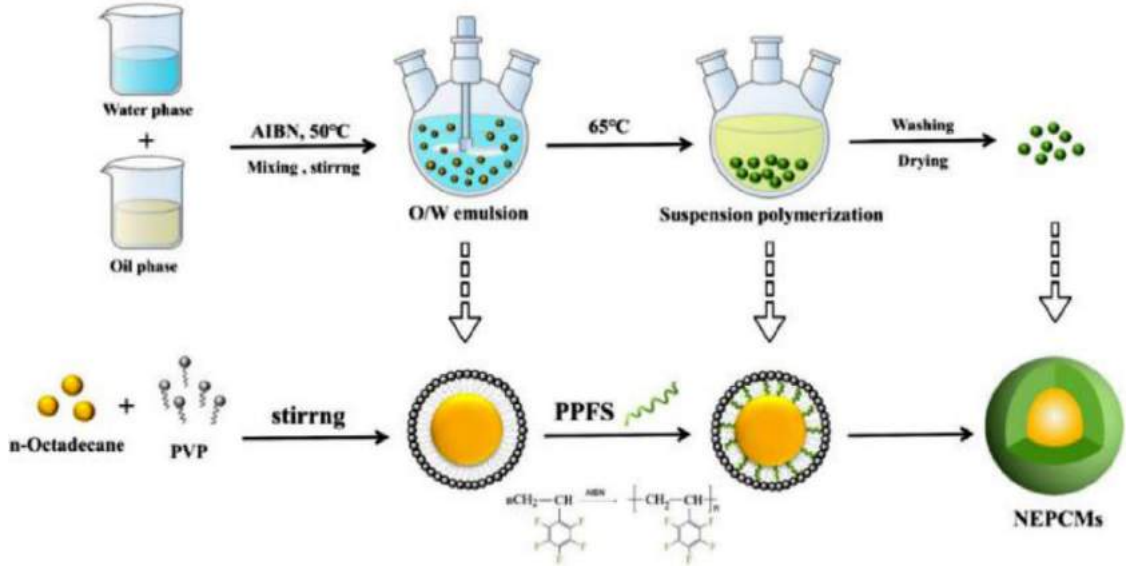

Fig. 70. The preparation process of nanocapsules [163].

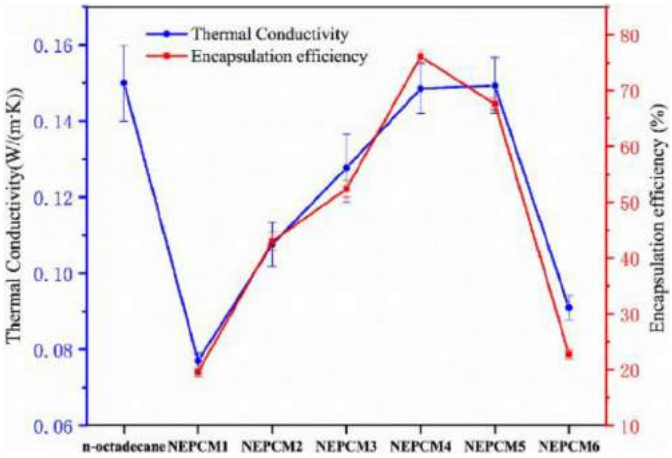

Fig. 71. The relationship between thermal conductivity and encapsulation efficiency as shell-core ratio increase [163].

Maithya et al. [164] implemented Pickering suspension polymerization to synthesize microcapsules containing n-eicosane as the core, and polyurea (PUA), modified with GO as the shell. The function of GO is to stabilize emulsion droplets. The droplet size decreases with the increase in GO concentration (Fig. 72 below). The SEM images tell us that the microcapsules have approximately spherical shapes. The higher the GO concentration, the smaller the microcapsules, and the better the GO coverage (see Fig. 73). Although they found 1 g/L of GO is enough to stabilize the emulsion, the higher concentration of 4 g/L and 8 g/L is optimal to give it leakage-proof property, because the higher concentration of GO results in a well-covered polymer shell. Furthermore, given that microstructure, reliability, the capability of leakage proof, 8 g/L GO is the most suitable in this case. This can be derived from the leakage test where incorporation of GO largely decrease the rate of leakage, and the lowest leakage rate in a long term is achieved while GO concentration is 8 g/L (black line in Fig. 74 b below). The authors placed microcapsules with different GO concentrations on filter papers and then heated them to 60°C. The largest area stained means the most leakage occurred (microcapsules with no GO incorporated, Fig. 74 a below).

Oktay et al. [165] compared two methods to prepare bio-based microcapsules, suspension polymerization and UV-curing (see Fig. 75 below). The poly(stearyl methacrylate-co-hydroxyethyl methacrylate) (Poly(SMA-co-HEMA)) shell material comes from the copolymerization of hydroxylethyl methacrylate (HEMA) and stearyl methacrylate (SMA), and the core material is natural coconut oil (CO). These two techniques can be used to effectively sta-

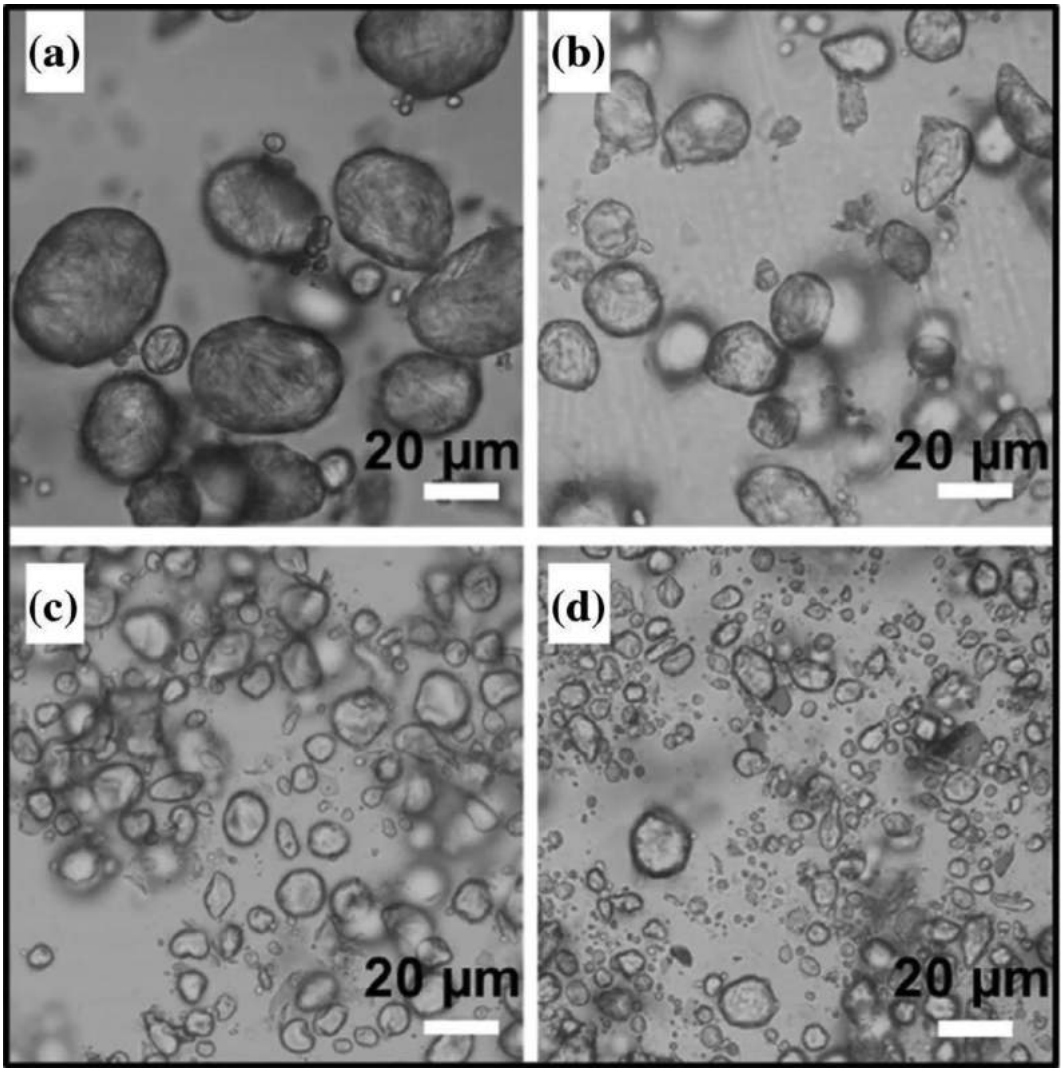

Fig. 72. Optical microscope of emulsion droplet at GO concentration of 1(a), 2(b), 4(c) and 8 g/L (d) [164].

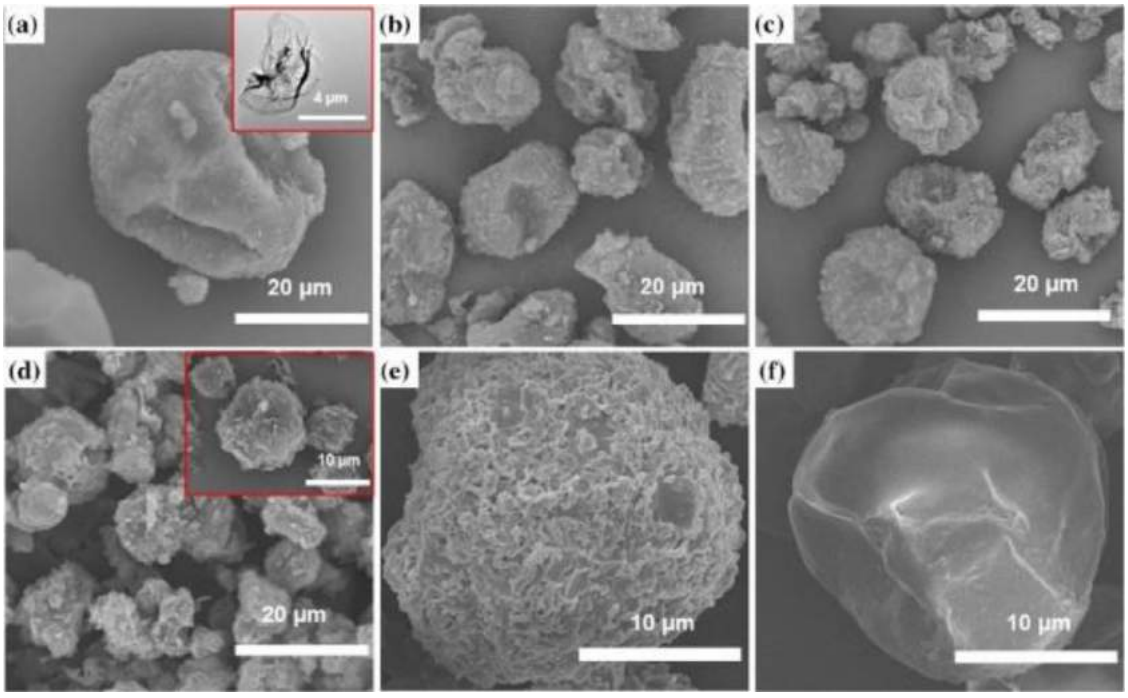

Fig. 73. The morphology of GO-modified microcapsules (a-e with increasing GO concentration) and microcapsule with no GO (f) [164].

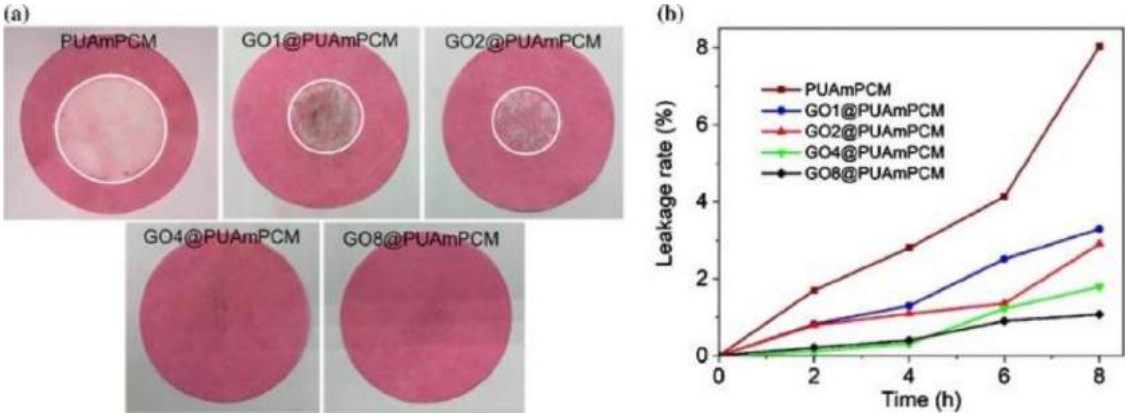

Fig. 74. The picture of leakage area (a) and leakage rate at a different time (b), PUAmPCM (0 g/L GO), GO1@PUAmPCM (1 g/L GO), GO2@PUAmPCM (2 g/L GO), GO4@PUAmPCM (4 g/L GO), GO8@PUAmPCM (8 g/L GO) [164].

bilize the shape of PCMs and prevent leakage problems. However, the latent heat obtained by using the encapsulation technique is two times larger than that by using UV-curing.

The research by Szczotok et al. [32] is a milestone for the prediction of microparticle morphology and encapsulation efficiency. According to previous research [166,167], they calculated the spreading coefficient theory and polar surface energy component parameters to achieve this by measuring the interfacial tension. St, Hexa(methacryloylethylenedioxy) cyclotriphosphazene (PNC-HEMA) and divinylbenzene (DVB) are used as monomers to form the shell because different shell materials give different polarity. The PCM used in this case is Rubitherm®RT27. If the interfacial tension between oil and water is larger than that between polymer and water, three conditions could predict the possible morphology (see Fig. 76 below). Conditions at the second, third and fourth quadrant correspond to core-shell morphology, acorn-shaped morphology and drop separation, respectively. The microcapsules have a matrix structure due to P(S-DVB) formed as the shell. As they further copolymerize PNC-HEMA, the morphology turns into a core-shell structure. By increasing the PVP concentration as a suspending agent, the decrease in the polar surface energy component of the water phase results in a slight increase in encapsulation efficiency (see Fig. 77 below). Another fact is that the incorporation of PNC-HEMA significantly improves the encapsulation efficiency due to less polymer being needed (see Fig. 78 below). Overall, they concisely concluded that the factors that make core-shell structure formation favourable would increase the encapsulation efficiency.

Zhao et al. [168] came up with a novel way to protect PCMs from UV damage by the incorporation of modified TiO_2 as a UV absorber. According to the SEM images (Fig. 79), there are some pits on the external surface due to the shrinkage of the core materials during the crystallization process. However, with the increase in the content of titanium dioxide, the shape tends to become more spherical due to enhanced mechanical properties by the incorporation of nanoparticles. These kinds of microcapsules can be promisingly used in intelligent textile and architectural coating.

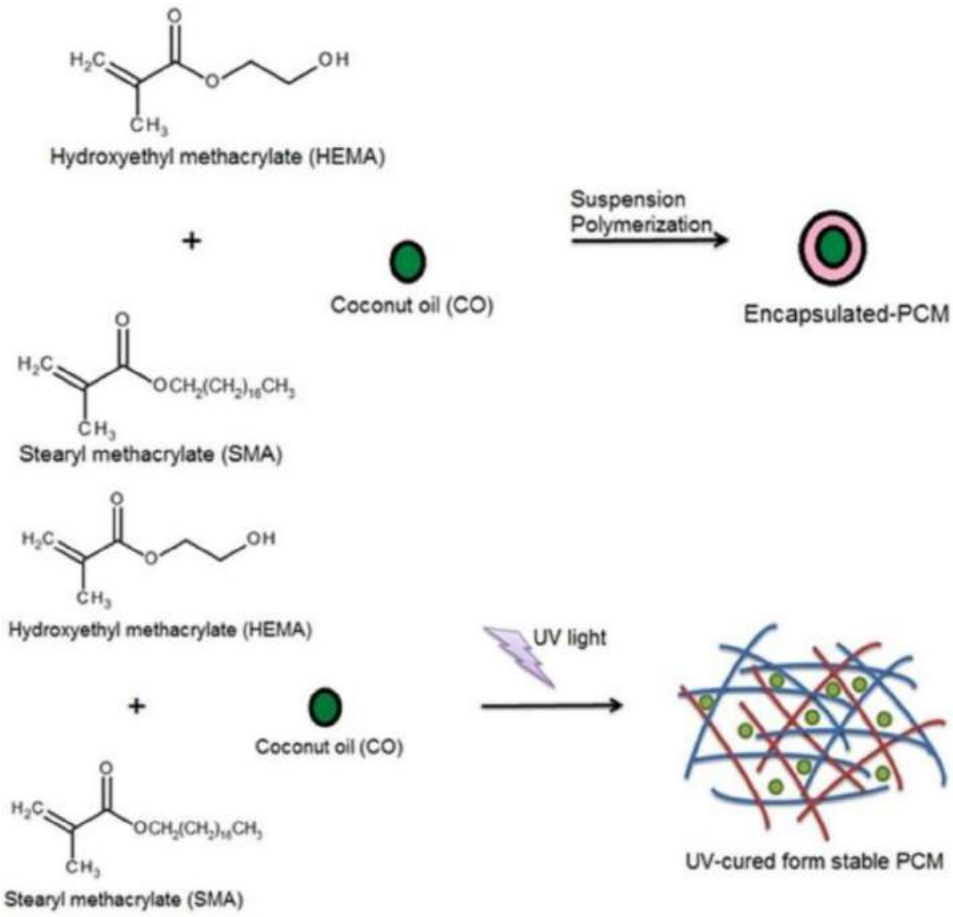

Fig. 75. Shape-stabilized PCM by using encapsulation and UV-curing techniques [165].

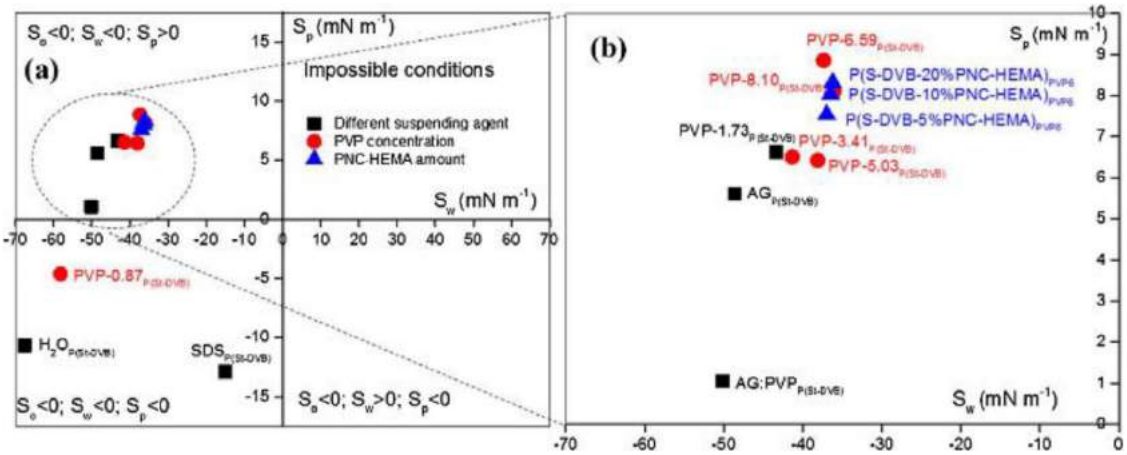

Fig. 76. Oil, water, polymer spreading coefficients of different suspending agents, PVP concentration and PNC-HEMA (a) full scale, (b) the second quadrant [32].

Parvate et al. [169] interlocked copper nanoparticles into the polydivinylbenzene (PDVB) shell for thermal buffering application in food industry. By using these microcapsules, 240 g of chocolate expend 6.5 h on rising temperature from 5 to 35°C. Differing to other research, they applied atomic force microscopy (AFM) to determine the roughness of microcapsules, showing higher than undoped microcapsules (Fig. 80). The dosage of copper nanoparticles is experimented to be 1.0% to achieve great performance on latent heat, encapsulation efficiency, reliability and thermal conductivity.

Some key works involved suspension polymerization for encapsulation are summarised in Table 9.

3.3.4. Emulsion polymerization

Emulsion polymerization involves polymerization in the aqueous phase. For suspension polymerization mentioned above, the initiator is oil soluble. However, for emulsion polymerization, the initiator is water-soluble. Fig. 81 is drawn according to the description of previous research [96,170]. The prepared oil phase containing PCMs and monomer is added to the aqueous phase con-

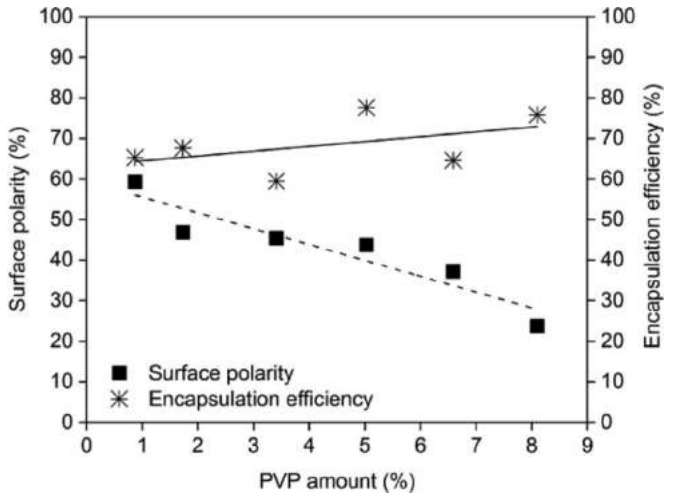

Fig. 77. The surface polarity and encapsulation efficiency affected by suspending agent (PVP) concentration [32].

taining water, suitable surfactant, and water-soluble initiator. As the concentration of surfactant excesses a critical value, micelles are formed generally in spherical shapes waiting for monomers to be input. Monomers from droplets are distributed to micelles. Then, the polymerization would happen due to the presence of surfactant in the aqueous phase to form microcapsule-containing micelles. After filtering, washing, and drying, the isolated microcapsules are obtained. The amount of monomer contained in micelles, the emulsifier concentration, polymerization temperature and initiator concentration, etc., all determine the particle size [171].

The earlier research by Sarı et al. [172] has drawn peoples' attention by using emulsion polymerization. N-octacosane was encapsulated by PMMA. The reliability of microcapsules is exceptional according to the 5000 times thermal cycling tests (see Fig. 82). Besides, the capability of resisting high temperature is excellent due to two-step degradation. Also, they explored the suitable emulsion stirring rate of 2000 rpm to obtain a narrow particle size distribution whilst synthesing (see Fig. 83).

A year after, Sarı et al. [173] used the same shell material (PMMA) but encapsulated another promising PCM (n-

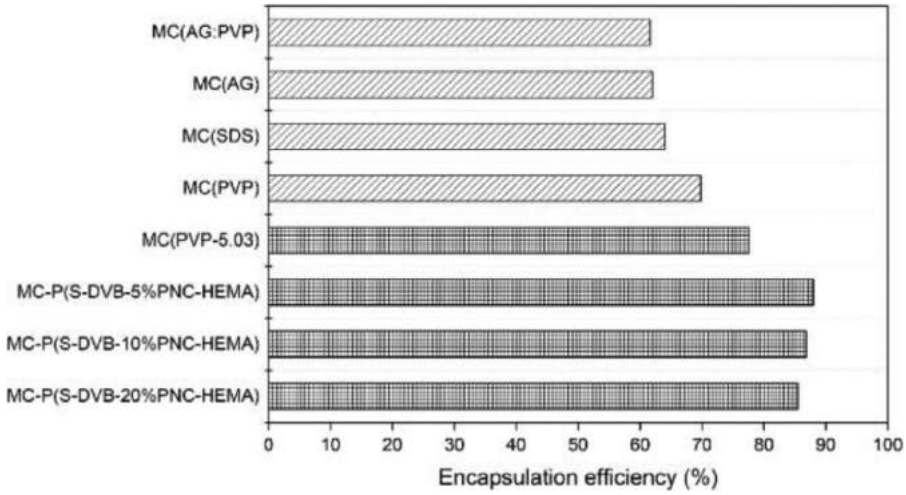

Fig. 78. The encapsulation efficiency of microcapsules containing different shells (note that the last three bars correspond to the incorporation of 5, 10, 20% PNC-HEMA respectively) [32].

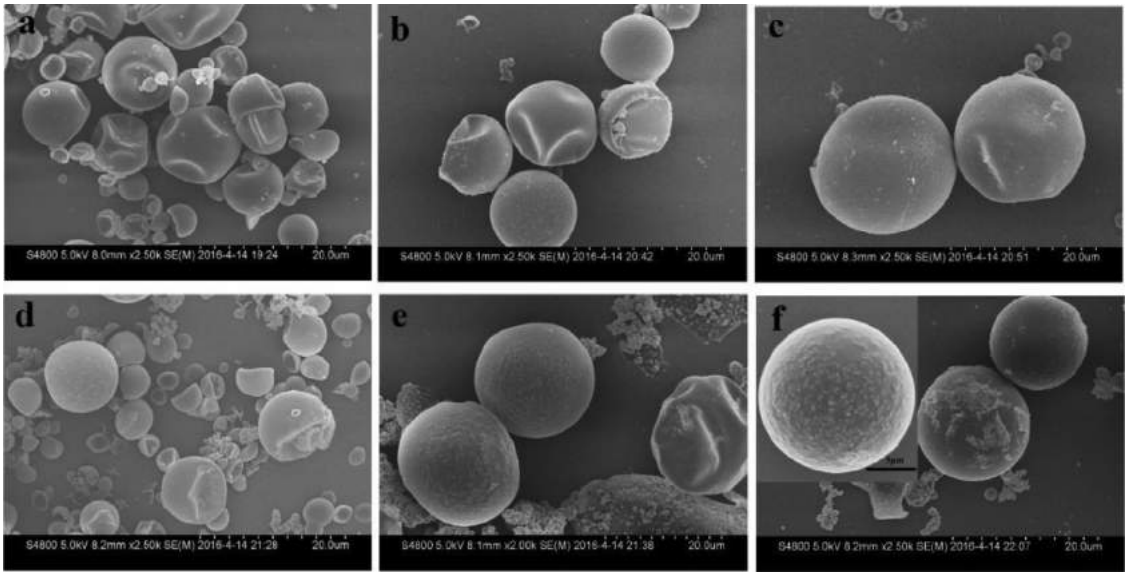

Fig. 79. SEM images of microcapsule containing different amount of titanium dioxide; (a) 0% (b) 2% (c) 4% (d) 6% (e) 8% (f) 10% [168].

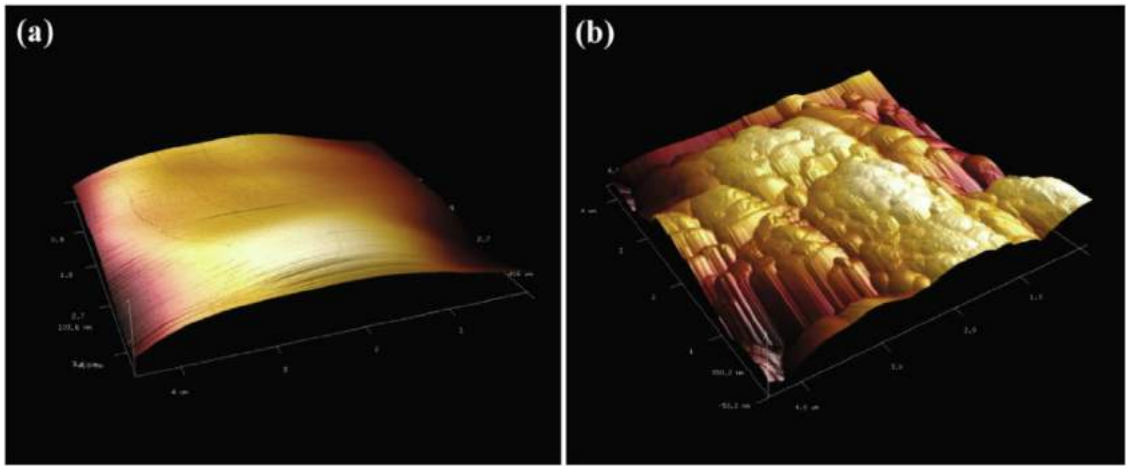

Fig. 80. AFM images of microcapsules with a) 0% and b) 1.0% copper nanoparticles [169].

Table 9
The properties of encapsulated capsules from previous research using suspension polymerisation.

Refs.	Core material	Shell material	Average diameter (μm)	Thermal cycling (cycles)	Encapsulation efficiency (%)	Heat of fusion (J/g)	Other properties of microcapsules
[157]	Paraffin	P(St-co-MMA)	182	-	-	84.04	• Core content: 41.46 wt.%
[158]	Paraffin	PS	330	-	-	148.5	
[159]	N-octadecane	PMMA-silica hybrid	10	-	-	178.9	• Core content: 74 wt.%
[160]	Rubitherm®RT21	PMMA	10	2000	-	110.42	• Melting/freezing Temp.: 22.8/17.51°C
[161]	Hexadecane	PMMA and P(BA-co-MMA)	100–200	500	96.3	63.1	• Good shell flexibility • Smooth surface • The core content is 28.9%
[162]	Hexadecane	Poly(MeS-co-DVB) (incorporated with TiO_2 nanopowder)	5–50	100	76.6	63.1	• The optimal core-shell ratio of 0.5:1 • Optimal nanoparticle content of 2.6 wt %
[163]	N-octadecane	PPFS	490–620	200	76.1	171.8	• Thermal conductivity of 0.149 W/mK
[164]	N-eicosane	GO-modified PUA	4	100	70.5	181	• Optimal GO concentration is 8 g/L • Low leakage rate around 1% after 8 h • Approximately spherical shape • The photothermal conversion efficiency of 60%
[165]	Coconut oil	Poly(HEMA-co-SMA)	100–150	-	84	119	• No leakage • Encapsulated PCM increases the degradation temperature • Two melting points: 5 and 18°C • Two freezing points: -7 and -8°C
[168]	N-octadecane	Titanium dioxide enhanced PMMA	10–20	500	-	139.26	• UV-shielding function
[169]	Hexadecane	Copper nanoparticles enhanced polydi-vinylbenzene	~1	100	60.5	132	• Improved thermal conductivity from 0.0813 to 0.3411 W/m°C after 1% copper doping • Rough shell surface

heptadecane) by using emulsion polymerization. By following the optimal emulsion stirring rate of 2000 rpm derived from the last paper [172], the size of the microcapsule is close to nanoscale dimensions (0.26 μm). As for the chemical and thermal stability, 5000 times cycling is conducted with little degradation and latent heat change. What makes it superior is the three-step degradation compared to n-octacosane/PMMA with just two-step degradation, meaning better resistance to high temperature.

Unlike the last two research papers discussed, which achieved narrow particle size distribution by controlling the stirring rate, Alay et al. [174] achieve unimodal particle size distribution by introducing cross-linker, like allyl methacrylate (AMA), ethylene glycol dimethacrylate (EGDMA) and glycidyl methacrylate (GMA). Herein, they encapsulated n-hexadecane with poly(butyl acrylate) (PBA). As the SEM images (Fig. 84) show, the morphology is different from normal spherical shape, instead, particles tend to agglomerate to form clusters. The use of EGDMA and GMA decrease

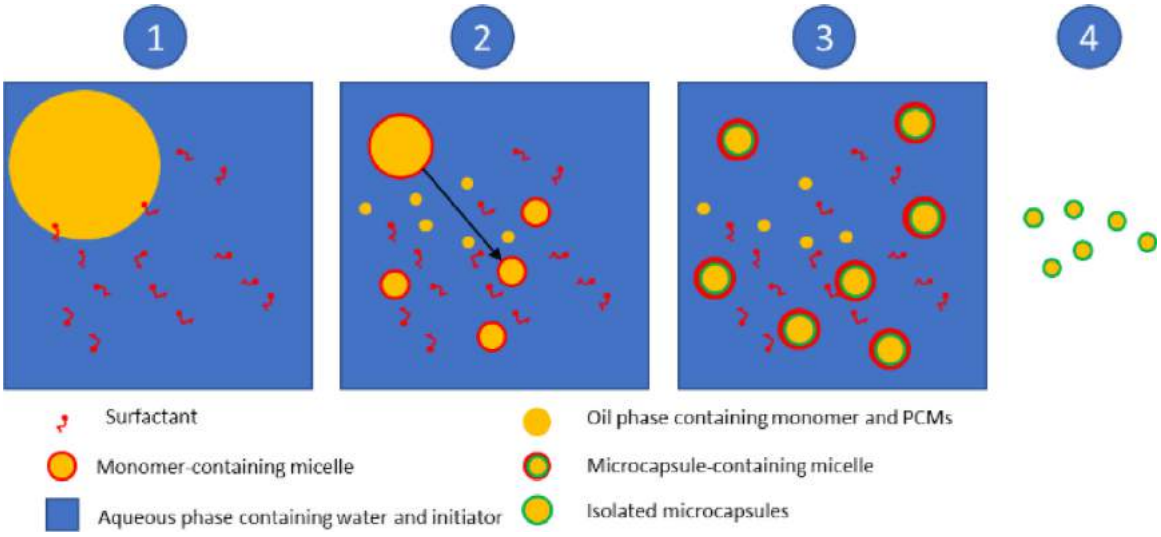

Fig. 81. The process of emulsion polymerization.

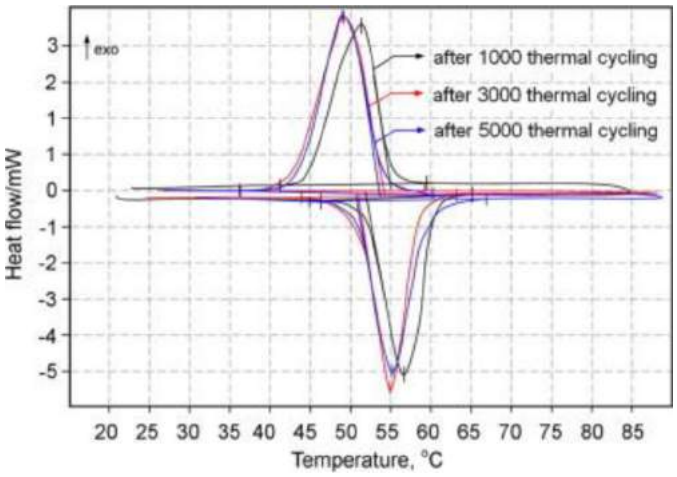

Fig. 82. The DSC thermogram of microcapsules after 1000, 3000, 5000 cycling [172].

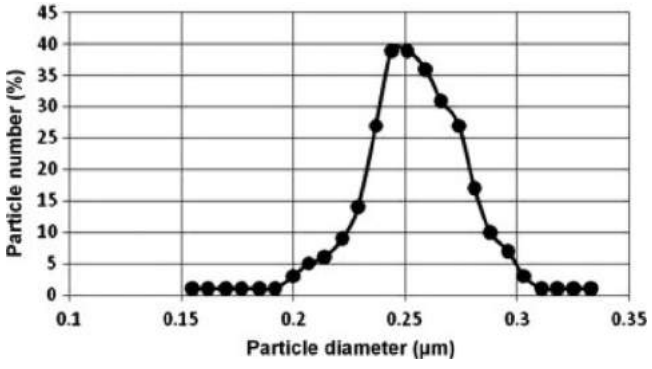

Fig. 83. The particle size distribution [172].

the particle size to the nanoscale. Besides, they also found EGDMA gives the highest heat capacity, whilst GMA gives the lowest. According to the DSC data, encapsulation has little impact on the change in phase change temperature.

As time goes by, Sarı et al. [175] turned their attention to studying encapsulation of paraffin eutectic mixtures (C_{17}-C_{24}, C_{19}-C_{18}, C_{19}-C_{24}, C_{20}-C_{24}) with PMMA as the shell. For the morphology study, all types of microcapsules have a wide range of particle size (see Fig. 85), and the surface is rough with some agglomeration, forming clusters (see Fig. 86). The particle size proportion within the nanoscale varies from 6.34 to 15.27%. They also measured the thermal conductivity, where the four different kinds of eutectic mixture mentioned above have the value of 0.21, 0.21, 0.21, 0.22, and 0.23 W/mK, respectively, and the test data shows the values do not significantly drop after encapsulation (0.19, 0.19, 0.19 and 0.20 W/m K, respectively).

Jiang et al. [176] innovated the encapsulation of a paraffin wax core by using poly(methyl methacrylate-co-methyl acrylate) (P(MMA-co-MA)) as the shell and alumina nanoparticles as the filler to study how this nanoparticle influences the morphology and thermal performance. The modification of the shell largely boosts the thermal conductivity, since Al_2O_3 nanoparticle is highly thermally conductive. They found the optimal proportion of nanoparticles added is 16 wt% so that the best performance is achieved. Besides, the morphology depends on the dosage of the nanoparticle. As we can see in Fig. 87, the best shape and dispersity are achieved when the dosage of the nanoparticle is 16 wt%, which is one of the reasons why this dosage is the most appropriate. As the dosage increase, the number of particles increases because nanoparticles act as nucleating agents (a-c). Uneven distribution and less favourable morphology can be seen (c-f), especially for 38% dosage, which is caused by the increase in surface energy. However, as we increase the dosage of nanoparticles to achieve better thermal conductivity, the authors pointed out a limitation where useful encapsulation is hard to conduct, and the latent heat tends to decrease.

Abdeali et al. [177] investigated the effect of a key aspect, droplet size distribution, on the thermal properties. They enclosed the paraffin wax core with polyurethane shell (coming from IPDI and PEG as monomers). The droplet size distribution is affected by the reaction temperature and the ultrasonic time during the emulsion polymerization. After adjusting these two parameters, the most optimal condition was when the paraffin and PEG addition temperature, ultrasonic intensity, ultrasonic time, and volume ratio of oil and aqueous phase are 80°C, 90%, 20 min, 1:10, respectively. Herein, it is worth mentioning that the authors introduced polycaprolactone diol (PCL) as the improvement agent to thermal and mechanical properties, and evidence was given in Fig. 88. Although the enthalpy of paraffin wax (PW) is much higher than

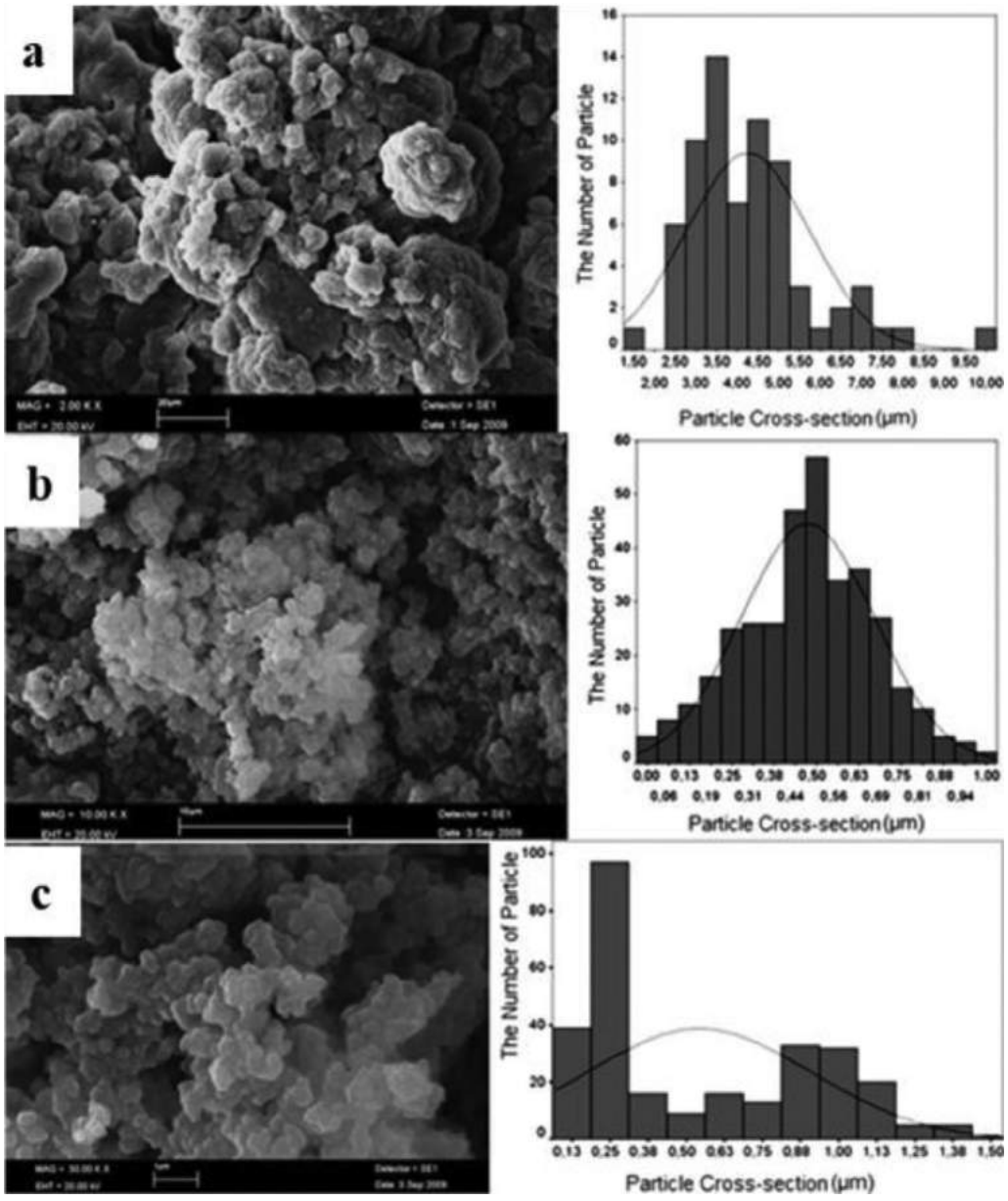

Fig. 84. The SEM images and particle size distribution of particles incorporated with (a) AMA, (b) EGDMA and (c) GMA as cross-linkers [174].

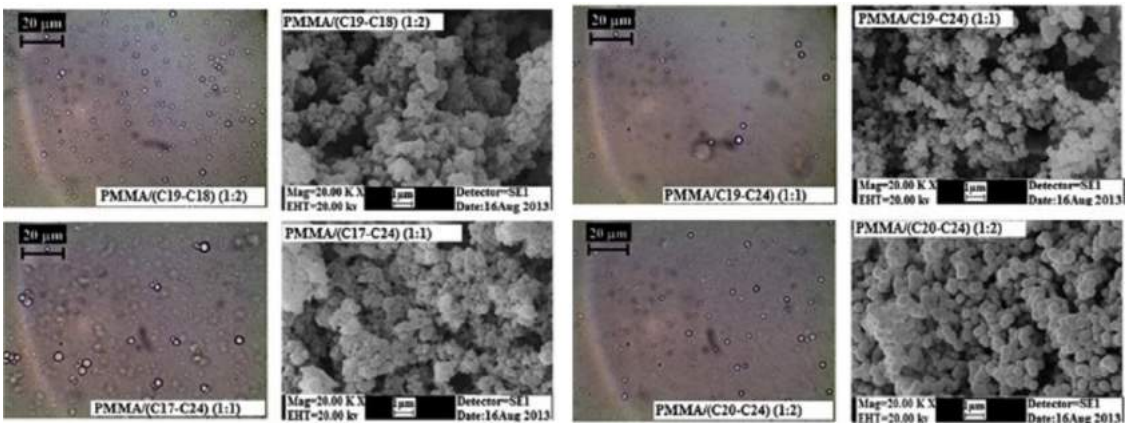

Fig. 85. The SEM images of microcapsule with different paraffin eutectic mixtures [175].

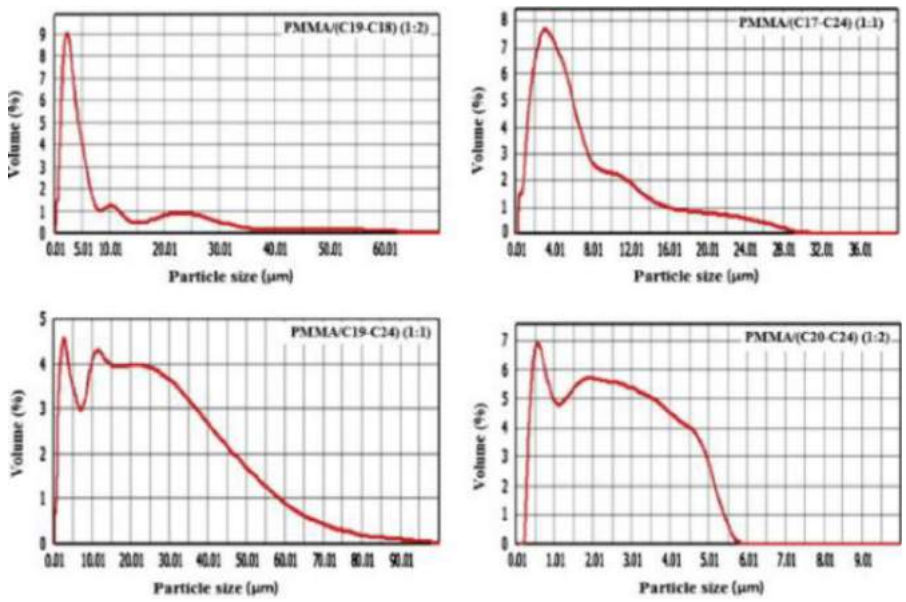

Fig. 86. The particle size distribution of microcapsule with different paraffin eutectic mixtures [175].

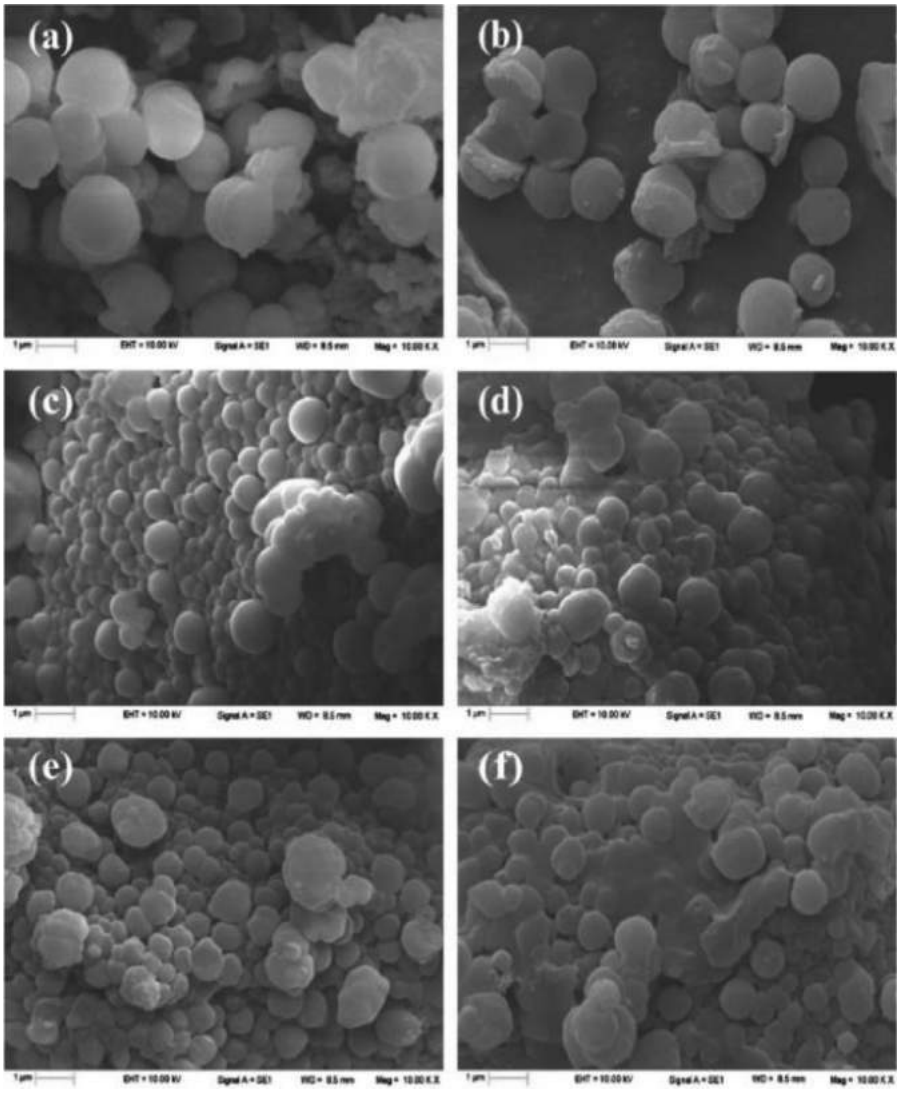

Fig. 87. The SEM images of microcapsules containing different dosage of nanoparticles, (a) 0%, (b) 5%, (c) 16%, (d) 27%, (e) 33%, and (f) 38% [176].

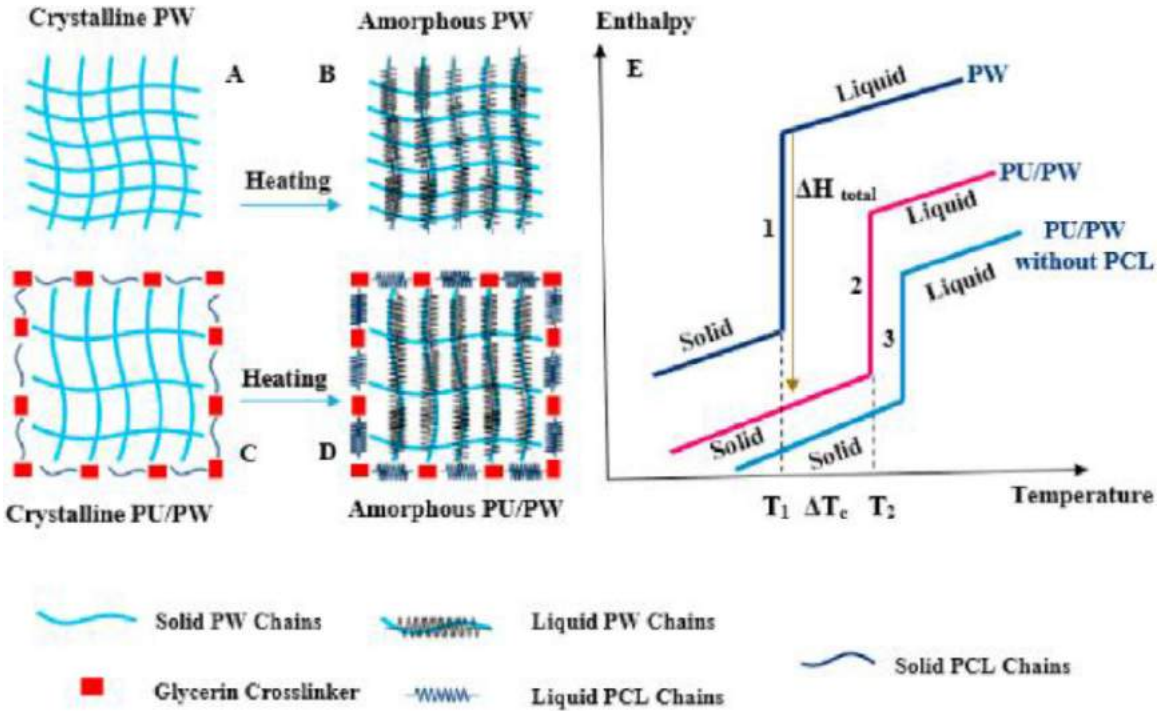

Fig. 88. The schematic of PW and nanoparticle structure before and after melting (left), and the enthalpy comparison [177].

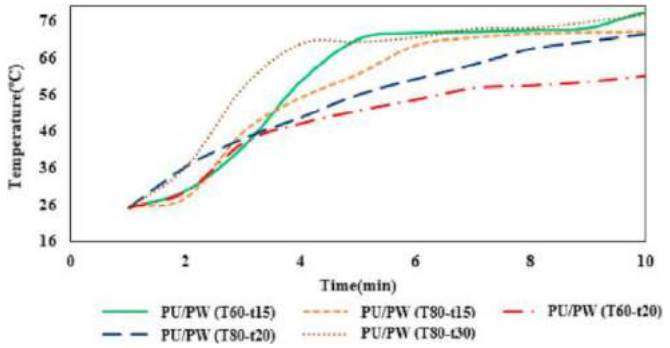

Fig. 89. The time-temperature response of all different candidates (note: T60 means reaction temperature at 60°C, and t15 means ultrasonic time is 15 min) [177].

nanocapsules, leakage is a serious problem. The presence of PLC increases the enthalpy of capsules due to sharing its melting enthalpy. According to the time-temperature response for all candidates (different reaction temperature and ultrasonic time) (see Fig. 89), the nanoparticles under optimal conditions (T80-t20) give a homogeneous melting profile compared to other candidates, due to their uniform particle size distribution, their same core content and shell thickness for each nanocapsule (see Fig. 90).

Singh et al. [178] adopted emulsion polymerization to encapsulate 1-dodecanol with the copolymer, poly(styrene-co-n-butyl acrylate-co-divinylbenzene), as the shell. Apart from testing the properties of microcapsules, they applied them to PVC film for thermal buffering ability investigation, and the process is depicted in Fig. 91. Findings show that the 1.5 core-shell ratio gives the highest encapsulation efficiency and core content. Although the latent heat is reduced by 30.45% after applying microcapsules on PVC film, the thermal stability is largely improved. This thermal stability can be ensured in Fig. 92 where the area within red dashed circles corresponding to leakage on the surface is found before applying to PVC.

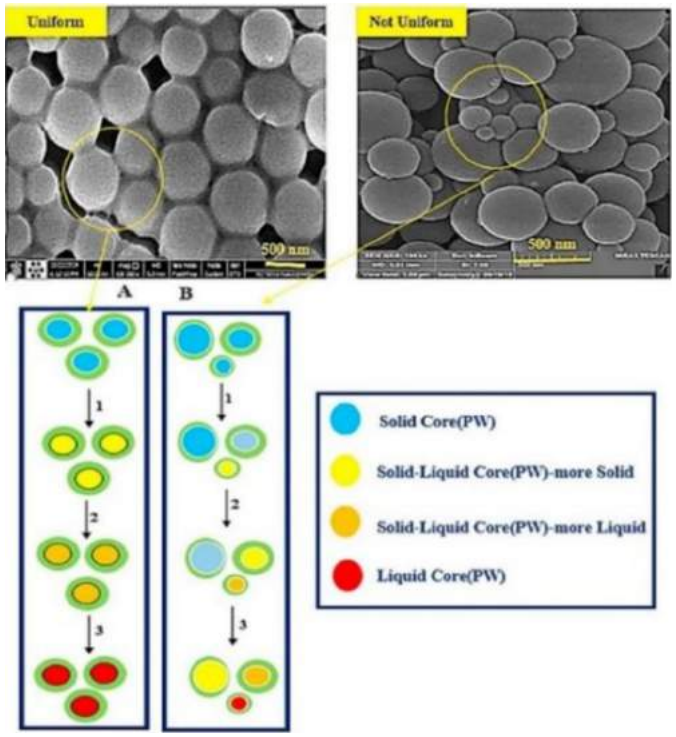

Fig. 90. The SEM comparison images of uniform and not uniform particle size distribution [177].

Zhao et al. [179] conducted a series of encapsulation processes with 28#paraffin (industrial paraffin) as a core material, a hybrid shell of crosslinked polystyrene (CLPS) and modified nano SiO2 (MS). The reason why they employed these inorganic nanoparticles is that they would improve the mechanical properties, thermal reliability, and reduce the surface tension of the water, thus, boosting the emulsification process. The nanoparticles used in this

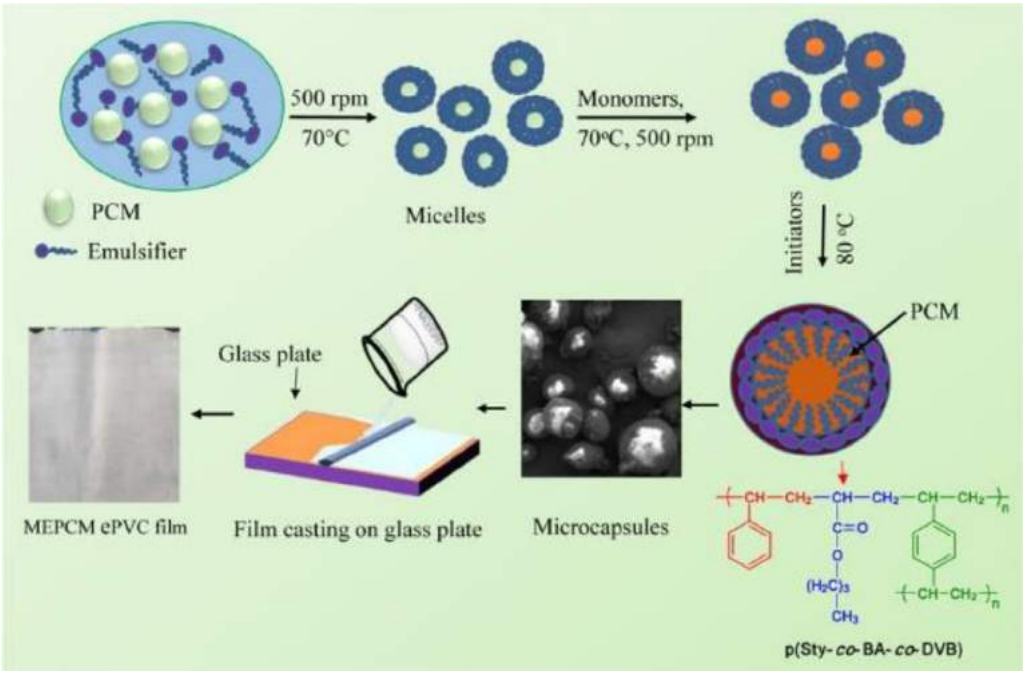

Fig. 91. The fabrication process of the microcapsule and microcapsule-embedded PVC film [178].

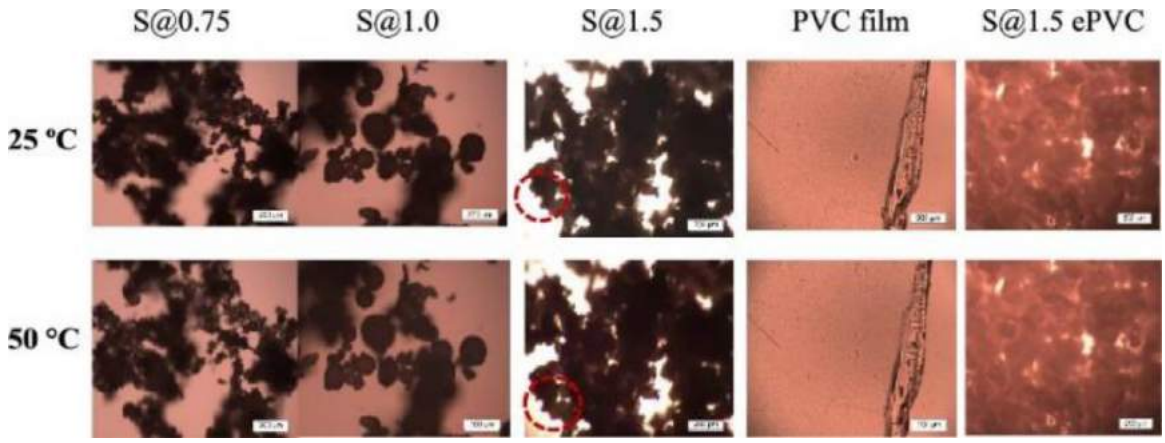

Fig. 92. Optical microscope images of different core-shell ratios at different temperatures for 10 min exposure [178].

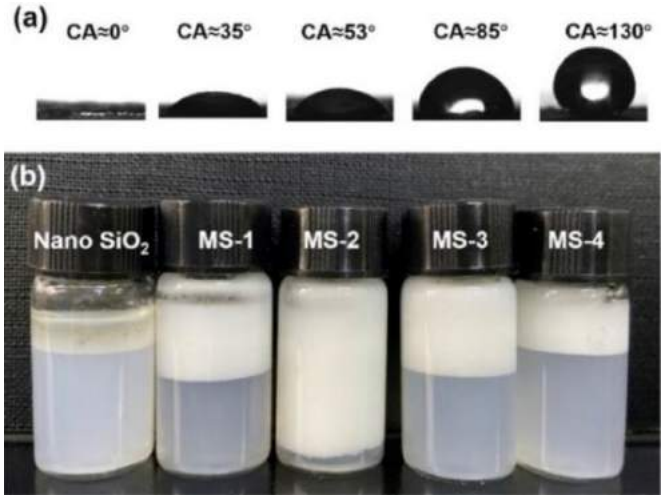

Fig. 93. The pre-emulsions containing different amounts of TTCS (b) with their contact angles (CA) [179].

case are modified by triethoxyoctylsilane (TTCS), changing their hydrophilicity, which has great effects on the morphology. As Fig. 93 below shows, the pre-emulsions formed have phase separation in varying extents, except the MS-2 pre-emulsion with its contact angle of 53 °. The SEM images (Fig. 94) confirms the finding above, where microcapsules (b, d, e) made from MS-2 pre-emulsion are well-dispersed with comparable size, despite some small pits caused by a volume change after the PCMs solidification. Plus, energy dispersive X-Ray spectroscopy (EDX) (f) ensures C, O, Si atoms are present. After several experiments, the 4.2% graft ratio of the nanoparticle is the most suitable for providing the highest paraffin content, latent heat, and encapsulation efficiency.

Wang et al. [180] fabricated the microcapsules containing a 1-tetradecanol (TDA) core and PMMA shell with the help of a natural biopolymer (lignin) as the emulsion stabilizer, and pentaerythritol tetraacrylate (PETRA) as the crosslinking agent. Fig. 95 is the fabrication process. There are two key factors, core monomer ratio and crosslinking agent dosage, that influence the morphology and latent heat. By looking at the formulation and SEM images (Figs. 96

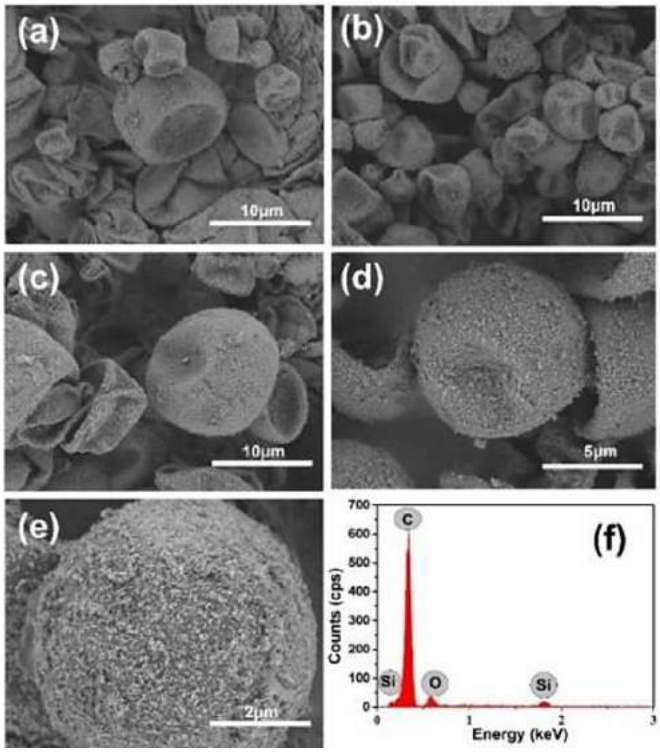

Fig. 94. The SEM images of microcapsules made from MS-1 (a), MS-2 with different magnifications of 10 μm (b), 5 μm (d), 2 μm (e), and MS-3 (c); and EDX map of microcapsules made from MS-2 [179].

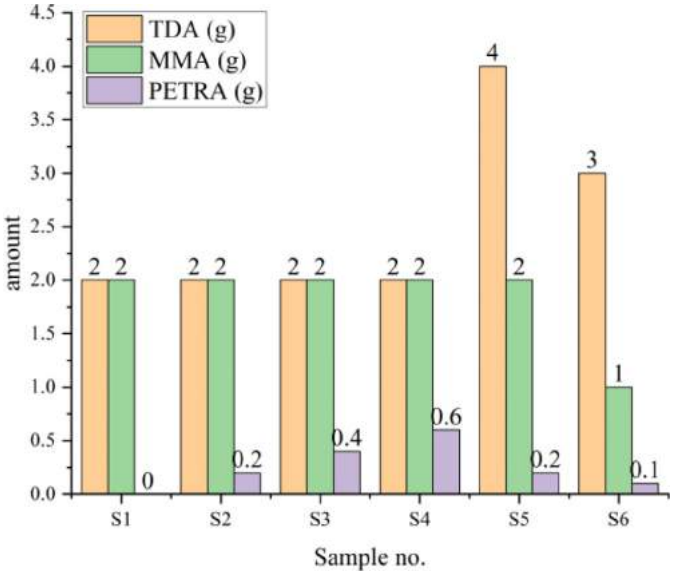

Fig. 96. The formulation of different microcapsule [180].

and 97), the effects of changing the dosage of crosslinking agent on morphology can be seen from S1 to S4 where the particle size becomes smaller with an increase in PETRA. As for the consequence of changing the core-monomer ratio, the images of S2 and S5 tell us that the surface tends to be smoother with an increase in ratio. Comprehensively, the PETRA-monomer ratio of 1:10 and core-monomer ratio of 2:1 is the optimal condition for the best thermal performance and morphology.

Şahan and Paksoy [181] firstly encapsulated behenic acid (BA) as the core with four kinds of shells, PMMA and its three copolymers with GMA, 2-hydroxyethyl acrylate (HEA) and 2- hydroxyethylmethyl acrylate (HEMA). They aimed to select the most suitable shell by various characterization techniques; the process and reaction are given in Fig. 98. SEM images are shown in Fig. 99, and all types of microcapsules have a regular spherical shape with a narrow size range below 500 nm. However, microcapsules made from HEMA have a higher thermal stability, latent heat, and core content.

Zhou et al. [182] synthesized microcapsules that could absorb UV radiation by incorporating TiO_2 within the polyacrylate shell. They found that, when the nanoparticle content, monomer conversion and thermal conductivity increases, and particle size and its distribution decreased when the content is below 0.2 wt%. Furthermore, they applied these nanocapsules to textiles. Not only can it enhance the enthalpy (see Fig. 100), but also exhibit gentle temperature change meaning smaller temperature fluctuation (see Fig. 101).

Fig. 95. The fabrication processes [180].

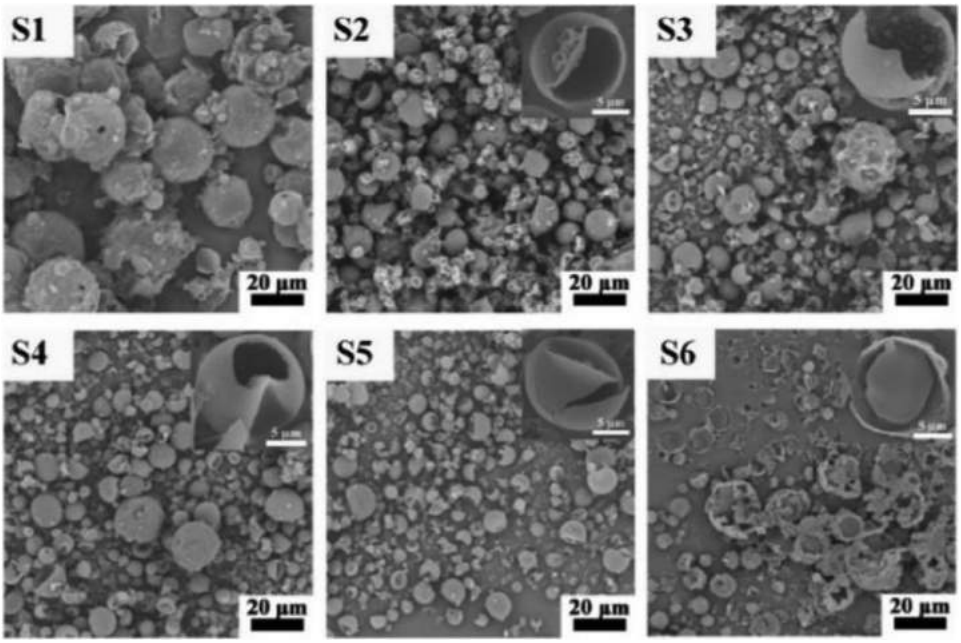

Fig. 97. The SEM images of microcapsule with different formulations [180].

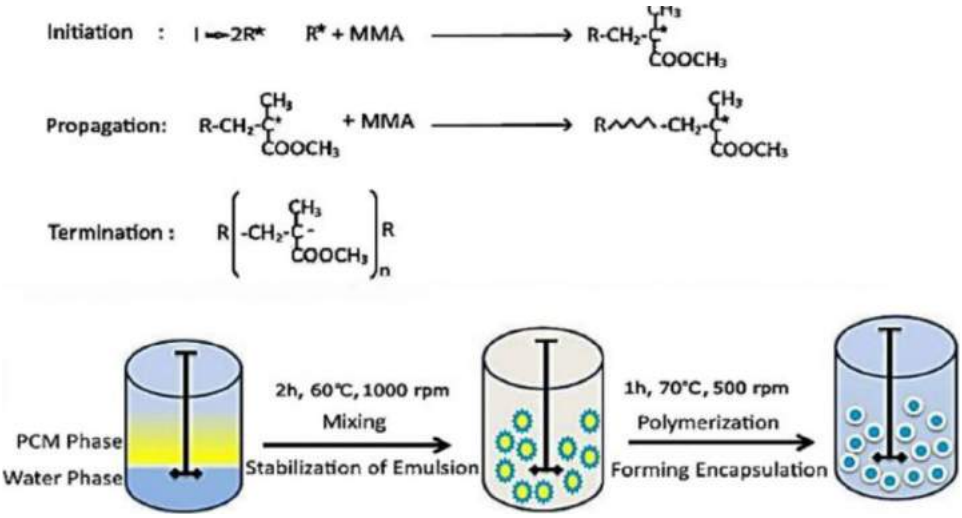

Fig. 98. The chemical reaction of shell and process of microcapsules [181].

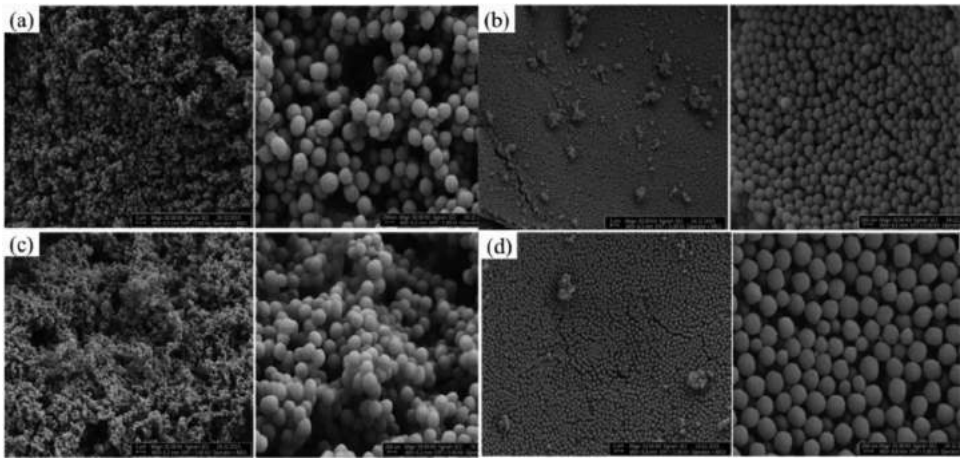

Fig. 99. The SEM images of microcapsule with different shell material, (a) PMMA, (b) P(MMA-co-GMA), (c) P(MMA-co-HEA), (d) P(MMA-co-HEMA), 10 K (left) and 50 K (right) magnification [181].

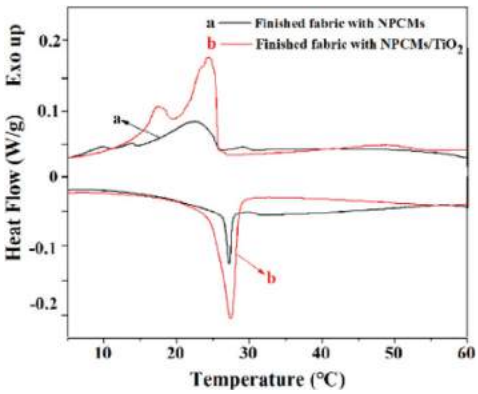

Fig. 100. DSC curves of nanocapsules used in textile (a) with and (b) without nanoparticles [182].

Currently, Li and Yuan [183] have achieved exceptionally high encapsulation efficiency of 99.6% by a combination of emulsion and suspension polymerization (Fig. 102). Moreover, the microcapsules have a double shell (polyacrylate and silica). They investigated the morphology by tuning the Janus silica particles and monomers, finding that the suitable core/inner shell/ourter shell is 70:21:1. In terms of thermal stability and reliability, double-shell microcapsules can withdraw temperature up to 150°C and have an unchanged latent heat after 7560 thermal cycles. Fig. 103 indicate that the appearance of the microcapsules are nearly unchanged.

Table 10 shows previous progress by using emulsion polymerization for encapsulation.

3.4. Physical and chemical combined encapsulation methods

3.4.1. Ionic gelation

The pharmaceutical and food industry commonly use the ionic gelation method to deliver drugs and synthesize nanoparticles

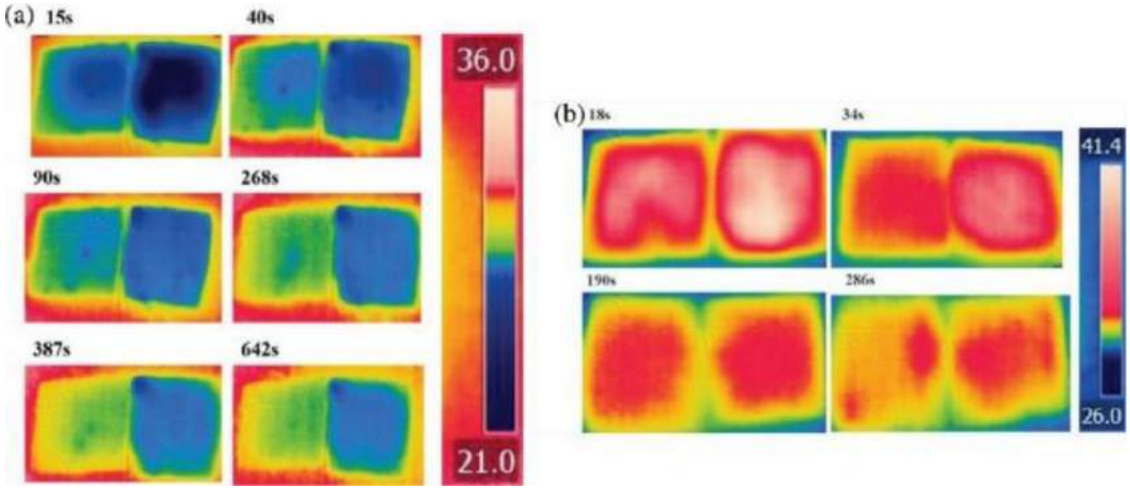

Fig. 101. Thermal images of (a) heating and (b) cooling process of nanocapsules (left) with and (right) without nanoparticles [182].

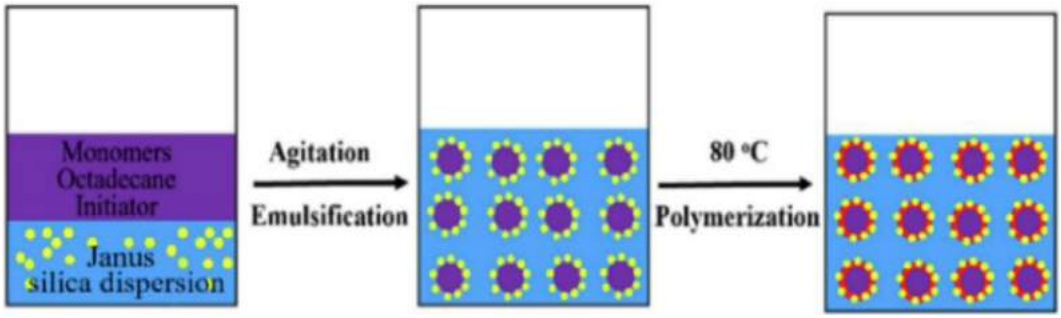

Fig. 102. The preparation process of microcapsules.

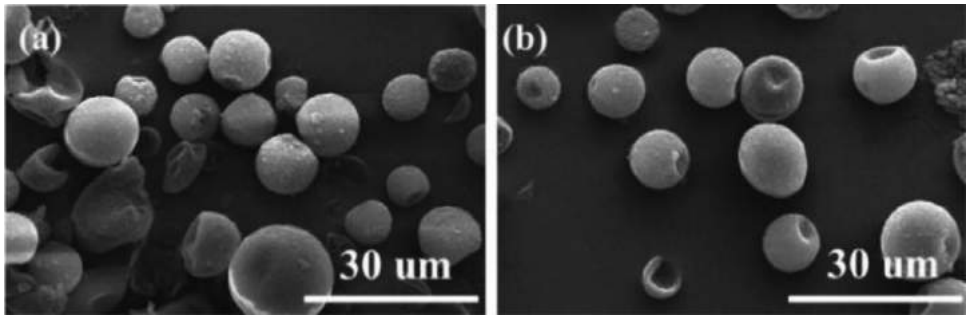

Fig. 103. The SEM images of morphology a) before cycling and b) after 7560 thermal cycles..

Table 10
The properties of encapsulated capsules using emulsion polymerisation.

Refs.	Core material	Shell material	Particle size (μm)	Thermal cycling (cycles)	Encapsulation efficiency (%)	Heat of fusion (J/g)	Other properties of microcapsules
[172]	N-octacosane	PMMA	0.25	5000	-	86.4	• Melting temperature: 50.6°C • Freezing temperature: 53.2°C • Good chemical stability • Narrow particle size distribution • Smooth and compact surface • Core content: 43 wt% • Two-step degradation
[173]	N-heptadecane	PMMA	0.26	5000	-	81.5	• Smooth and compact surface • Melting point: 18.2°C • Freezing point: 18.4°C • Core content: 38 wt% • Three-step degradation
[174]	N-hexadecane	Poly(butyl acrylate) (PBA)	0.47–4.5	-	-	120.16	• Melting point: 17°C • Freezing point: 15°C • Core content: 50.69
[175]	Paraffin eutectic mixtures: 1: C_{17}-C_{24}; 2: C_{19}-C_{18}; 3: C_{19}-C_{24}; 4: C_{20}-C_{24}	PMMA	1: 2.97; 2: 2.36; 3: 6.42; 4: 1.16	5000	-	169	• Melting point: 26–30°C • Rough surface • Cluster • Thermal conductivity: 0.19–0.20 W/m K
[176]	Paraffin wax	P(MMA-co-MA) incorporated with alumina nanoparticles	~1	-	-	105.50	• Highest thermal conductivity: 0.3816 W/m K (0.2442 W/m K for unmodified shell) • Smooth surface • Good microcapsule distribution and dispersity at optimal nanoparticle dosage • Core content: 61.2%
[177]	Paraffin wax	Polyurethane shell	0.205–0.260	100	-	7.83	• Melting point: 32.57°C • Freezing point: 65.67°C • Uniform and narrow particle size distribution • Homogeneous melting • Good high-temperature resistance
[178]	1-dodecanol	p(Styco-BA-co-DVB)	16.9–41.3	30	93.5	132	• Core content: 69.89% • Optimal core-shell ratio: 1.5
[179]	28#paraffin	Crosslinked polystyrene (CLPS) and modified nano SiO_2 (MS) hybrids	1–5	500	95.15	86.35	• Optimal nanoparticle ratio: 4.2% • Core content:54.37% • Melting point: 28.20°C • Irrigation shape with the narrow particle size distribution
[180]	TDA	PMMA	2–20	200	97.4	190	• Core content: 81.4% • Melting point: 43.48 • Optimal core-monomer ratio: 2:1
[181]	BA	Poly(MMA-co-2-HEA)	0.1–0.477	-	-	58	• Uniform spherical shape with a smooth surface • Core content: 25% • Degradation temperature: 335°C • Melting point: 69–79°C
[182]	N-octadecane and n-butyl stearate eutectics	Titanium dioxide reinforced polyacrylate	0.07–0.1	-	61.54	62.85	• Melting and freezing point: 26.49 and 22.86 °C • Spherical shape with well-defined core-shell structure • Ultraviolet (UV) absorption • Gentle temperature change
[183]	N-Octadecane	Silica and polyacralate	15	7560	99.6	175.1	• Melting point: 30.1°C • Freezing point: 22.2°C • Exceptional thermal reliability

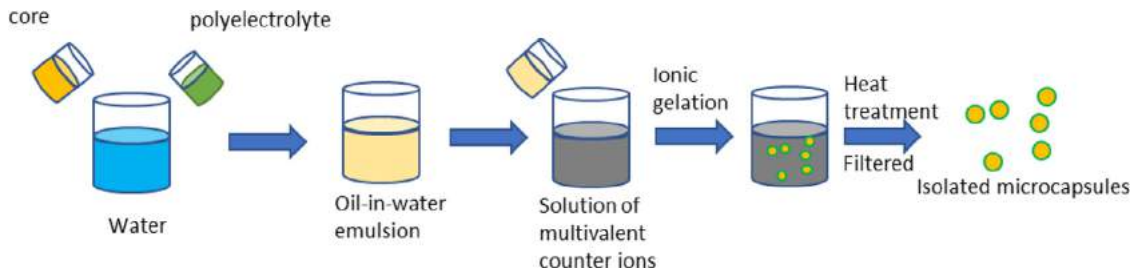

Fig. 104. The general process of ionic gelation.

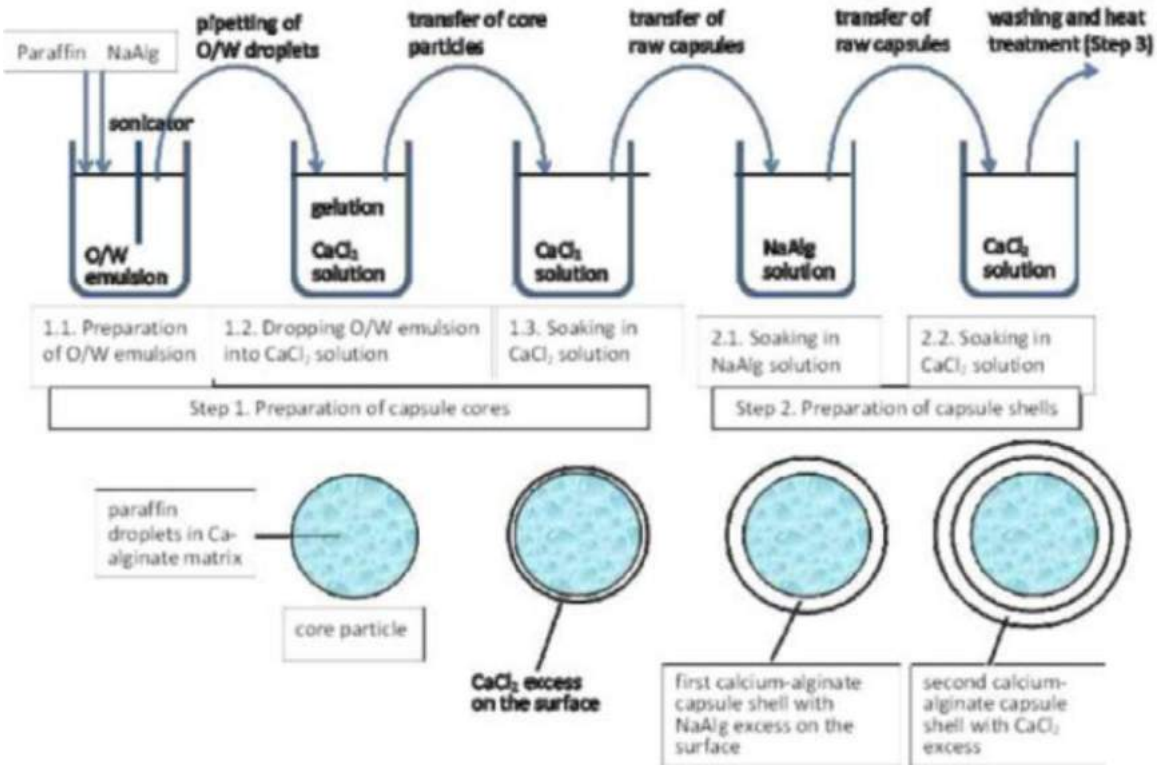

Fig. 105. The process and mechanism of the raw capsule with double shell [187].

[184]. However, it is rarely applied in the thermal energy storage field for the encapsulation of PCMs. In this process, the core material is dissolved in a suitable solvent, followed by the addition of a polyelectrolyte solution to form the emulsion, under a suitable stirring rate. Then, the hydrogels from the ionic gelation process are obtained when the emulsion is added to a solution containing multivalent cations, like Ca^{2+}, Ba^{2+}, and Al^{3+} [185]. Finally, the consolidation through the heat post-treatment is needed to solidify obtained capsules. The process has illustrated in Fig. 104 based on the description of the previous work [96]. The most used polyelectrolyte is alginate which can be crosslinked. The consequence of gelation is the formation of CaAlg, which occurs when alginate encounters Ca^{2+} [186].

Németh et al. [187] used ionic gelation in recent years to encapsulate paraffin within a non-porous double shell. As the process and the mechanism of the shell formation in Fig. 105 show, initially, the sonicator is used to mix the oil phase (melted paraffin) and aqueous phase (sodium alginate).

Then, the emulsion formed is added to a $CaCl_2$ solution, drop by drop, with a slow stirring rate, where the droplets are approximately uniform. To provide an environment of excess $CaCl_2$ on the surface, the particles are transformed to another $CaCl_2$ solution with various concentrations. The core particles with abundant $CaCl_2$ surface concentration are transferred to a sodium alginate solution with the same gradient concentration as the previous step, where not only the calcium-alginate shell is formed but the sodium alginate excess on the shell surface is ready for the next layer of shell formation. The second crosslinked layer of the shell is obtained after the raw capsules are withdrawn to the $CaCl_2$ solution with the same gradient concentration. The heat treatment illustration is not given in this research. However, according to their description, it has been drawn in Fig. 106, where the raw capsules are placed on a hot plate followed by the continuous rolling movement to consolidate capsules and evaporate the water. According to this fabrication process, they found three factors that could influence particle size. The increase in soaking time and sodium alginate concentration results in a reduction in particle size, unless they exceed the 8 min and 8 wt%, respectively. The size is proportional to calcium chloride concentration until a plateau shows at high concentration.

Similar to the previous research, Miloudi and Zerrouki [188] designed a fabrication device of microcapsules named microfluidic coaxial device in Fig. 107. The melted glycerid wax core material is pumped into the inner container, whereas the sodium alginate (shell material) solution, containing sodium silicate (Na_2SiO_3) and sodium carbonate (Na_2CO_3) as reinforcement components, is added

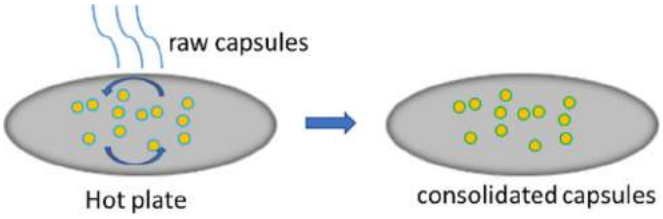

Fig. 106. The heat treatment of raw capsule.

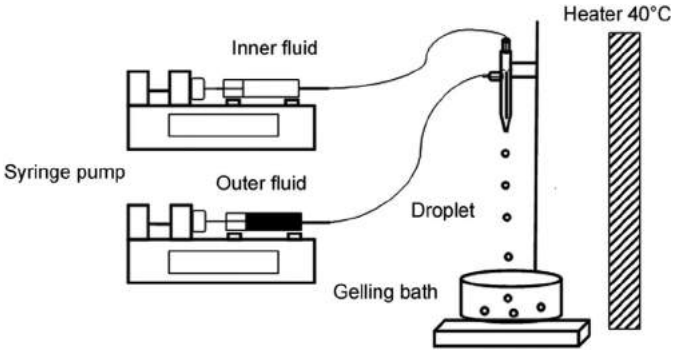

Fig. 107. The fabrication device [188].

into the outer container by a syringe pump. Under a programmed flow rate, mixture droplets are surrounded by calcium chloride, the crosslinking agent, in a gelling bath to form simple capsules. Then, by transferring them to other calcium chloride solutions with higher concentrations for a longer time, raw capsules are formed. To incorporate the enhancement agents, raw capsules are transferred to their continuous solution for a short time. Before the final products are obtained, the same heat treatment as the previous research is needed. According to results from characterization, the shell consists of the double-shell (Alg-Ca, Alg-$CaSiO_3$, and Alg-$CaSiO_3$) and hybrid shell (Alg-$CaSiO_3$/Alg-$CaCO_3$). They conclude that the incorporation of highly compatible and stable inorganic components, such as carbonate and silicate, have positive effects on the reliability and mechanical properties.

Key works using ionic gelation for encapsulation are summarized in Table 11.

3.4.2. Coacervation

Coacervation is a method where the separation of two liquid phases occurs by an electrostatic, hydrophilic hydrogen bonding interaction between two polymers in the aqueous phase, after adjustments are made to the pH, temperature, ionic strength, etc. [96]. These interactions are affected by the biopolymer with different molecular weights, pH, ionic strength etc. [189]. The coacervation is divided into simple and complex, where they follow the same mechanism of microcapsule formation, but different phase separation based on different polymer systems. The mechanism of phase separation for complex coacervation follows the complexation between the opposite charged proteins or polyelectrolytes, whereas the phase separation for simple coacervation is achieved with the help of desolvation agents. Speaking of particle size, complex coacervation results in smaller particles. The fabrication process is shown in Fig. 108. Initially, the prepared oil phase containing PCM and aqueous phase containing polymer are mixed to form an emulsion. By adding salt and another polymer, followed by adjustment of the pH and temperature, the shell material is gathered on the core particle surface. The crosslinking process then proceeds by addition of the crosslinking agent, heat treatment or desolvation, to form stable microcapsules.

Hawlader et al. [190] initially applied coacervation to encapsulate paraffin within acacia and gelatine gum, and investigated the factors that influence the encapsulation efficiency, latent heat, and hydrophilicity of capsules so that the optimal fabrication process was attained. Here the crosslinking agent they selected is formaldehyde (HCHO). They found the hydrophilicity increases by lowering the core-shell ratio and amount of HCHO used, and the encapsulation efficiency is improved while decreasing the core-shell ratio, meaning the more shell material used, the better capsule is sealed. Thus, the most suitable emulsion time and crosslinking agent amount added is 10 min and 6–8 ml, respectively. With the same leading author, Hawlader et al. [113] combined this method and traditional spray drying together to prepare a paraffin-wax microcapsule encapsulated in the same shell, where the main results have been discussed in the spray drying section before.

Onder et al. [191] fabricated three kinds of microcapsules in the same shell of acacia and gelatine gum: n-hexadecane, n-octadecane and n-nonadecane, and studied their thermal performance. Unlike other research using repeated thermal cycling, they evaluated the leakage by applying centrifugal shear force plus a fabric surface staining check, and the test result showed that the obtained microcapsule is robust enough, without leakage problems. According to DSC data, the latent heat of the n-hexadecane microcapsule (165.8 J/g) is slightly higher than that of the n-octadecane microcapsule (144.7 J/g), approximately corresponding to three times n-nonadecane microcapsule (57.5 J/g).

Deveci and Basal [192] explored other shell materials by using complex coacervation. In this case, a silk fibroin (SF) and chitosan (CHI) shell is chosen to seal the n-Eicosane (ES) core. The effects of polymer ratio, the amount of crosslinking agent and core content on the thermal properties and morphology of the microcapsule are studied. The morphology of the microcapsule varies with the SF-CHI ratios; when the ratio is close to 5, a smooth monolayer is formed (Fig. 109 b). As the ratio increases beyond 14, this morphology then is transformed to double-layer morphology where the inner layer is dense and compact, and the outer layer is porous (Fig. 109 c). Supportively, SEM images (Fig. 110) show the obtained microcapsules at different magnification. The smooth inner layer

Table 11
The properties of encapsulated capsules using ionic gelation.

Refs.	Core material	Shell material	Particle size (μm)	Thermal cycling (cycles)	Encapsulation efficiency (%)	Heat of fusion (J/g)	Other properties of microcapsules
[187]	Paraffin	Double calcium-alginate shell	2160	1000	-	95.5	• Core content: 48% • Air content: 38.7% • Spherical shape with a smooth surface • Shell thickness: 40 μm
[188]	Glycerid wax	Sodium silicate and sodium carbonate modified calcium-alginate shell	In Millimetre (can be seen with naked eyes)	100	-	-	• Shell thickness: 35 μm • Good reliability • Good mechanical properties

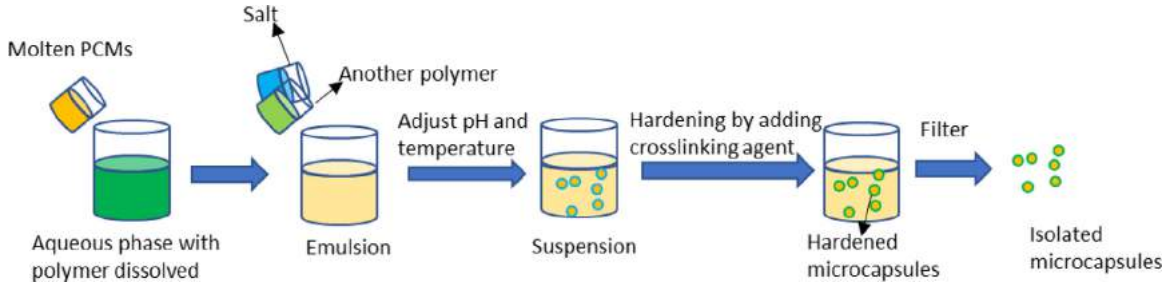

Fig. 108. The process of coacervation.

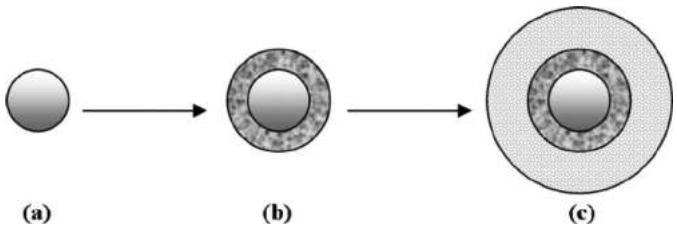

Fig. 109. The structure schematic of (a) ES droplet, (b) SF/CH coacervate monolayer, and (c) SF (excess in the outer layer)/CH bilayer [192].

is exposed when microcapsules are cracked Fig. 110 c), and the outer SF layer is more porous and homogeneous (Fig. 110 b). To achieve the highest microcapsule efficiency, the optimal condition is obtained with the SF-CHI ratio of 20, the content of crosslinking agent of 0.9% and core content of 1.5%. The properties of these microcapsules has been further discussed in following research [193], where they had pointed out that it is necessary to study the mechanical properties and durability while applying them on textiles.

Demirbağ et al. [194] integrated clay nanoparticles into microcapsules composed of ES as the core and acacia/gelatine as the conventional shell. The thermal stability and capability of flame retardation were investigated. Findings illustrated that the incorporation of clay nanoparticles largely increase the thermal stability and comfort in cotton fabrics, with an average ignition time of 2.4 s, extended to 3.6 s.

Differing from other research using conventional paraffin as the core, Huo et al. [13] used CHI alone as the shell to seal a side-

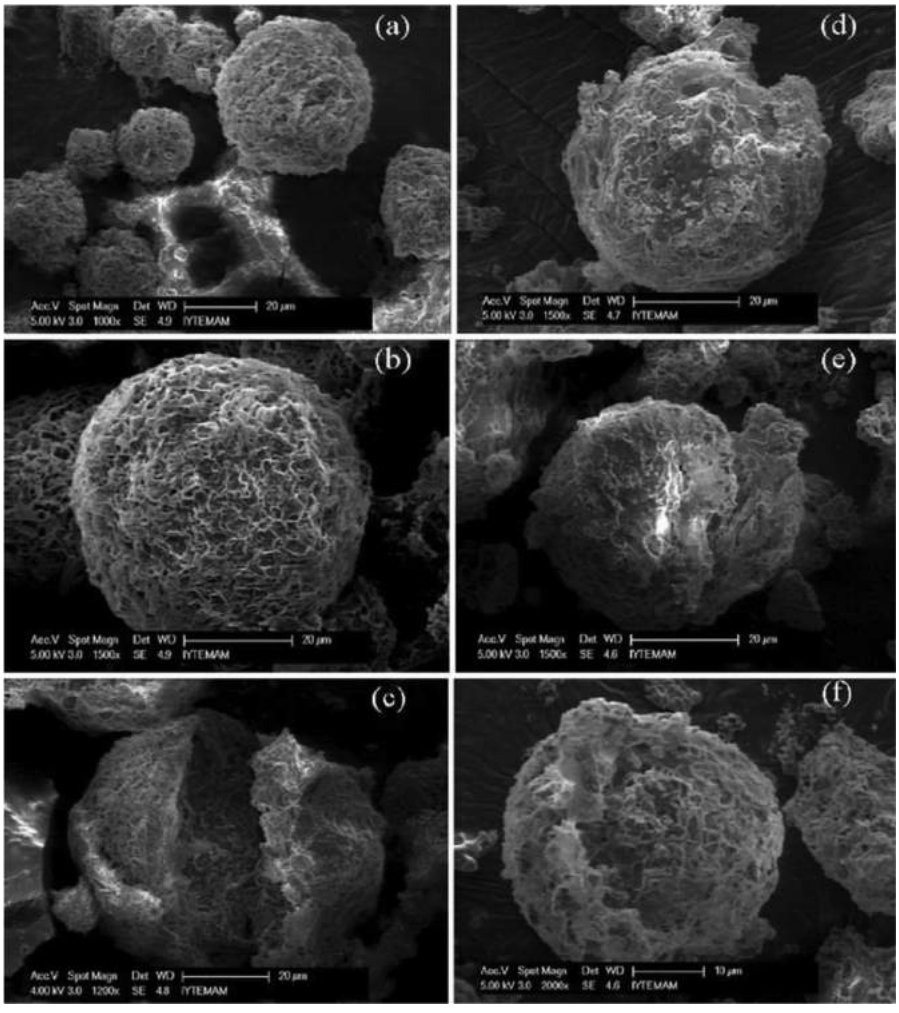

Fig. 110. SEM images of microcapsules at magnification of (a) 1000, (b) 1500, (c, cracked) 1200, (d, e, cracked) 1500, (f, cracked) 2000 [192].

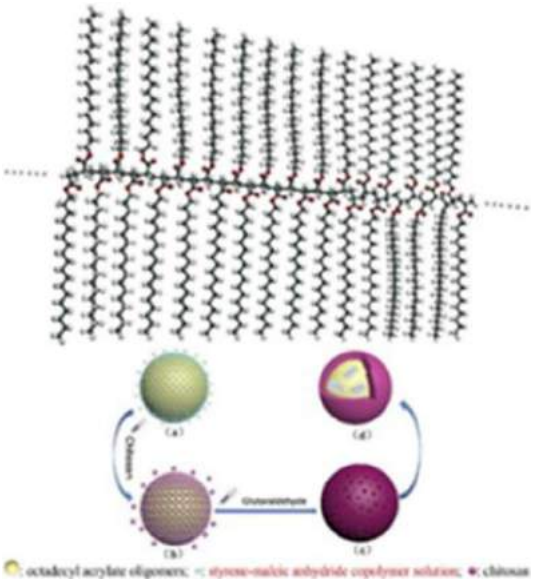

Fig. 111. The structure of core polymer (a) and fabrication process (b) of microcapsules [13].

chain crystallizable comb-like polymer, poly (octadecyl acrylate) (POA), as the core material; the structure of this polymer and fabrication process is given in Fig. 111. They found that the most suitable core-shell ratio was 1:2, and the formation of microcapsules increase the zeta-potential compared with that of emulsion, meaning that it is more favourable and stable to form microcapsules. According to the morphology study in Fig. 112, some wrinkles appear on the surface of spherical microcapsules, and some particles are sticking together (particles of CHI aggregation and prepared microcapsules). After detaching, the microcapsules exhibits a hollow core-shell structure. Due to their eco-friendly nature, the authors suggested it is promising to apply it in medical treatments.

Roy et al. [195] focused on the various process parameters while synthesizing n-hexadecane microcapsules sealed by chitosan (CH) and type-B gelatine (GB) shell materials. The parameters, like homogenization time, CH-GB ratio and polymer concentration have great effects on the mean diameter and its distribution, shell thickness, etc. They found that as they increase the homogenization time, polymer concentration and CH-GB ratio, the mean diameter and distribution is reduced. It can be validated in Fig. 113, where the smallest emulsion droplets, dispersed ideally, can be observed at the bottom left image. Besides, if the core-shell ratio is lower, higher encapsulation efficiency can be obtained.

Wu et al. [196] developed colour-visualized microcapsules, named reversible thermochromic MicroPCMs, resulting from colour former and developer chemicals. The promising application is an intelligent adjustment-based garment for thermoregulation and temperature management [197]. The core and shell materials they used were 1-hexadecanol and modified gelatine and gum arabic. The fabrication process is depicted in Fig. 114, where DVB and GLA are used as crosslinkers. As Fig. 115 shows, the colour-changing

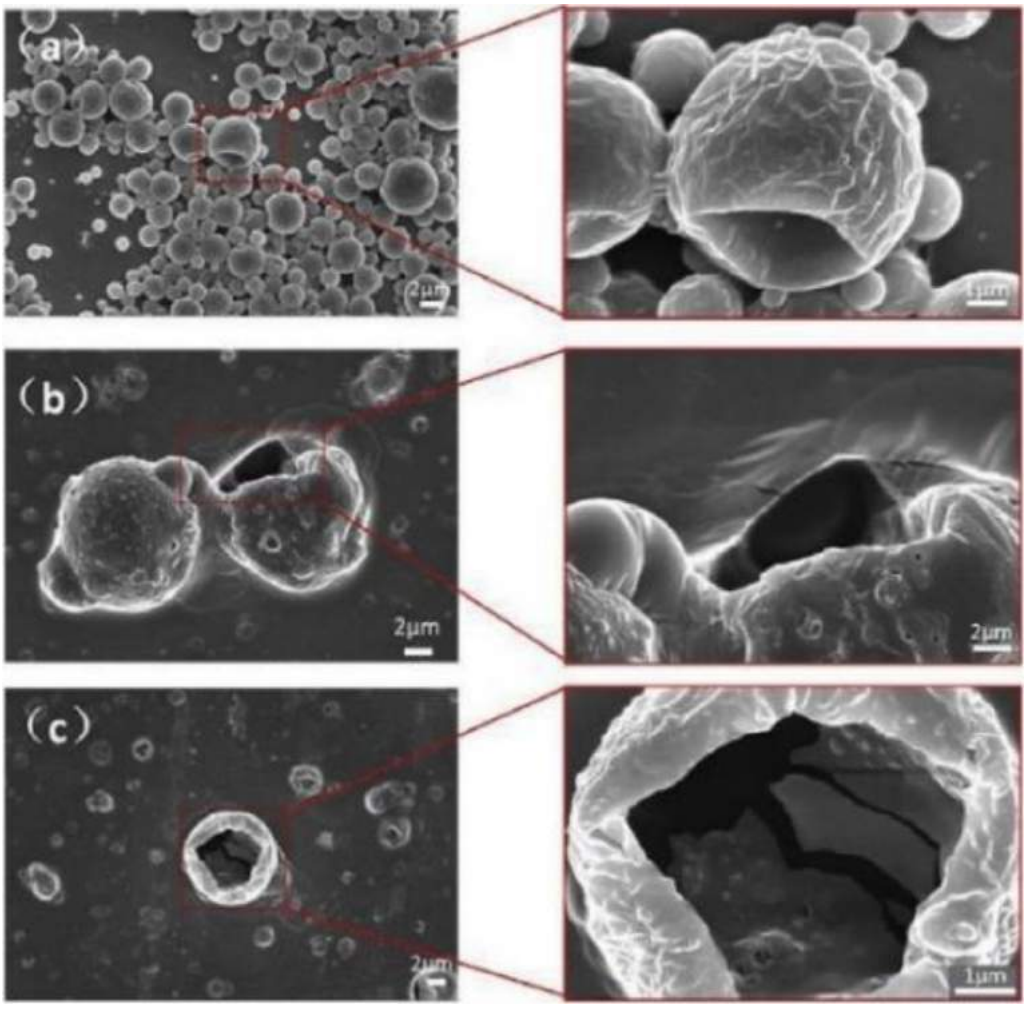

Fig. 112. The SEM images of microcapsules, before (a) and after (b, c) rupture [13].

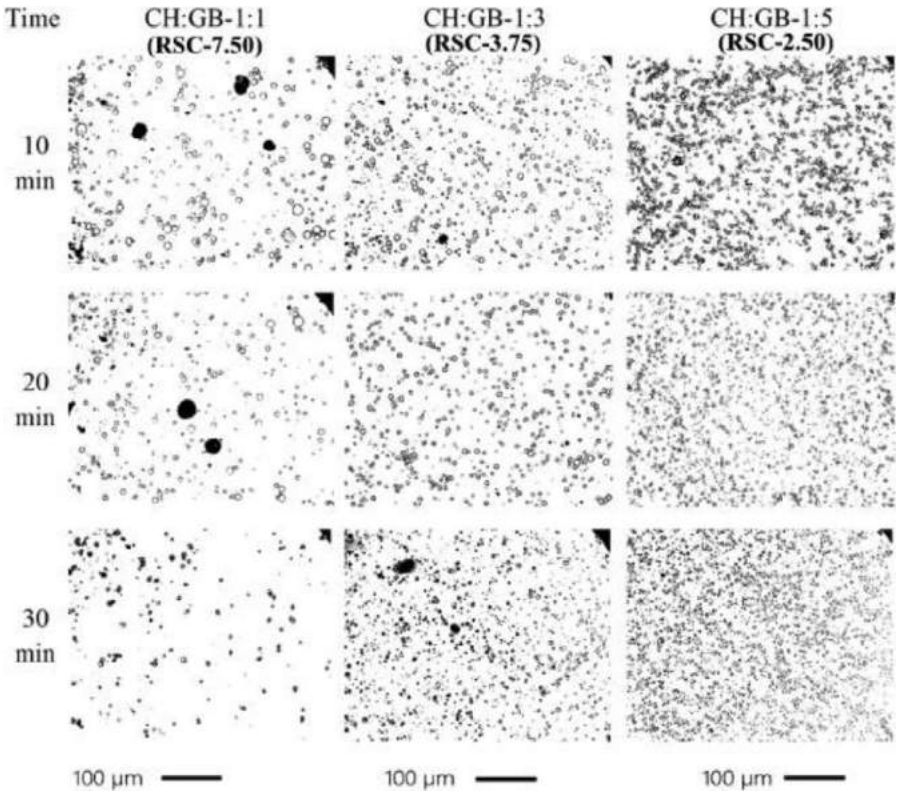

Fig. 113. The emulsion droplet size distribution varied with stirring time and core-shell ratio (RSC) [195].

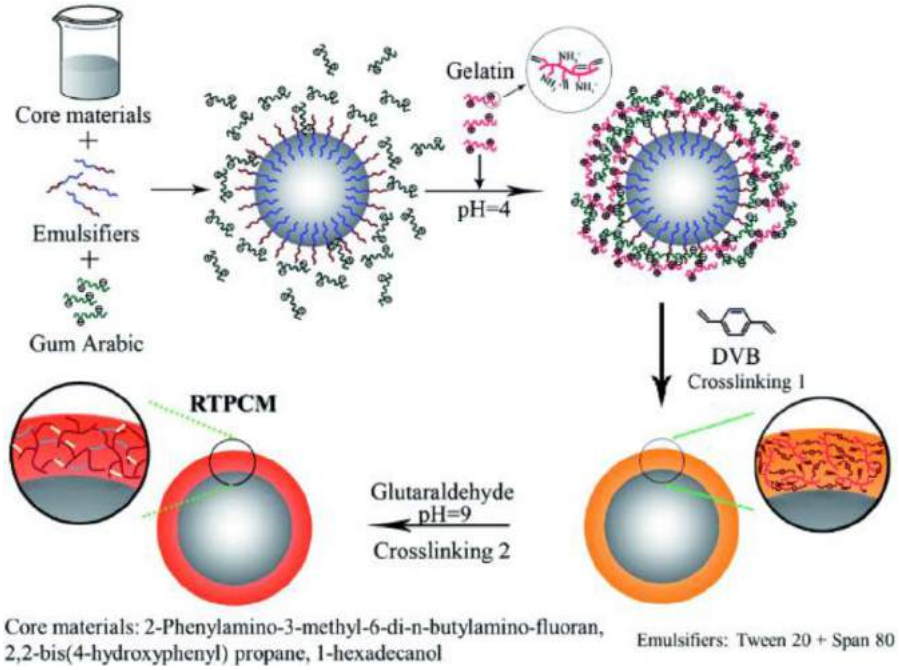

Fig. 114. The fabrication process of microcapsules [196].

mechanism of microcapsules is achieved by the reaction of the colour former and developer. The obtained sample is milky white with light pink at 60°C. As the temperature decreases to 15°C, the core material solidifies boosting interaction between the colour former and developer, and the ring-opening reaction of the colour former, which generates black colour. On the contrary, if the sample is heated to 60°C, the colour former and developer tends to be dissolved in the co-solvent leading to a ring-closing reaction. In this case, the ratio of colour former, developer, and core material is 1:2:20.

Considering the encapsulation of fatty acids, Konuklu et al. [198] successfully prepared the microcapsules containing caprylic and decanoic acid (DA) as core and chitosan-gelatine as the shell. The morphology of microcapsules containing different fatty acids is shown in Fig. 116. Although a continuous wall with no surface cracks can be seen, the shape is irregular due to the nat-

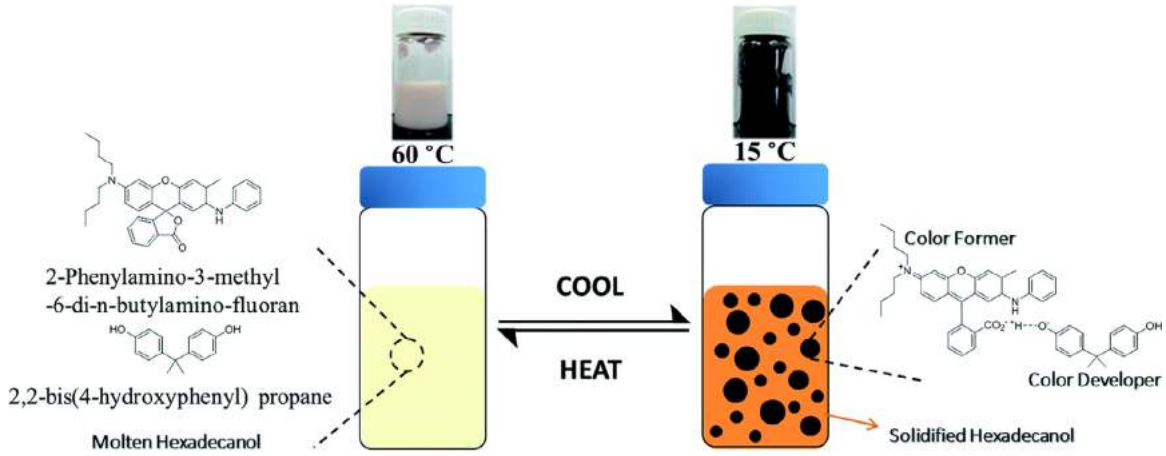

Fig. 115. Thermochromic mechanism of microcapsules [196].

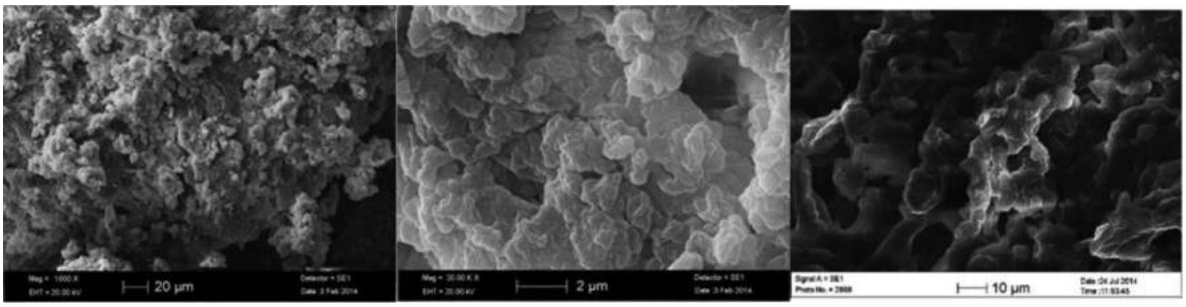

Fig. 116. The morphology of microcapsules containing caprylic acid (the first and second images) and DA (the last image) [198].

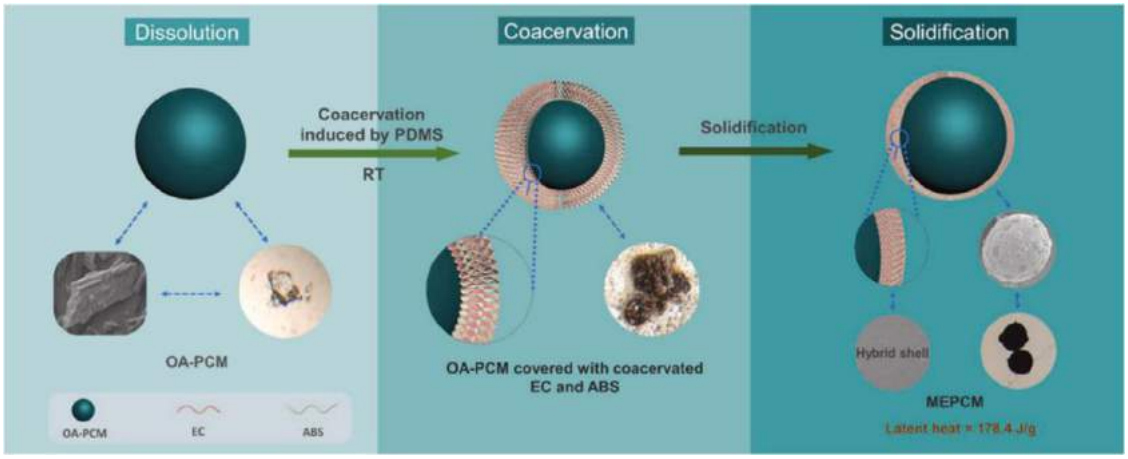

Fig. 117. The process/mechanism of microcapsules with oxalic acid dihydrate/boric acid as core and EC/ABS as shell.

ural materials used. Conversely, they had studied encapsulation with MF shell leading to regular and spherical shape [199], which gave the information that it is more difficult for the natural shell to control the morphology compared with using the inorganic shell.

Recently, eutectic PCMs composed of oxalic acid dihydrate/boric acid were encapsulated by ethyl cellulose (EC) and an acrylonitrile-butadinene-styrene (ABS) hybrid shell with the help of polydimethylsiloxane using coacervation (Fig. 117). This research is contributed by Ma et al. [200], and they claimed the suitable EC:ABS:PCMs ratio is 1:1:2 to give optimal performance.

Table 12 shows previous progress by using Coacervation for encapsulation.

3.4.3. Sol-gel method

The sol-gel method involves the combination of solution and gelation, and it also can be called a polycondensation reaction. The shell precursor exists as the stable colloidal dispersion in the aqueous phase followed by the gel formation (an oxide network) where dispersion particles aggregate together by different interactions, such as electrostatic interaction, van der Waals forces, hydrogen bonds, covalent bonds [51,170,201]. To be more specific, the shell precursor, catalyst, complexing agent, surfactants are initially dissolved in a solvent, followed by stirring to form a stable dispersion resulting from the hydrolysis reaction of the precursor [202]. After oil-in-water emulsion the core material is added under desired conditions, gel walls are formed surrounding PCM droplets.

Table 12
The properties of encapsulated capsules using complex coacervation.

Refs.	Core material	Shell material	Particle size (μm)	Thermal cycling (cycles)	Encapsulation efficiency (%)	Heat of fusion (J/g)	Other properties of microcapsules
[190]	Paraffin	Acacia and gelatine	2833	2000	-	90	
[191]	N-hexadecane n-octadecane n-nonadecane	Acacia and gelatine	-	-	-	165.8	• Resistance to high shear centrifugation and compression. • Higher heat absorption
[192,193]	ES	Silk fibroin and CHI	23	-	72	93.04	• Can form monolayer or bilayer • Inner layer: thin, dense, and smooth • Outer layer: thick, porous • Core content: 45.7 wt%
[194]	ES	Acacia and gelatine doped with clay nanoparticles	1.37–1.6	-	-	114	• Core content: 41.47 • Excellent thermal stability and flame retardation • Spherical shape
[13]	POA	CHI	1.47	-	68.99	129.9	• Shell thickness: 20 nm • High-temperature resistance • Roughly spherical shape • core-shell ratio: 1:2
[195]	N-hexadecane	CHI and type-B gelatine	0.1–4.0	-	96.7	115.0	• The most suitable shell materials ratio: 1:5
[196]	1-hexadecanol	Modified gelatine and gum arabic	7–10	100	85	72	• Good thermal and colour reliability • Colour-visualized phase change
[198]	Caprylic acid decanoic acid	Chitosan and gelatine	0.22 1.06	400	-	79 73	• Core content: 50.58% • Both with irregular shape
[200]	Oxalic acid dihydrate/boric acid	EC/ABS	76.27	100	51.9	178.4	• Hybrid shell • Melting point: 77.9°C • Quasi-spherical shape

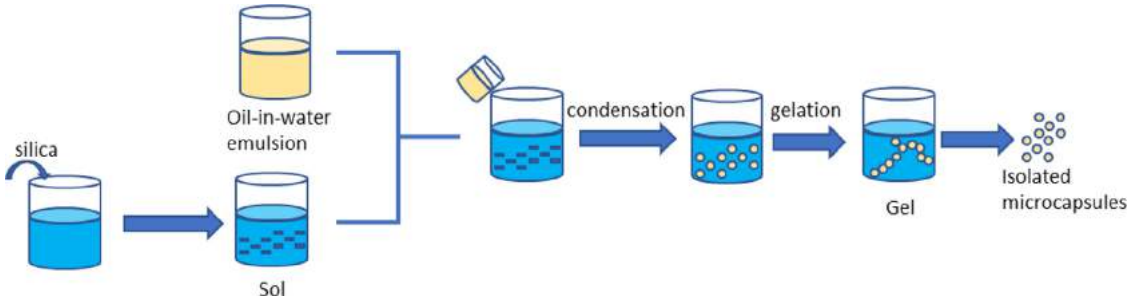

Fig. 118. The process of the sol-gel method.

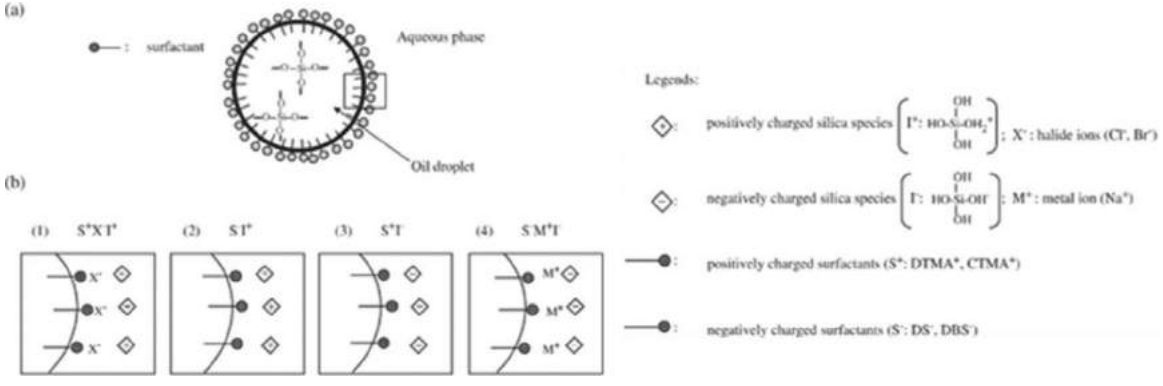

Fig. 119. The formation process of silica shell (a) and the different interfacial interaction [202].

Fig. 118 shows the process of the sol-gel method mentioned just above.

Wang et al. [202] are the first group that employed the silica microspheres as the inorganic shell by using the sol-gel method (Fig. 119). In their research, the emulsifiers used are the key to achieving successful small particle encapsulation. Acidic solutions achieved by adding cationic surfactants facilitate the electrostatic interactions between positively charged surfactant, halide ion, and positively charged silica. Based on the acidic conditions and emulsifiers, the pH and type of ionic surfactant are investigated. After they examined several experiments using different surfactants, cetyltrimethylammonium chloride (CTMAC), Dodecyltrimethyl-ammonium chloride (DTMAC) and Dodecyltrimethylammonium bromide (DTMAB) can successfully encapsulate the PCM through the formation of a silica shell, compared with unsuccessful synthesis using common surfactants like SDS

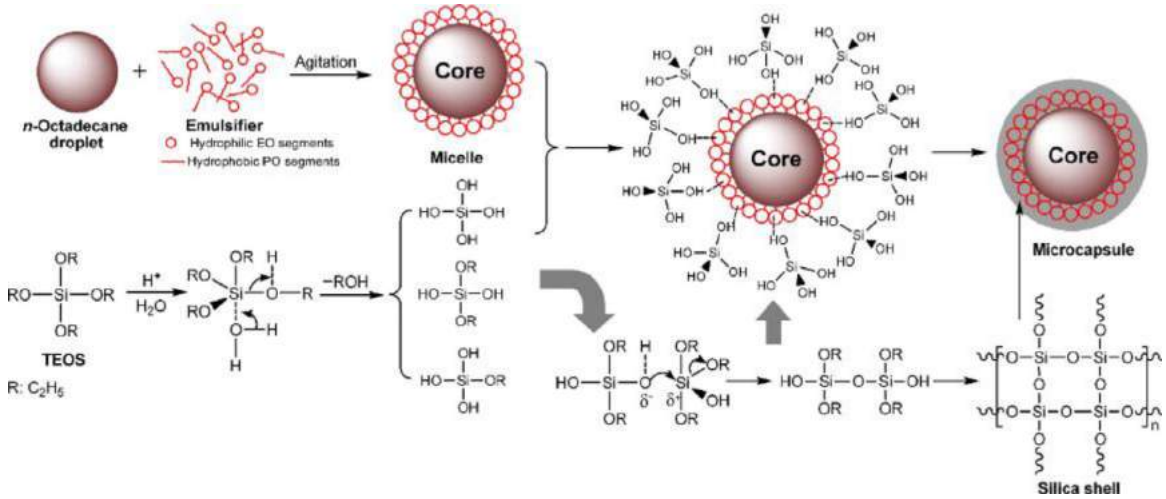

Fig. 120. The mechanism of silica shell formation [203].

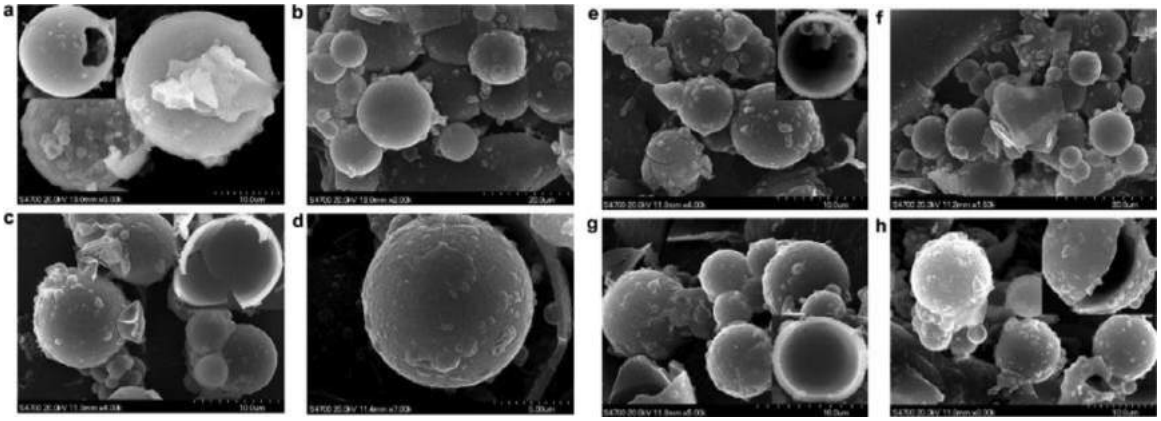

Fig. 121. The morphology of microcapsules derived from different core-shell ratio and pH; (a, b) 70/30 and 2.26, (c, d) 70/30 and 2.45, (e, f) 60/40 and 2.45, (g) 50/50 and 2.45, (h) 70/30 and 2.89 [203].

and SDBS under the same condition. Thus, the most suitable pH value obtained is -0.16. As Fig. 119 shown, the $S^+X^-I^+$ interaction (b1) is preferred to form the silica shell.

Since the silica shell had been used for enhancement of thermal conductivity, Zhang et al. [203] made another attempt to encapsulate n-octadecane, and the mechanism of shell formation is shown in Fig. 120 where the TEOS is used as silica precursor. They prepared several samples with different core-shell ratios and pH values. Their morphologies are shown in Fig. 121. A rough and thin shell that is easily cracked by force can be observed due to the slow condensation rate depositing a small amount of silica on the surface under a pH of 2.26 (Fig. 121 a, b). However, with the pH increase to 2.45, a compact and smooth surface can be obtained (Fig. 121 c–f) where the condensation rate matches the aggregation rate of silica. The higher the pH, the thicker the shell is (Fig. 121 g, h), whereas pH should not be more than 3 or less than 2 due to the much higher aggregation rate of silica failing to wrap the core particles.

Unlike previous research using TEOS as the silica precursor, Fang et al. [29] applied tetraethyl silicate to generate silica shell encapsulating paraffin with fusion heat of 189.24 J/g. they provided three kinds of microcapsule morphologies with different core contents and concluded that the inhomogeneous morphology is formed if the PCM dosage is not sufficient due to silica self-aggregation (see Fig. 122 a, b). The resultant microcapsules exhibit excellent thermal stability owing to paraffin-silica synergy for which carbonaceous-silicate charred layer are build up on the surface limiting the transfer of heat and flammable molecules.

Tahan Latibari et al. [204] is the first group to conduct the sol-gel method under a high pH value of 11, 11.5 and 12. the core and shell materials they used are PA and silica. The particle size distributions of macrocapsules successfully lowered to nano-range. Higher pH results in larger particle size (see Fig. 123). For the latent heat and enhancement of thermal conductivity, microcapsules obtained under a pH of 12 have the highest value. The thermal conductivity is enhanced by roughly 2 times that of pure PA.

Similarly, Luan et al. [205] studied the effect of an acid and alkali reaction system on the microcapsule in the sol-gel method. They found a significant reduction in the particle size and the latent heat in the alkali system compared with that in the acid system.

He et al. [206] further had explored the new silica precursor, sodium silicate. They again confirmed the mechanism of shell formation driven by the balance between self-assembly and the condensation rate of precursors. The excellent thermal performance, desired morphology, and high encapsulation efficiency can be obtained if the core-shell ratio and pH value is 3:2 and in the range of 2.95–3.05, respectively.

Chai et al. [207] firstly achieved the preparation of microcapsules via titanium dioxide shell. The resultant bifunctional microcapsules that came from the photocatalysis of titanium dioxide

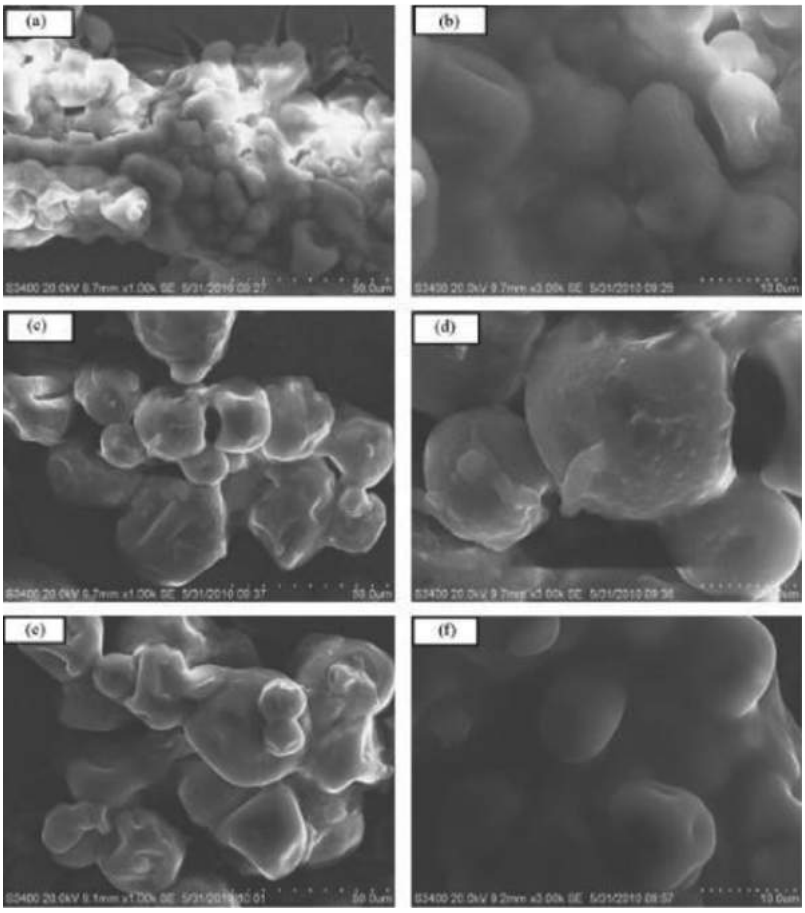

Fig. 122. SEM images of microcapsules with different core-shell ratio, (a) 10:20, (b) 15:20, (c) 20:20 [29].

are synthesized by the sol-gel method (see Fig. 124), and they found that during the fabrication process the fluorinions help the transition from amorphous to brookie-form crystal structure wrapping around core particles. The core-shell ratio of 3:2 gives the best thermal performance in this research. For the photocatalysis effect, they designed an experiment where methylene blue is added to a solution containing prepared microcapsules, and the result shows that the degradation reaction of methylene blue takes place by photocatalysis of titanium dioxide at different finite UV exposure times (see Fig. 125). The colour is changed from blue to colourless. The good antimicrobial function can be vividly observed by applying UV light to an incubator containing microcapsules and *Escherichia coli* at different radiation times. With the radiation time, the number of living *Escherichia coli* decreases, especially after 105 min (see Fig. 126 d).

Mo et al. [208] used silica to encapsulate inorganic PCM, ternary carbonates (lithium carbonate, sodium carbonate, potassium carbonate), and investigate the differences of obtained microcapsules produced with and without heating. Fig. 127 illustrates the two fabrication processes of carbonates/silica microcapsules. They found that the supercooling degree of unheated microcapsules (G-LiNaK-Si) is up to 22.2°C due to insufficient nucleation sites generated, while this is decreased by 43.7% for HG- LiNaK-Si. Thus, they clearly explained heat treatment affecting positively the thermal performance of this kind of microcapsule.

Srinivasaraonaik et al. [209] combined the stearic acid (SA) and capric acid (CA) (75:25) as core materials wrapped by the silica shell by using the sol-gel method. They compared the thermal conductivity, specific heat, and mechanical properties between microcapsules with MF and silica as shells, then incorporated to cement paste. The result shows that the mechanical strength and thermal conductivity of cement paste containing microcapsules with silica shell are improved by 10%, 9% than that of containing MF shell.

Lee et al. [210] achieved successful encapsulation without using surfactant as the stabilizer. Fig. 128 shows a simple fabrication process. The most important stage is stage 2 where added $NaNO_3$ acts as impurities for the heterogeneous nucleation, encouraging the polycondensation reaction. The obtained silica particles are then aggregated on the surface of the core material to form the shell. They investigated the effects of precursor concentration, the amount of catalyst added, and synthesis time consumed. Findings revealed that the concentration of precursor is not a dominating parameter, despite the small increase in condensation rate. Secondly, the catalyst concentration largely influences the shell formation, where more catalyst would promote the dense and rigid silica shell formation, thus the ratio of precursor and catalyst should be considered during synthesis. Lastly, the duration of synthesis should be prolonged if the precursor-catalyst ratio is large, otherwise, broken and incomplete microcapsules might be obtained.

According to the research by Subramanian [211], aluminium isopropoxide was used to generate alumina as the shell encapsulating the MA core. The process is like previous research using silica (see Fig. 129). They designed three kinds of microcapsules derived from the core-shell ratio of 1:1, 1:0.75, and 1:0.5. The results show that the ratio of 1:1 is preferred due to the best thermal performance.

Ishak et al. [212] encapsulated SA with a silica shell. They investigated the most suitable core-shell ratio by adding 5, 10, 15, 20, 30, and 50 g core material into 10 ml of TEOS. After the experiment, the combination of 50 g core material and 10 ml precursor is the most desired in terms of latent heat,

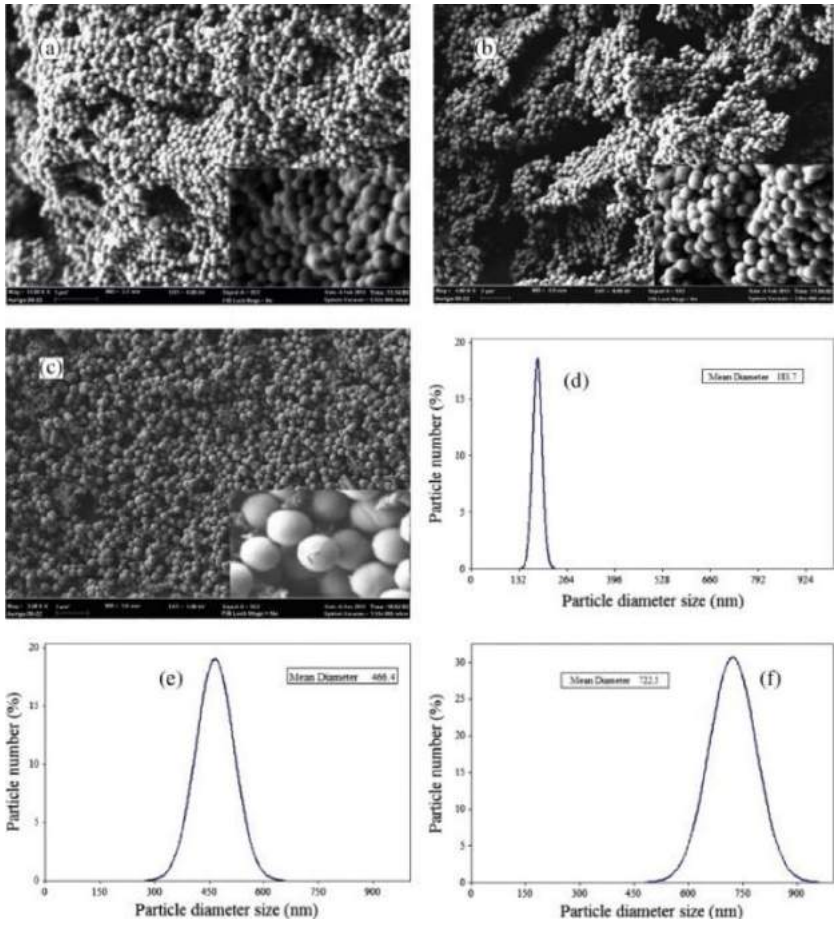

Fig. 123. SEM images of microcapsules and their particle diameter size distribution derived under the pH of 11 (a, d), 11.5 (b, e), and 12 (c, f) [204].

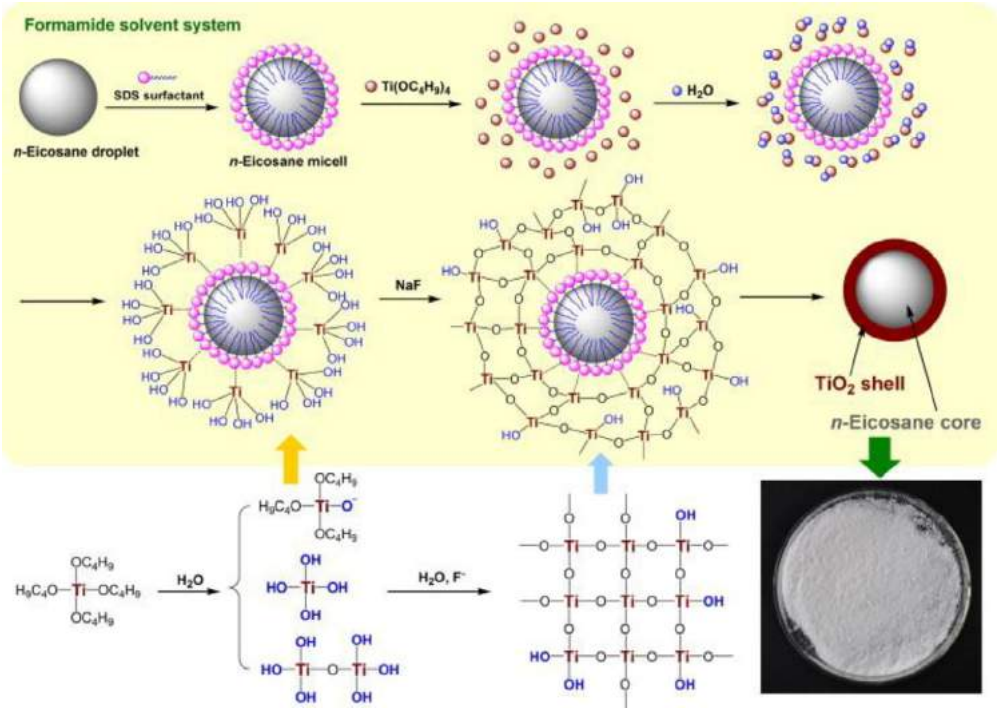

Fig. 124. The fabrication process [207].

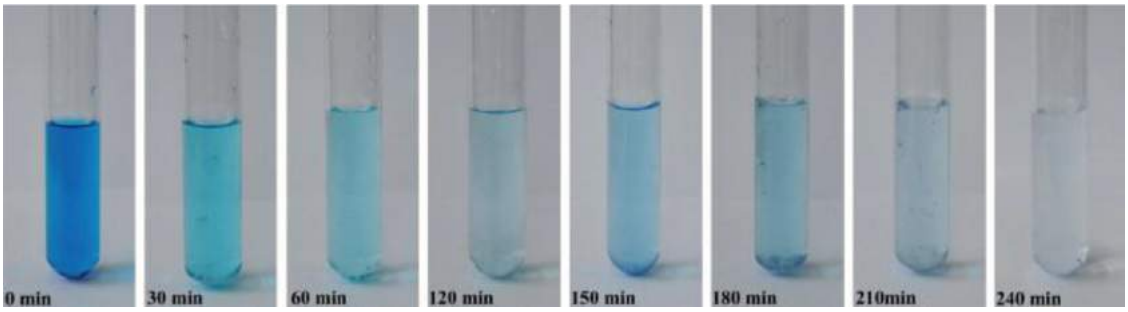

Fig. 125. The discolouration behaviour of solution containing methylene blue and obtained microcapsules at different UV-exposure times [207].

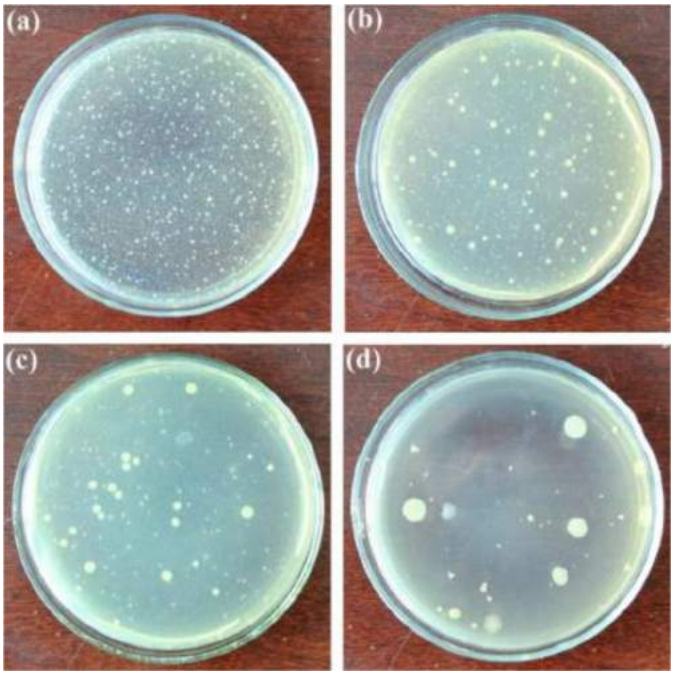

Fig. 126. The antimicrobial experiment at different UV radiation time; (a) 0 min, (b) 45 min, (c)75 min, (d) 105 min [207].

encapsulation efficiency, thermal stability, due to inhibition of aggregations.

Subramanian and Appukuttan [213] provided another shell option, strontium titanate, to encapsulate MA. They found that the increase in surface area negatively effects the microencapsulation ratio, and the most suitable MA/$SrTiO_3$ ratio is 1:2. The leakage test is shown in Fig. 130, where obtained microcapsules remain unchanged without any leakage after 16 min at 70°C, whereas the bulk MA turns into liquid, indicating that the resultant microcapsules have good thermal endurance.

Hussain et al. [214] improved another function, electrical energy storage (for electronic chip applications), by coating chips with nanocapsules consisting of OA-polyethene glycol eutectic core and SiO_2/SnO_2 shell. Apart from the excellent electronic conductivity (1.08 × 10–7 S/cm), they also conducted the measurement of mechanical properties (see Fig. 131). After incorporation of SnO_2, the hardness, elastic modulus, and resistance to plastic deformation are significantly enhanced.

Ishak et al. [215] optimized parameters for production of lauric acid (LA)/silicon dioxide microcapsules. The pH is controlled at 2.5. The core and shell mixture conditions are 800 rpm and 65°C for 6 h. The ratio of shell precursor TEOS and LA should be 1:5, otherwise aggregation appears.

Generally speaking, sol-gel method is mainly used for organic PCMs encapsulation. However, Milian and Ushak [216] empowered this method to encapsulate inorganic PCMs but using ethanol and only TEOS as precursor. During this study, they employed different monomer and solvent. The different monomers used affect the visible physical forms, morphology, crystallinity and thermal properties. Particularly, the Trimethoxy (2-phenylethyl) silane monomer has a positive impact on cyclic stability. For changing the solvent, there is significant change in stored heat, though physical difference is slight. Also, they found that the solvent polarity is crucial where the more PCMs can dissolved in solvent, the better homogeneity within the silica shell, the less supercooling engaged.

Cheng et al. [217] realized a hierarchical structure by Ni and MXene film formation to encapsulate PEG with the help of the sol-gel method. Interestingly, apart from high conventional thermal properties, this material has the function of shielding electromagnetic interference, which is important when used in electronic devices.

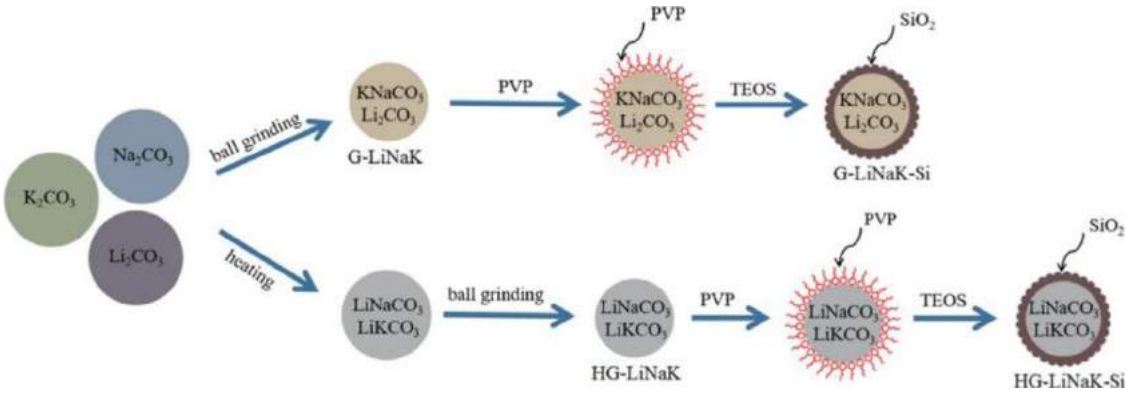

Fig. 127. The fabrication process with and without heating treatment [208].

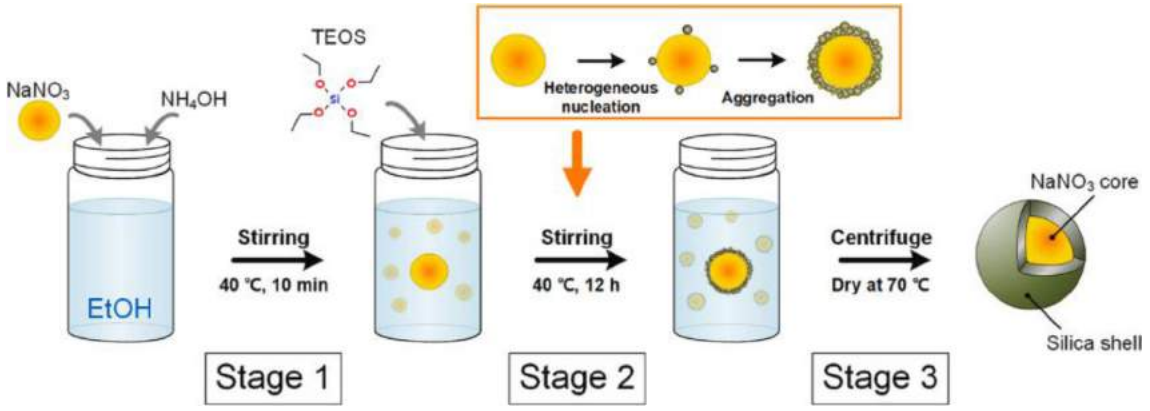

Fig. 128. The fabrication of $NaNO_3$@SiO_2 microcapsule without using surfactant; NH4OH and TEOS are the catalyst and silica precursor [210].

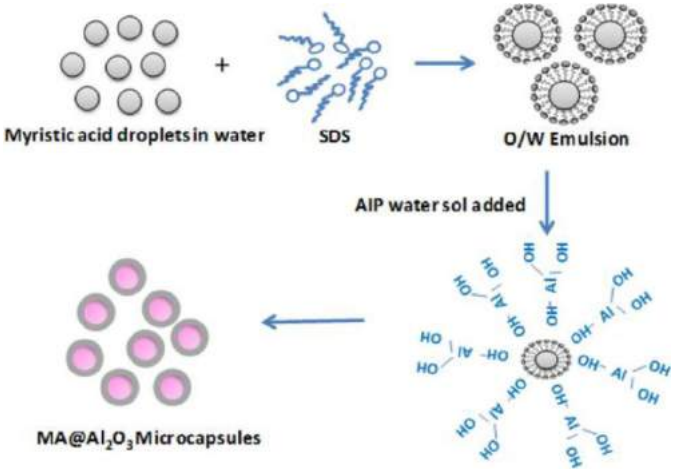

Fig. 129. The fabrication process of MA@Al2O3 microcapsules [211].

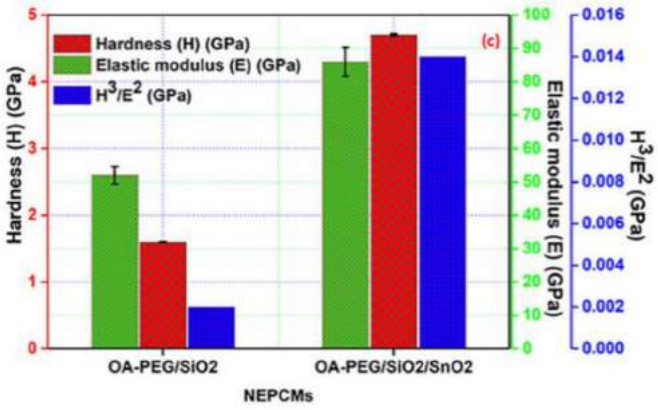

Fig. 131. The mechanical properties of OA-PEG/SiO_2 and OA-PEG/SiO_2/SnO_2 (H^3E^2 means the resistance to plastic deformation) [214].

Some works using the sol-gel method for encapsulation developed by previous researchers are included in Table 13.

3.5. Comparison of encapsulation techniques

Although there are plenty of methods to achieve encapsulation, researchers should be aware of the prerequisites for their use, advantages and disadvantages, and which method could effectively meet the application requirements. In terms of physical methods, they are simple to conduct, energy-saving, low production cost and ease of control due to the absence of complicated chemical reactions, meaning that fabrication can be done at scale [115,117]. Despite feasible production at the industry scale, the properties are lowered at their expense, with leakage occurring sometimes, lower mechanical strength resulting from large particle size and incomplete coating. Amongst the physical methods, only spray-drying and solvent evaporation are academically worth noting for scholars, because it is feasible to combine them with other methods for better performance [117]. As for chemical methods, they have the potential to be used for mass production owing to superior encapsulation efficiency, nano/micro-sized capsule, and narrow particle size distribution. Nevertheless, the selection of the most suitable encapsulation method is crucial. For example, although suspension polymerisation provides excellent encapsulation, not all monomers are water-soluble. Thus, the formation mechanism of shells by monomers decides what chemical method is the most suitable. Given the limitations of physi-

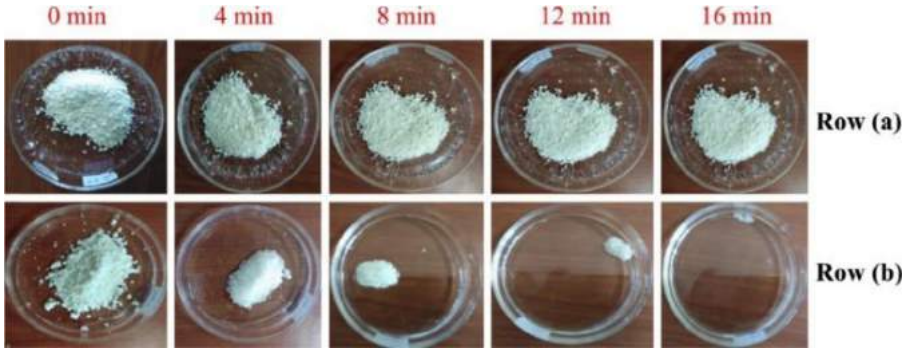

Fig. 130. Photograph of obtained MA/$SrTiO_3$ microcapsule (a) and MA for different heating times [213].

Table 13
The properties of encapsulated capsules using the sol-gel method.

Refs.	Core material	Shell material	Particle size (μm)	Thermal cycling (cycles)	Encapsulation efficiency (%)	Heat of fusion (J/g)	Other properties of microcapsules
[202]	N-pentadecane	Silica	4–8	-	-	46.4	• Core content: 29.8% • Spherical shape
[203]	N-octadecane	Silica	7–16	-	86.40	184.9	• Spherical shape with smooth and compact surface • Core maintain good crystallinity • Good thermal stability: two-step degradation • Good anti-osmosis property • Good thermal conductivity: 0.6213 W/mK • Core content: 69.5 wt.% • Melting point: 27.1°C
[29]	Paraffin	Silica	8–15	-	87.50	165.68	• Fire resistance • Freezing point: 58.27°C • Melting point: 58.37°C
[204]	PA	Silica	0.18–0.72	2500	89.55	180.91	• Melting point: 61.6°C • Freezing point: 57.08°C • Thermal conductivity: 0.47–0.49 W/mK
[206]	N-octadecane	Silica	8	100	41.83	87.46	• Thermal conductivity: 0.891 W/mK • Melting and freezing point: 27.96 and 23.72°C
[207]	ES	Titanium dioxide	1.5–2	100	77.97	152.5	• Melting and freezing point: 42.73 and 36.29°C • Thermal conductivity: 0.749 • Antimicrobial function to Gram-negative bacteria
[208]	Ternary carbonates	Silica	~3	50	84.8	192.2	• Melting and freezing point: 397.8 and 385.3°C • No leakage and chemical decomposition
[209]	Binary mixture of SA + CA	Silica	6.03	1000	71	86.5	• Melting point: 34.8°C • Shell thickness: 0.12 um • Thermal conductivity: 0.47 W/mK • Smooth and regular shape
[210]	NaNO3	Silica	3–10	50	94.0	168.6	• Improved high-temperature resistance • Shell thickness: 180 nm
[211]	MA	Alumina	2–5	500	92	150	• Spherical shape with smooth and compact surface • Good thermal endurance due to alumina shell
[212]	SA	Silica	10–20	30	86.68	182.53	• Good thermal stability • Melting and freezing point: 70.37 and 64.27°C
[213]	MA	Strontium titanate	5–10	500	46	91.90	• Melting point: 53.41°C • Good thermal endurance
[214]	Eutectics of OA and PEG	SiO_2/SnO_2	0.53–0.61	1000	51.58	58.79	• Thermal conductivity: 0.7053 W/mK • Electronic conductivity: 1.08×10^{-7} S/cm • Exceptional mechanical properties: yield load of 89.65 μN and hardness of 4.7 GPa
[215]	Lauric acid	Silicon dioxide	160	30	96.5	152.82	• Melting point: 44.30°C • Freezing point: 38.01°C
[216]	$LiNO_3$	Silicon dioxide	-	50		202	• Core content: 70% • Melting point: 153°C
[217]	PEG	MXene/Ni		50	-	154.3	• Thermal conductivity: 0.47 W m^{-1} K^{-1} • electromagnetic interference

Table 14
The summary of particle size and encapsulation efficiency from the aforementioned research by using different encapsulation methods.

Categories	Methods	Particle size (μm)	Encapsulation efficiency (%)
Physical	Spray-drying	0.1–11.5	63–91.98
	Solvent evaporation	3–159	57.7–97.6
	Pan-coating	-	-
	Air-suspension	-	-
	Centrifugal extrusion	-	-
Physio-chemical	Ionic gelation	Macro	-
	Complex coacervation	0.1–2833	68.99–96.7
	Sol-gel method	0.18–20	41.83–94
Chemical	*In-situ*	0.1–65	52–83
	Interfacial	1–400	73–95
	Suspension	4–620	70.5–96.3
	Emulsion	0.1–41.3	93.5–97.4

Table 15
the advantages and disadvantages of each encapsulation method along with some limitations.

Methods	Advantages	Disadvantages and limitations
Physical [127,170,218,219]		
Spray-drying	Can enhance thermal conductivity by adding carbon nanotube in feed stream [220] Flexible (easy to combine with other methods) [117] Can scale-up Widely available equipment Smaller capsules within micrometre Organic and inorganic shell is feasible	Difficult to control Agglomeration occurring in drying chamber [115] High temperature needed Remaining leakage due to small portion of uncoated particles Only used for encapsulation of organic PCMs
Solvent evaporation	Easy to conduct Low cost Smaller capsules within micrometre	Difficult to scale up Volatile
Pan-coating	Easy to conduct Low-cost equipment	Difficult to control Hard to isolate capsules
Air-suspension	Easy to conduct Higher production volume	Difficult to control Particle agglomeration
Centrifugal extrusion	Easy to conduct Suitable for bio-encapsulation	High temperature needed
Physio-chemical [170,185,219]		
Ionic gelation	Suitable for thermal conductivity enhancement Simple Low cost	Only suitable for the inorganic shell, like silica or titanium oxide The high temperature for heat treatment High shell permeability
Complex coacervation	Versatile Can produce particles within the nanometre Easy to control particles size Low cost	Agglomeration Difficult to scale up Hardening agent needed Use a large amount of consumption of other solvents [221]
Sol-gel method	High thermal conductivity shell produced Can produce particles within the nanometre mild condition Flexible	pH is needed to be very low formation of continuous gel if the stirring rate or adding rate is not suitable Expensive shell precursors
Chemical [222]		
in-situ	Organic and inorganic shells are feasible The organic and inorganic core can be encapsulated Give rise to large encapsulation efficiency, core content	Might produce harmful substances for the environment [223]
Interfacial	High reaction speed Low permeability	Might produce harmful substances for the environment [223] Fewer kinds of shells available (usually PU)
Suspension	Good heat control More kinds of shells (copolymer, organic and inorganic hybrid)	The water-soluble monomer is not common High cost due to high energy consumption while scale-up Only used for organic PCMs
Emulsion	Used for obtained nanocapsules More kinds of shells (copolymer, organic and inorganic hybrid)	High cost due to high energy consumption while scale-up

cal and chemical methods, the combination of them is a compromise but still needs further deep study especially for the sol-gel method, for which an inorganic shell can be formed. Ionic gelation complex coacervation can result in large particle size, but the former is mainly used in drug delivery. Table 14 summarized the particle size and encapsulation efficiency of collected papers in previous sections, and Table 15 comprehensively summarized the advantages and disadvantages of each specific encapsulation method.

Encapsulation efficiency is a crucial parameter that determines the amount of PCMs encapsulated, and is visualized in Fig. 132. The emulsion polymerisation is efficient (93.4%) and is a highly feasible (smallest interval) technique to produce microcapsules, compared to others. This is mainly because miniemulsion can be

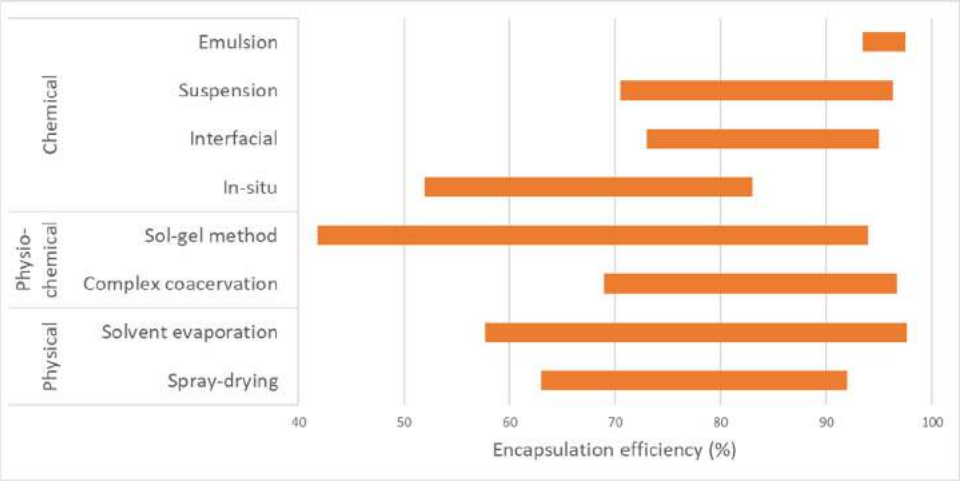

Fig. 132. The encapsulation efficiency comparison of different encapsulation techniques.

Table 16
The latent heat of different kinds of nanocapsules.

Encapsulations	Nanocapsules	Latent heat (kJ/kg)
Spray drying	Paraffin/PS	220.3
In-situ	$Mg(NO_3)_2{\cdot}6H_2O$-$Na_2SO_4{\cdot}10H_2O$/PECA	126.8
	n-Nonadecane/P(St-co-MMA)	76.9
Emulsion	n-heptadecane/PMMA	81.5
	n-hexadecane/PBA	120.16
	Paraffin/PU	7.83
	BA/Poly(MMA-co- 2-HEA)	58
	n-octadecane-n-butyl stearate/Polyacrylate@Titanium dioxide	62.85
Complex coacervation	n-hexadecane/CHI&type-B gelatine	115
	Caprylic acid/Chitosan and gelatine	79
Sol-gel	PA/Silica	180.91
	OA-PEG/SiO_2&SnO_2	58.79

achieved with the help of sonication, meaning that shells can be better formed on these small droplets. The largest difference and the lowest value can be seen for the sol-gel method. This is not only because of the introduction of a new silica precursor (sodium silicate), instead of TEOS, but also the low pH condition. Thus, increasing the encapsulation efficiency of the sol-gel method is a challenge.

The diameter of capsules is another vital parameter. The lower the diameter, the smaller the possibility there is to develop flaws leading to cracked capsules. Table 16 and Fig. 133 illustrate the latent heat of different kinds of nanocapsules produced by different encapsulation techniques. The nanocapsules of paraffin/PS and PA/silica, produced by spray drying and sol-gel method respectively, exhibit high latent heat compared to others. Also, paraffin/PU nanocapsules produced by emulsion polymerisation show poor latent heat. If researchers would like to synthesize nanocapsules by using inorganic shells such as silica to obtain higher thermal conductivity than a polymeric shell, the only way that can be achieved is the sol-gel method, and this again emphasizes the importance of developing this encapsulation technique.

Incorporation of high-performance materials has been recognized as one of the enhancement ways. Table 17 summarizes the heat of fusion and diameter of encapsulated capsules with doped shells, and they are depicted as Fig. 134 (bubble size represents the size of capsules). High-performance material doping can boost the mechanical and thermal conductivity, but the capsule diameter is increased especially while incorporating CNCs achieved by interfacial polymerisation. It is worth noting that after the encapsulation of hexadecane by copolymer and inorganic material doping shell,

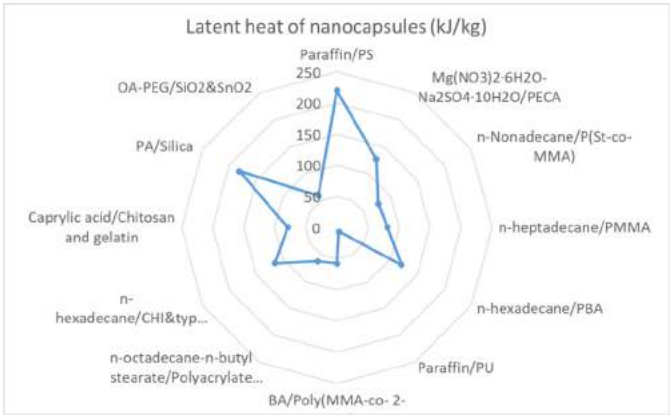

Fig. 133. The radar chart of different nanocapsules and their latent heats.

the latent heat is significantly decreased from more than 200 to 63.1 kJ/kg. Often, researchers will not investigate the thermal conductivity of the encapsulated PCMs they have produced, which is in agreement with the review article by Stonehouse and Abeykoon [15], who was not able to acquire sufficient data on the thermal conductivity of encapsulated PCMs.

Encapsulation by copolymer shell is another effective way to make capsules flexible and durable. Table 18 and Fig. 135 shows the latent heat and diameter after encapsulation by using copolymer. Compared with the doping method, using copolymer for enhancement usually gives a lower latent heat (below 100 kJ/kg).

Table 17
The latent heat and diameter of encapsulated capsules with doped shell by using different encapsulation techniques.

Encapsulations	No.	Encapsulated capsules with doped shell	Heat of fusion (kJ/kg)	Diameter (μm)
Spray drying	1	Rubitherm®RT27/LDPE-PEVA@CNFs	98.1	3.9
In-	2	Paraffin/UF@GO	155.3	42.5
situ	3	1-Decanol/UF@GnP&CuO	120.12	-
Interfacial	4	Methyl laurate/PUU@CNCs	148.43	210
Suspension	5	n-Octadecane/PMMA@Silica	178.9	10
	6	Hexadecane/Poly(MeS-co-DVB)@Titanium dioxide	63.1	27.5
	7	n-eicosane/PUA@GO	181	4
	8	n-octadecane/PMMA@Titanium dioxide	139.26	15
	9	Paraffin/P(MMA-co-MA)@Alumina	105.5	1
Emulsion	10	28#paraffin/PS@Modified silica	86.35	3
	11	n-octadecane@n-butyl stearate/Polyacrylate@Titanium dioxide	62.85	0.085
Complex	12	n-Eicosane/CHI@Silk fibroin	93.04	23
coacervation	13	n-Eicosane/Acacia&gelatine@Clay nanoparticles	114	1.485

Table 18
The heat of fusion and diameter of copolymer-encapsulated PCMs by using different techniques.

Encapsulations	No.	Capsules by using copolymer	Heat of fusion (kJ/kg)	Diameter (μm)
Solvent evaporation	1	Paraffin/Poly (MMA-co-HEMA)	61.8	5
In-situ	2	n-Nonadecane/Poly(St-co-MMA)	76.9	0.16
Suspension	3	Hexadecane/Poly(BA-co-MMA)	63.1	250
	4	Hexadecane/Poly(MeS-co-DVB)@Titanium dioxide	63.1	27.5
	5	Coconut oil/Poly(HEMA-co-SMA)	119	125
Emulsion	6	Paraffin/P(MMA-co-MA)@Alumina	105.5	1
	7	1-dodecanol/Poly(St-co-BA-co-DVB)	132	29.1
	8	Behenic acid/Poly(MMA-co- 2-HEA)	58	0.29

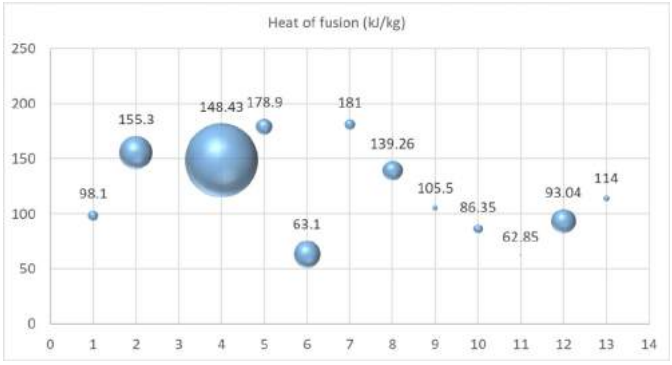

Fig. 134. The bubble chart of differently doped capsules with their heat of fusion and diameter.

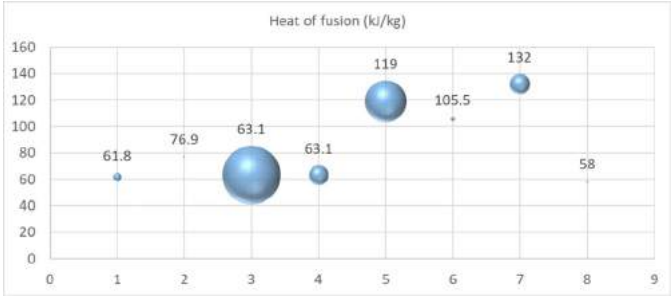

Fig. 135. The bubble chart of copolymer-encapsulated PCMs with their heat of fusion and diameter.

Amongst these capsules, the encapsulation of hexadecane by using Poly(BA-co-MMA) results in large capsules, thus it is a challenge to achieve them with a small diameter. Even with the incorporation of enhancement particles, paraffin capsules can be produced with relatively high latent heat and a small diameter that is close to nanoscale dimensions by using P(MMA-co-MA).

4. Possible directions for future research

As reviewed above, the majority of PCMs, including organic, inorganic, eutectic materials, with a large amount of latent heat, have been listed and compared. Also, the encapsulation methods to use them safely and durably have been reviewed, and some of the latest research has been discussed. However, there is much more potential to be exploited and improved. Suggestions for future research works are given as follows:

- More eutectic and metallic PCMs need to be investigated. It is crucial to explore the different combinations of PCMs. Eutectic and metallic PCMs act as the compromise for overcoming shortcomings from pristine materials. For example, if people are trying to combine two or more materials for higher performance, it is likely to turn out the same or even lower performance than they wish for. Thus, researchers need to guide them.
- The thermal conductivity and mechanical properties play important roles. Many researchers are dedicated to encapsulate PCMs with numerous shell materials and study morphology, encapsulation efficiency, core content, thermal conductivity, thermal reliability, but thermal conductivity and mechanical properties are less focused on. Future researchers could complete these data, because these two properties determin the energy exchange efficiency, especially for organic PCMs, and the strength of preventing leakage. Also, a standard mechanical testing method should be developed.
- The problems of the spray-drying method should be solved for further mass production. The agglomeration in the drying chamber is obvious. Thus, a better design of devices is needed.
- Complex coacervation should be more investigated under neutral and alkaline conditions because it is conducted only under very low pH. Therefore, encapsulation under higher pH should be explored.
- The sol-gel method needs to be further studied. The paper issued about this method is insufficient. If it is well-developed in the future, capsules with superior properties and nano/micrometre size could be obtained for commercial use.

- Multi-functional microcapsules are another promising field. In the previous section, the colour-changeable, antibacterial, electrical energy storage, light-thermal energy conversion, and UV-shielding microcapsules have been discussed. However, this area has not been widely researched yet.
- The incorporation of high-performance materials in the shell could be further studied. This is an effective way to enhance the properties, like adding GO or inorganic particles to improve thermal conductivity and mechanical strength.
- The use of different copolymers to enhance the PCMs properties is an area that could be more investigated because flexible capsules with high mechanical strength can be achieved by designing the copolymer sections. Besides, it is crucial to improve the latent heat after encapsulation because this method is less competitive compared with the incorporation of high-performance materials currently.

7. Conclusions

Energy storage is ever significant due to global warming caused by excessive reliance on traditional resources. PCMs, regarded as alternatives, have lots of benefits that can be drawn upon. Based on this critical review, the pertinent conclusions are drawn below:

- PCMs with various properties from different categories, like organic, inorganic, and eutectic PCMs, are summarized. The advantages and disadvantages of each category are listed along with the analysis indicating their melting point and latent heat ranges. Metallic and inorganic compounds are the most suitable to be used in areas that need high-temperature energy storage and fast energy exchanging. Other PCMs are more advantageous in mild temperature energy storage fields which are mostly paid attention to. For example, organic PCMs are stable, non-toxic, but have a poor thermal conductivity that needs to be enhanced. Inorganic PCMs exhibit excellent thermal conductivity, but also corrosion and supercooling. Eutectic PCMs properties depend on the composition of PCMs and the production methods used, careful choice is required to obtain improved performance for different compositions.
- Moreover, encapsulation methods such as chemical, physical, and physio-chemical methods, are investigated by consulting a large amount of research, followed by the integration of key thermophysical properties. Solvent evaporation and spray-drying are two effective physical methods used in the encapsulation of PCMs, which give smaller particle sizes and high feasibility. Apart from ionic gelation, merely used in PCMs, complex coacervation and sol-gel methods are advantageous for the formation of the inorganic shell with high thermal conductivity like silica, but agglomeration and low pH conditions limit their application. All chemical methods including *in-situ*, interfacial, suspension and emulsion polymerisation can obtain smaller capsule sizes with narrow distributions. Also, tunable morphology and the possibility to incorporate reinforced materials are promising, but still face the difficulty of massive production.
- For possible future research areas, the thermal conductivity of capsules should be measured because previous researchers usually neglect this critically useful property. Test methods of mechanical properties should be standardized by using one criterion so that researchers can universally compare. Also, eutectic and metallic PCMs, sol-gel encapsulation method, complex coacervation method, and spray drying are the areas that can be further investigated for better microcapsule performance, high microcapsule yield, and improved synthesis conditions. In the future, bifunctional microcapsules, copolymer encapsulation, and doped high-performance materials are highly promising for developing applications like textiles, construction, etc.

Data availability

No data was used for the research described in the article.

Acknowledgments

We would like to acknowledge the funding support provided by Engineering and Physical Sciences Research Council (EPSRC), UK under the grant number EP/T517823/1.

References

[1] R. Huang, et al., Carbon precursors in coal tar: extraction and preparation of carbon materials, Sci. Total Environ. 788 (2021) 147697, doi:10.1016/j.scitotenv.2021.147697.
[2] R. Pradhan, Energy geopolitics and the new great game in Central Asia, Millenn. Asia (2021) 097639962110032, doi:10.1177/09763996211003260.
[3] T. Kober, H.W. Schiffer, M. Densing, E. Panos, Global energy perspectives to 2060 – WEC's World Energy Scenarios 2019, Energy Strategy Rev. 31 (2020) 100523 /09/01/2020, doi:10.1016/j.esr.2020.100523.
[4] Z. Zhang, et al., A review of technologies and applications on versatile energy storage systems, Renew. Sustain. Energy Rev. 148 (2021) 111263 /09/01/2021, doi:10.1016/j.rser.2021.111263.
[5] International Energy Agency, World Energy Outlook 2011, 666, International Energy Agency, 2011.
[6] S.A. Alkaff, S.C. Sim, M.N. Ervina Efzan, A review of underground building towards thermal energy efficiency and sustainable development, Renew. Sustain. Energy Rev. 60 (2016) 692–713 /07/01/2016, doi:10.1016/j.rser.2015.12.085.
[7] B. Akhmetov, A.G. Georgiev, A. Kaltayev, A.A. Dzhomartov, R. Popov, M.S. Tungatarova, Thermal energy storage systems - review, Bulg. Chem. Commun. 48 (2016) 31–40.
[8] U. Stritih, E. Osterman, H. Evliya, V. Butala, H. Paksoy, Exploiting solar energy potential through thermal energy storage in Slovenia and Turkey, Renew. Sustain. Energy Rev. 25 (2013) 442–461 /09/01/2013, doi:10.1016/j.rser.2013.04.020.
[9] N. Yu, R.Z. Wang, T.X. Li, L.W. Wang, in: Progress in Sorption Thermal Energy Storage, Springer International Publishing, 2017, pp. 541–572.
[10] A.A. Al-Abidi, S. Bin Mat, K. Sopian, M.Y. Sulaiman, C.H. Lim, A. Th, Review of thermal energy storage for air conditioning systems, Renew. Sustain. Energy Rev. 16 (8) (2012) 5802–5819 /10/01/2012, doi:10.1016/j.rser.2012.05.030.
[11] G. Raam Dheep, A. Sreekumar, Influence of nanomaterials on properties of latent heat solar thermal energy storage materials – a review, Energy Convers. Manag. 83 (2014) 133–148, doi:10.1016/j.enconman.2014.03.058.
[12] N. Zhang, Y. Yuan, X. Cao, Y. Du, Z. Zhang, Y. Gui, Latent heat thermal energy storage systems with solid-liquid phase change materials: a review, Adv. Eng. Mater. 20 (6) (2018) 1700753, doi:10.1002/adem.201700753.
[13] X. Huo, et al., Chitosan composite microencapsulated comb-like polymeric phase change material via coacervation microencapsulation, Carbohydr. Polym. 200 (2018) 602–610.
[14] F. Souayfane, F. Fardoun, P.H. Biwole, Phase change materials (PCM) for cooling applications in buildings: a review, Energy Build. 129 (2016) 396–431.
[15] A. Stonehouse, C. Abeykoon, Thermal properties of phase change materials reinforced with multi-dimensional carbon nanomaterials, Int. J. Heat Mass Transf. 183 (2022) 122166 /02/01/2022, doi:10.1016/j.ijheatmasstransfer.2021.122166.
[16] Z. Ling, F. Wang, X. Fang, X. Gao, Z. Zhang, A hybrid thermal management system for lithium ion batteries combining phase change materials with forced-air cooling, Appl. Energy 148 (2015) 403–409, doi:10.1016/j.apenergy.2015.03.080.
[17] E. Alehosseini, S.M. Jafari, Micro/nano-encapsulated phase change materials (PCMs) as emerging materials for the food industry, Trends Food Sci. Technol. 91 (2019) 116–128 /09/01/2019, doi:10.1016/j.tifs.2019.07.003.
[18] M.H. Abokersh, M. Osman, O. El-Baz, M. El-Morsi, O. Sharaf, Review of the phase change material (PCM) usage for solar domestic water heating systems (SDWHS), Int. J. Energy Res. 42 (2) (2018) 329–357, doi:10.1002/er.3765.
[19] H. Akeiber, et al., A review on phase change material (PCM) for sustainable passive cooling in building envelopes, Renew. Sustain. Energy Rev. 60 (2016) 1470–1497 /07/01/2016, doi:10.1016/j.rser.2016.03.036.
[20] L.F. Cabeza, A. Castell, C. Barreneche, A. de Gracia, and A.I. Fernández, Materials used as PCM in thermal energy storage in buildings: a review, Renew. Sustain. Energy Rev., vol. 15, no. 3, pp. 1675–1695, 2011/04/01/2011, doi: 10.1016/j.rser.2010.11.018.
[21] M. Mastani Joybari, F. Haghighat, J. Moffat, and P. Sra, Heat and cold storage using phase change materials in domestic refrigeration systems: the state-of-the-art review, Energy Build., vol. 106, pp. 111–124, 2015/11/01/2015, doi: 10.1016/j.enbuild.2015.06.016.

[22] N. Sarier, E. Onder, Organic phase change materials and their textile applications: an overview, Thermochim. Acta 540 (2012) 7–60 /07/20/2012, doi:10.1016/j.tca.2012.04.013.
[23] G. Li, Y. Hwang, R. Radermacher, Review of cold storage materials for air conditioning application, Int. J. Refrig. 35 (8) (2012) 2053–2077 /12/01/2012, doi:10.1016/j.ijrefrig.2012.06.003.
[24] S.N. Gunasekara, V. Martin, J.N. Chiu, Phase equilibrium in the design of phase change materials for thermal energy storage: state-of-the-art, Renew. Sustain. Energy Rev. 73 (2017) 558–581.
[25] S. Chandel, T. Agarwal, Review of current state of research on energy storage, toxicity, health hazards and commercialization of phase changing materials, Renew. Sustain. Energy Rev. 67 (2017) 581–596.
[26] L. Zhang, et al., Graphene oxide-modified microencapsulated phase change materials with high encapsulation capacity and enhanced leakage-prevention performance, Appl. Energy 197 (2017) 354–363.
[27] L. Fan, J.M. Khodadadi, Thermal conductivity enhancement of phase change materials for thermal energy storage: a review, Renew. Sustain. Energy Rev. 15 (1) (2011) 24–46.
[28] Y. Zhang, S. Zheng, S. Zhu, J. Ma, Z. Sun, M. Farid, Evaluation of paraffin infiltrated in various porous silica matrices as shape-stabilized phase change materials for thermal energy storage, Energy Convers. Manag. 171 (2018) 361–370 /09/01/2018, doi:10.1016/j.enconman.2018.06.002.
[29] G. Fang, Z. Chen, H. Li, Synthesis and properties of microencapsulated paraffin composites with SiO_2 shell as thermal energy storage materials, Chem. Eng. J. 163 (1) (2010) 154–159 /09/15/2010, doi:10.1016/j.cej.2010.07.054.
[30] Y. Zhu, et al., Nanoencapsulated phase change materials with polymer-SiO2 hybrid shell materials: compositions, morphologies, and properties, Energy Convers. Manag. 164 (2018) 83–92 /05/15/2018, doi:10.1016/j.enconman.2018.02.075.
[31] Q. Lian, Y. Li, A.A.S. Sayyed, J. Cheng, J. Zhang, Facile strategy in designing epoxy/paraffin multiple phase change materials for thermal energy storage applications, ACS Sustain. Chem. Eng. 6 (3) (2018) 3375–3384 /03/05 2018, doi:10.1021/acssuschemeng.7b03558.
[32] A.M. Szczotok, I. Garrido, M. Carmona, A.L. Kjøniksen, J.F. Rodriguez, Predicting microcapsules morphology and encapsulation efficiency by combining the spreading coefficient theory and polar surface energy component, Colloids Surf. A 554 (2018) 49–59 /10/05/2018, doi:10.1016/j.colsurfa.2018.06.022.
[33] B.K. Green, Pressure sensitive record material, ed: Google Patents, 1955.
[34] A.M. Pisoschi, A. Pop, C. Cimpeanu, V. Turcuş, G. Predoi, F. Iordache, Nanoencapsulation techniques for compounds and products with antioxidant and antimicrobial activity-a critical view, Eur. J. Med. Chem. 157 (2018) 1326–1345.
[35] X. Liu, H. Liu, S. Wang, L. Zhang, H. Cheng, RETRACTED: Preparation and Thermal Properties of Form Stable Paraffin Phase Change Material Encapsulation, Elsevier, 2006 ed.
[36] G.H. Zhang, S.A. Bon, C.Y. Zhao, Synthesis, characterization and thermal properties of novel nanoencapsulated phase change materials for thermal energy storage, Sol. Energy 86 (5) (2012) 1149–1154.
[37] N. Zhang, Y. Yuan, Synthesis and thermal properties of nanoencapsulation of paraffin as phase change material for latent heat thermal energy storage, Energy Built Environ. 1 (4) (2020) 410–416.
[38] T.A. Comunian, C.S. Favaro-Trindade, Microencapsulation using biopolymers as an alternative to produce food enhanced with phytosterols and omega-3 fatty acids: a review, Food Hydrocoll. 61 (2016) 442–457.
[39] J. Li, M. Yao, Y. Shao, D. Yao, The application of bio-nanotechnology in tumor diagnosis and treatment: a view, Nanotechnol. Rev. 7 (3) (2018) 257–266.
[40] D.Q. Ng, Y.L. Tseng, Y.F. Shih, H.Y. Lian, Y.H. Yu, Synthesis of novel phase change material microcapsule and its application, Polymer 133 (2017) 250–262.
[41] R. Pichandi, K. Murugavel Kulandaivelu, K. Alagar, H.K. Dhevaguru, S. Ganesamoorthy, Performance enhancement of photovoltaic module by integrating eutectic inorganic phase change material, Energy Sources Part A Recovery Util. Environ. Eff. 42 (2020) 1–18.
[42] M.K. Rathod, J. Banerjee, Thermal stability of phase change materials used in latent heat energy storage systems: a review, Renew. Sustain. Energy Rev. 18 (2013) 246–258 /02/01/2013, doi:10.1016/j.rser.2012.10.022.
[43] S. Xie, et al., A thermally stable phase change material with high latent heat based on an oxalic acid dihydrate/boric acid binary eutectic system, Sol. Energy Mater. Sol. Cells 168 (2017) 38–44.
[44] V.J. Reddy, K. Akhila, P. Dixit, J. Singh, S. Parvate, S. Chattopadhyay, Thermal buffering performance evaluation of fatty acids blend/fatty alcohol based eutectic phase change material and simulation, J. Energy Storage 38 (2021) 102499.
[45] Y. Konuklu, N. Şahan, H. Paksoy, 2.14 latent heat storage systems, Comprehensive Energy Systems 11 (11) (2018) 396–434.
[46] Z. Li, E. Gariboldi, Review on the temperature-dependent thermophysical properties of liquid paraffins and composite phase change materials with metallic porous structures, Mater. Today Energy 20 (2021) 100642 /06/01/2021, doi:10.1016/j.mtener.2021.100642.
[47] I. Sarbu, A. Dorca, Review on heat transfer analysis in thermal energy storage using latent heat storage systems and phase change materials, Int. J. Energy Res. 43 (1) (2019) 29–64.
[48] A.A. Abuelnuor, A.A. Omara, K.M. Saqr, I.H. Elhag, Improving indoor thermal comfort by using phase change materials: a review, Int. J. Energy Res. 42 (6) (2018) 2084–2103.
[49] J. Radulovic, D. Nikolic, M. Blagojevic, I. Miletic, M. Vaskovic, A review of new materials used for building integrated systems, in: Proceedings of the First International Conference on Building Integrated Renewable Energy Systems BIRES, 2017.
[50] S.M. Merritt, et al., Gas barrier polymer nanocomposite films prepared by graphene oxide encapsulated polystyrene microparticles, ACS Appl. Polym. Mater. 2 (2) (2020) 725–731.
[51] Y.E. Milian, A. Gutierrez, M. Grageda, S. Ushak, A review on encapsulation techniques for inorganic phase change materials and the influence on their thermophysical properties, Renew. Sustain. Energy Rev. 73 (2017) 983–999.
[52] S.A. Mohamed, et al., A review on current status and challenges of inorganic phase change materials for thermal energy storage systems, Renew. Sustain. Energy Rev. 70 (2017) 1072–1089.
[53] B. Zhao, et al., Thermal conductivity enhancement and shape stabilization of phase change thermal storage material reinforced by combustion synthesized porous Al_2O_3, J. Energy Storage 42 (2021) 103028 /10/01/2021, doi:10.1016/j.est.2021.103028.
[54] E.H. Benchara, S. Jennah, N. Belouggadia, K. Mansouri, O. Bouattane, Thermal energy storage by phase change materials suitable for solar water heaters: an updated review, in: Proceedings of the IEEE 2nd International Conference on Electronics, Control, Optimization and Computer Science (ICECOCS), IEEE, 2020, pp. 1–10.
[55] W. Su, J. Darkwa, G. Kokogiannakis, Review of solid–liquid phase change materials and their encapsulation technologies, Renew. Sustain. Energy Rev. 48 (2015) 373–391, doi:10.1016/j.rser.2015.04.044.
[56] V. Tatevskii, in: Physicochemical Properties of Individual Hydrocarbons, Gostoptekhizdat, Moscow, 1960, pp. 21–57.
[57] F. Javadi, H. Metselaar, P. Ganesan, Performance improvement of solar thermal systems integrated with phase change materials (PCM), a review, Sol. Energy 206 (2020) 330–352.
[58] S. Rostami, et al., A review of melting and freezing processes of PCM/nano-PCM and their application in energy storage, Energy 211 (2020) 118698.
[59] S. Kashyap, S. Kabra, B. Kandasubramanian, Graphene aerogel-based phase changing composites for thermal energy storage systems, J. Mater. Sci. 55 (10) (2020) 4127–4156.
[60] S. Lieskoski, Developing a demo environment on phase change materials, 2020.
[61] S.J. Chang, Y. Kang, S. Wi, S.G. Jeong, S. Kim, Hygrothermal performance improvement of the Korean wood frame walls using macro-packed phase change materials (MPPCM), Appl. Therm. Eng. 114 (2017) 457–465.
[62] C. Cárdenas-Ramírez, M.A. Gómez, F. Jaramillo, A.G. Fernández, L.F. Cabeza, Thermal reliability of organic-organic phase change materials and their shape-stabilized composites, J. Energy Storage 40 (2021) 102661 /08/01/2021, doi:10.1016/j.est.2021.102661.
[63] D.G. Atinafu, W. Dong, X. Huang, H. Gao, G. Wang, Introduction of organic-organic eutectic PCM in mesoporous N-doped carbons for enhanced thermal conductivity and energy storage capacity, Appl. Energy 211 (2018) 1203–1215 /02/01/2018, doi:10.1016/j.apenergy.2017.12.025.
[64] K. Pielichowska, K. Pielichowski, Phase change materials for thermal energy storage, Prog. Mater. Sci. 65 (2014) 67–123 /08/01/2014, doi:10.1016/j.pmatsci.2014.03.005.
[65] J. Pereira Da Cunha, P. Eames, Thermal energy storage for low and medium temperature applications using phase change materials – a review, Appl. Energy 177 (2016) 227–238, doi:10.1016/j.apenergy.2016.05.097.
[66] X. Huang, G. Alva, Y. Jia, G. Fang, Morphological characterization and applications of phase change materials in thermal energy storage: a review, Renew. Sustain. Energy Rev. 72 (2017) 128–145.
[67] Y. Jiang, Y. Sun, M. Liu, F. Bruno, S. Li, Eutectic Na_2CO_3-NaCl salt: a new phase change material for high temperature thermal storage, Sol. Energy Mater. Sol. Cells 152 (2016) 155–160 /08/01/2016, doi:10.1016/j.solmat.2016.04.002.
[68] D. Groulx, Thermal energy storage for temperature management of electronics, in: Advances in Thermal Energy Storage Systems, Elsevier, 2021, pp. 725–748.
[69] T. Zhao, M. Zheng, A. Munis, J. Hu, H. Teng, L. Wei, Corrosion behaviours of typical metals in molten hydrate salt of $Na_2HPO_4 \cdot 12H_2O$–$Na_2SO_4 \cdot 10H_2O$ for thermal energy storage, Corros. Eng. Sci. Technol. 54 (5) (2019) 379–388.
[70] H. Faraji, A. Benkaddour, K. Oudaoui, M. El Alami, M. Faraji, Emerging applications of phase change materials: a concise review of recent advances, Heat Transf. 50 (2) (2020) 1443–1493.
[71] A. El-Sebaii, S. Al-Amir, F. Al-Marzouki, A.S. Faidah, A. Al-Ghamdi, S. Al-Heniti, Fast thermal cycling of acetanilide and magnesium chloride hexahydrate for indoor solar cooking, Energy Convers. Manag. 50 (12) (2009) 3104–3111.
[72] P.J. Shamberger, N.M. Bruno, Review of metallic phase change materials for high heat flux transient thermal management applications, Appl. Energy 258 (2020) 113955.
[73] J. Hirschey, K.R. Gluesenkamp, A. Mallow, and S. Graham, Review of Inorganic Salt Hydrates with Phase Change Temperature in Range of 5 to 60°C and Material Cost Comparison with Common Waxes, 2018.
[74] B. Kocak, A.I. Fernandez, H. Paksoy, Review on sensible thermal energy storage for industrial solar applications and sustainability aspects, Sol. Energy 209 (2020) 135–169.
[75] M. Mofijur, et al., Phase change materials (PCM) for solar energy usages and storage: an overview, Energies 12 (16) (2019) 3167.
[76] C.E. Andraka, A.M. Kruizenga, B.A. Hernandez-Sanchez, E.N. Coker, Metallic phase change material thermal storage for dish Stirling, Energy Procedia 69 (2015) 726–736.

[77] M. Guo, M. Liang, Y. Jiao, W. Zhao, Y. Duan, H. Liu, A review of phase change materials in asphalt binder and asphalt mixture, Constr. Build. Mater. 258 (2020) 119565.
[78] N.R. Jankowski, Phase Change Materials For Vehicle and Electronic Transient Thermal Systems, University of Maryland, College Park, 2020.
[79] M.I. Lone, R. Jilte, A review on phase change materials for different applications, Mater. Today Proc. 46 (20) (2021) 10980–10986.
[80] W. Kraft, V. Stahl, P. Vetter, Thermal storage using metallic phase change materials for bus heating-state of the art of electric buses and requirements for the storage system, Energies 13 (11) (2020) 3023.
[81] E.A. Brandes, G. Brook, Smithells Metals Reference Book, Elsevier, 2013.
[82] K. Dutkowski, M. Kruzel, B. Zajączkowski, Determining the heat of fusion and specific heat of microencapsulated phase change material slurry by thermal delay method, Energies 14 (1) (2021) 179.
[83] A.E. Gheribi, A.D. Pelton, J.P. Harvey, Determination of optimal compositions and properties for phase change materials in a solar electric generating station, Sol. Energy Mater. Sol. Cells 210 (2020) 110506.
[84] M.M. Kenisarin, High-temperature phase change materials for thermal energy storage, Renew. Sustain. Energy Rev. 14 (3) (2010) 955–970, doi:10.1016/j.rser.2009.11.011.
[85] S. Koohi-Fayegh, M.A. Rosen, A review of energy storage types, applications and recent developments, J. Energy Storage 27 (2020) 101047.
[86] J. Hadiya, A.K.N. Shukla, Thermal energy storage using phase change materials: a way forward, Int. J. Glob. Energy Issues 41 (1-4) (2018) 108–127.
[87] K. Iqbal, et al., Phase change materials, their synthesis and application in textiles-a review, J. Text. Inst. 110 (4) (2019) 625–638.
[88] N. Şahan, H. Paksoy, Determining influences of SiO2 encapsulation on thermal energy storage properties of different phase change materials, Sol. Energy Mater. Sol. Cells 159 (2017) 1–7.
[89] U. Berardi, S. Soudian, Experimental investigation of latent heat thermal energy storage using PCMs with different melting temperatures for building retrofit, Energy Build. 185 (2019) 180–195.
[90] S. Kahwaji, M.A. White, Prediction of the properties of eutectic fatty acid phase change materials, Thermochim. Acta 660 (2018) 94–100 /02/10/2018, doi:10.1016/j.tca.2017.12.024.
[91] A. Gaur, Latent heat utilization approach and the role of phase change materials, World Sci. News 112 (2018) 118–129.
[92] M. Ismail, Intensification of Heat Transfer in Thermal Energy Storage Systems With Phase Change Materials, Nothumbria University, 2019.
[93] H.M. Ali, Applications of combined/hybrid use of heat pipe and phase change materials in energy storage and cooling systems: a recent review, J. Energy Storage 26 (2019) 100986.
[94] B. Cambou, P. Dubujet, Difficulties and limitation of statistical homogenization in granular materials, in: Continuous and Discontinuous Modelling of Cohesive-Frictional Materials, Springer, 2001, pp. 205–214.
[95] L. Cong, X. She, G. Leng, G. Qiao, C. Li, Y. Ding, Formulation and characterisation of ternary salt based solutions as phase change materials for cold chain applications, Energy Procedia 158 (2019) 5103–5108, doi:10.1016/j.egypro.2019.01.690.
[96] A. Sivanathan, et al., Phase change materials for building construction: an overview of nano-/micro-encapsulation, Nanotechnol. Rev. 9 (1) (2020) 896–921, doi:10.1515/ntrev-2020-0067.
[97] S.A. Mohamed, et al., A review on current status and challenges of inorganic phase change materials for thermal energy storage systems, Renew. Sustain. Energy Rev. 70 (2017) 1072–1089, doi:10.1016/j.rser.2016.12.012.
[98] A. Sharma, V.V. Tyagi, C.R. Chen, D. Buddhi, Review on thermal energy storage with phase change materials and applications, Renew. Sustain. Energy Rev. 13 (2) (2009) 318–345, doi:10.1016/j.rser.2007.10.005.
[99] H. Nazir, et al., Recent developments in phase change materials for energy storage applications: a review, Int. J. Heat Mass Transf. 129 (2019) 491–523, doi:10.1016/j.ijheatmasstransfer.2018.09.126.
[100] J.L. Zeng, Z. Cao, D.W. Yang, L.X. Sun, L. Zhang, Thermal conductivity enhancement of Ag nanowires on an organic phase change material, J. Therm. Anal. Calorim. 101 (1) (2010) 385–389 2010/07/01, doi:10.1007/s10973-009-0472-y.
[101] A.H. Alkhazaleh, Preparation and characterization of isopropyl palmitate/expanded perlite and isopropyl palmitate/nanoclay composites as form-stable thermal energy storage materials for buildings, J. Energy Storage 32 (2020) 101679 /12/01/2020, doi:10.1016/j.est.2020.101679.
[102] S. Harikrishnan, S. Kalaiselvam, Preparation and thermal characteristics of CuO–oleic acid nanofluids as a phase change material, Thermochim. Acta 533 (2012) 46–55 /04/10/2012, doi:10.1016/j.tca.2012.01.018.
[103] A.M. Szczotok, M. Carmona, A.L. Kjøniksen, J.F. Rodriguez, The role of radical polymerization in the production of thermoregulating microcapsules or polymers from saturated and unsaturated fatty acids, J. Appl. Polym. Sci. 135 (10) (2018) 45970, doi:10.1002/app.45970.
[104] D. Dadarlat, D. Bicanic, J. Gibkes, W. Kloek, I. Van Den Dries, E. Gerkema, Study of melting processes in fatty acids and oils mixtures. A comparison of photopyroelectric (PPE) and differential scanning calorimetry (DSC), Chem. Phys. Lipids 82 (1) (1996) 15–23, doi:10.1016/0009-3084(96)02555-8.
[105] H. Kumano, A. Saito, S. Okawa, K. Takeda, A. Okuda, Study of direct contact melting with hydrocarbon mixtures as the PCM, Int. J. Heat Mass Transf. 48 (15) (2005) 3212–3220, doi:10.1016/j.ijheatmasstransfer.2005.01.040.
[106] G. Coccia, G. Di Nicola, S. Tomassetti, M. Pierantozzi, M. Chieruzzi, L. Torre, Experimental validation of a high-temperature solar box cooker with a solar-salt-based thermal storage unit, Sol. Energy 170 (2018) 1016–1025, doi:10.1016/j.solener.2018.06.021.
[107] Z. Li, M. Zhou, F. Wu, L. Shen, X. Lin, Y. Feng, Direct compaction properties of Zingiberis Rhizoma extracted powders coated with various shell materials: Improvements and mechanism analysis, Int. J. Pharm. 564 (2019) 10–21.
[108] S.S. Jyothi, A. Seethadevi, K.S. Prabha, P. Muthuprasanna, P. Pavitra, Microencapsulation: a review, Int. J. Pharm. Biol. Sci 3 (2012) 509–531.
[109] M.M. Umair, Y. Zhang, K. Iqbal, S. Zhang, B. Tang, Novel strategies and supporting materials applied to shape-stabilize organic phase change materials for thermal energy storage–a review, Appl. Energy 235 (2019) 846–873.
[110] M. Kazemi, M. Ghobadi, A. Mirzaie, Cobalt ferrite nanoparticles (CoFe2O4 MNPs) as catalyst and support: magnetically recoverable nanocatalysts in organic synthesis, Nanotechnol. Rev. 7 (1) (2018) 43–68.
[111] E.M. Shchukina, M. Graham, Z. Zheng, D.G. Shchukin, Nanoencapsulation of phase change materials for advanced thermal energy storage systems, (in English), Chem. Soc. Rev. 47 (11) (Jun 2018) 4156–4175 Review, doi:10.1039/c8cs00099a.
[112] C. Thies, Microencapsulation, Kirk-Othmer Encyclopedia of Chemical Technology, John Wiley & Sons, Inc., 2000, doi:10.1002/0471238961.1309031820080905.a01.
[113] M.N.A. Hawlader, M.S. Uddin, M.M. Khin, Microencapsulated PCM thermal-energy storage system, Appl. Energy 74 (1) (2003) 195–202 /01/01/2003, doi:10.1016/S0306-2619(02)00146-0.
[114] W. Wu, et al., Jet impingement and spray cooling using slurry of nanoencapsulated phase change materials, Int. J. Heat Mass Transf. 54 (13) (2011) 2715–2723 /06/01/2011, doi:10.1016/j.ijheatmasstransfer.2011.03.022.
[115] A.M. Borreguero, J.L. Valverde, J.F. Rodríguez, A.H. Barber, J.J. Cubillo, M. Carmona, Synthesis and characterization of microcapsules containing Rubitherm®RT27 obtained by spray drying, Chem. Eng. J. 166 (1) (2011) 384–390 /01/01/2011, doi:10.1016/j.cej.2010.10.055.
[116] W. Li, R. Huang, J. Zong, X. Zhang, Microencapsulation and morphological characterization of renewable microencapsulated phase-change materials with cellulose diacetate shell, ChemistrySelect 2 (21) (2017) 5917–5923, doi:10.1002/slct.201701078.
[117] R. Methaapanon, S. Kornbongkotmas, C. Ataboonwongse, A. Soottitantawat, Microencapsulation of n-octadecane and methyl palmitate phase change materials in silica by spray drying process, Powder Technol. 361 (2020) 910–916 /02/01/2020, doi:10.1016/j.powtec.2019.10.114.
[118] F. Ahangaran, A.H. Navarchian, F. Picchioni, Material encapsulation in poly(methyl methacrylate) shell: a review, J. Appl. Polym. Sci. 136 (41) (2019) 48039, doi:10.1002/app.48039.
[119] H. Es-haghi, S.M. Mirabedini, M. Imani, R.R. Farnood, Preparation and characterization of pre-silane modified ethyl cellulose-based microcapsules containing linseed oil, Colloids Surf. A 447 (2014) 71–80 /04/05/2014, doi:10.1016/j.colsurfa.2014.01.021.
[120] M. Fashandi, S.N. Leung, Preparation and characterization of 100% bio-based polylactic acid/palmitic acid microcapsules for thermal energy storage, Mater. Renew. Sustain. Energy 6 (3) (2017), doi:10.1007/s40243-017-0098-0.
[121] Y. Lin, C. Zhu, G. Alva, G. Fang, Microencapsulation and thermal properties of myristic acid with ethyl cellulose shell for thermal energy storage, Appl. Energy 231 (2018) 494–501 /12/01/2018, doi:10.1016/j.apenergy.2018.09.154.
[122] A. Khan, P. Saikia, R. Saxena, D. Rakshit, S. Saha, Microencapsulation of phase change material in water dispersible polymeric particles for thermoregulating rubber composites-a holistic approach, Int. J. Energy Res. 44 (3) (2020) 1567–1579, doi:10.1002/er.4925.
[123] S. Saha, Ifra, Fabrication of topologically anisotropic microparticles and their surface modification with pH responsive polymer brush, Mater. Sci. Eng. C 104 (2019) 109894 /11/01/2019, doi:10.1016/j.msec.2019.109894.
[124] F. Wang, et al., Cellulose nanocrystals-composited poly (methyl methacrylate) encapsulated n-eicosane via a Pickering emulsion-templating approach for energy storage, Carbohydr. Polym. 234 (2020) 115934 /04/15/2020, doi:10.1016/j.carbpol.2020.115934.
[125] Y. Chevalier, M.A. Bolzinger, Emulsions stabilized with solid nanoparticles: pickering emulsions, Colloids Surf. A 439 (2013) 23–34 /12/20/2013, doi:10.1016/j.colsurfa.2013.02.054.
[126] J. Xing, et al., Microencapsulation of fatty acid eutectic with polyvinyl chloride shell used for thermal energy storage, J. Energy Storage 34 (2021) 101998 /02/01/2021, doi:10.1016/j.est.2020.101998.
[127] P. Venkatesan, R. Manavalan, K. Valliappan, Microencapsulation: a vital technique in novel drug delivery system, J. Pharm. Sci. Res. 1 (4) (2009) 26–35.
[128] S.K. Ghosh, Functional coatings and microencapsulation: a general perspective, 2006 Funct. Coat. 1–28.
[129] Z. Chen, G. Fang, Preparation and heat transfer characteristics of microencapsulated phase change material slurry: a review, Renew. Sustain. Energy Rev. 15 (9) (2011) 4624–4632 /12/01/2011, doi:10.1016/j.rser.2011.07.090.
[130] D. Poncelet, Microencapsulation: fundamentals, methods and applications, in: Surface Chemistry in Biomedical and Environmental Science, Springer, 2006, pp. 23–34.
[131] J.P. Wang, X.X. Zhang, X.C. Wang, Preparation, characterization and permeation kinetics description of calcium alginate macro-capsules containing shape-stabilize phase change materials, Renew. Energy 36 (11) (2011) 2984–2991 /11/01/2011, doi:10.1016/j.renene.2011.03.039.
[132] A. Jamekhorshid, S. Sadrameli, M. Farid, A review of microencapsulation methods of phase change materials (PCMs) as a thermal energy storage (TES) medium, Renew. Sustain. Energy Rev. 31 (2014) 531–542.
[133] M. Graham, E. Shchukina, P.F. De Castro, D. Shchukin, Nanocapsules containing salt hydrate phase change materials for thermal energy storage, J. Mater. Chem. A 4 (43) (2016) 16906–16912, doi:10.1039/c6ta06189c.

[134] Z. Qiao, J. Mao, Enhanced thermal properties with graphene oxide in the urea-formaldehyde microcapsules containing paraffin PCMs, J. Microencapsul. 34 (1) (2017) 1–9 2017/01/02, doi:10.1080/02652048.2016.1267811.
[135] E. Morales-Narváez, L.F. Sgobbi, S.A.S. Machado, A. Merkoçi, Graphene-encapsulated materials: synthesis, applications and trends, Prog. Mater. Sci. 86 (2017) 1–24 /05/01/2017, doi:10.1016/j.pmatsci.2017.01.001.
[136] V. Pethurajan, S. Sivan, Fabrication, characterisation and heat transfer study on microencapsulation of nano-enhanced phase change material, Chem. Eng. Process. Process Intensif. 133 (2018) 12–23 /11/01/2018, doi:10.1016/j.cep.2018.09.014.
[137] S.R. Rakkappan, S. Sivan, V. Pethurajan, A. Aditya, H. Mittal, Preparation and thermal properties of encapsulated 1-Decanol for low- temperature heat transfer fluid application, Colloids Surf. A 614 (2021) 126167 /04/05/2021, doi:10.1016/j.colsurfa.2021.126167.
[138] M. Graham, J.A. Coca-Clemente, E. Shchukina, D. Shchukin, Nanoencapsulated crystallohydrate mixtures for advanced thermal energy storage, J. Mater. Chem. A 5 (26) (2017) 13683–13691, doi:10.1039/c7ta02494k.
[139] T. Khadiran, M.Z. Hussein, Z. Zainal, R. Rusli, Nano-encapsulated n-nonadecane using vinyl copolymer shell for thermal energy storage medium, Macromol. Res. 23 (7) (2015) 658–669, doi:10.1007/s13233-015-3088-z.
[140] C. Huang, et al., A novel bifunctional microencapsulated phase change material loaded with ZnO for thermal energy storage and light–thermal energy conversion, Sustain. Energy Fuels 4 (10) (2020) 5203–5214, doi:10.1039/d0se00718h.
[141] J. Cheng, et al., The thermal behavior and flame retardant performance of phase change material microcapsules with modified carbon nanotubes, Energy 240 (2022) 122821 /02/01/2022, doi:10.1016/j.energy.2021.122821.
[142] J.S. Cho, A. Kwon, C.G. Cho, Microencapsulation of octadecane as a phase-change material by interfacial polymerization in an emulsion system, Colloid Polym. Sci. 280 (3) (2002) 260–266 2002/03/01, doi:10.1007/s00396-001-0603-x.
[143] X.Z. Lan, Z.C. Tan, G.L. Zou, L.X. Sun, T. Zhang, Microencapsulation of n-eicosane as energy storage material, Chin. J. Chem. 22 (5) (2010) 411–414, doi:10.1002/cjoc.20040220502.
[144] F. Salaün, G. Bedek, E. Devaux, D. Dupont, L. Gengembre, Microencapsulation of a cooling agent by interfacial polymerization: Influence of the parameters of encapsulation on poly(urethane–urea) microparticles characteristics, J. Membr. Sci. 370 (1-2) (2011) 23–33, doi:10.1016/j.memsci.2010.11.033.
[145] Y. Yoo, C. Martinez, J.P. Youngblood, Synthesis and characterization of microencapsulated phase change materials with poly(urea–urethane) shells containing cellulose nanocrystals, ACS Appl. Mater. Interfaces 9 (37) (2017) 31763–31776, doi:10.1021/acsami.7b06970.
[146] S. Lu, J. Xing, Z. Zhang, G. Jia, Preparation and characterization of polyurea/polyurethane double-shell microcapsules containing butyl stearate through interfacial polymerization, J. Appl. Polym. Sci. 121 (6) (2011) 3377–3383, doi:10.1002/app.33994.
[147] X. Yang, et al., Synthesis of high latent heat lauric acid/silica microcapsules by interfacial polymerization method for thermal energy storage, J. Energy Storage 33 (2021) 102059 /01/01/2021, doi:10.1016/j.est.2020.102059.
[148] X. Wang, C. Li, M. Wang, T. Zhao, W. Li, Bifunctional microcapsules with n-octadecane/thyme oil core and polyurea shell for high-efficiency thermal energy storage and antibiosis, Polymers 12 (10) (2020) 2226 [Online]. Available https://www.mdpi.com/2073-4360 . /12/10/2226.
[149] C. Cai, et al., Co-solvent free interfacial polycondensation and properties of polyurea PCM microcapsules with dodecanol dodecanoate as core material, Sol. Energy 199 (2020) 721–730, doi:10.1016/j.solener.2020.02.071.
[150] Q. Hu, et al., Study on modification of room temperature vulcanized silicone rubber by microencapsulated phase change material, J. Energy Storage 41 (2021) 102842 /09/01/2021, doi:10.1016/j.est.2021.102842.
[151] D. Hu, Z. Wang, W. Ma, Fabrication and characterization of a novel polyurethane microencapsulated phase change material for thermal energy storage, Prog. Org. Coat. 151 (2021) 106006 /02/01/2021, doi:10.1016/j.porgcoat.2020.106006.
[152] M. Li, B. Mu, W.A. Altabey, A review study on preparation and application of microencapsulated phase change materials, Int. J. Sustain. Mater. Struct. Syst. 3 (2) (2018) 151–170.
[153] J.M. Stubbs, D.C. Sundberg, Core-shell and other multiphase latex particles-confirming their morphologies and relating those to synthesis variables, J. Coat. Technol. Res. 5 (2) (2008) 169–180, doi:10.1007/s11998-007-9060-x.
[154] R. Arshady, Suspension, emulsion, and dispersion polymerization: a methodological survey, Colloid Polym. Sci. 270 (8) (1992) 717–732, doi:10.1007/bf00776142.
[155] H.G. Yuan, G. Kalfas, W.H. Ray, Suspension polymerization, J. Macromol. Sci. Part C Polym. Rev. 31 (2-3) (1991) 215–299, doi:10.1080/15321799108021924.
[156] L. Sánchez, P. Sánchez, A. de Lucas, M. Carmona, J.F. Rodríguez, Microencapsulation of PCMs with a polystyrene shell, Colloid Polym. Sci. 285 (12) (2007) 1377–1385 2007/09/01, doi:10.1007/s00396-007-1696-7.
[157] L. Sánchez-Silva, J.F. Rodríguez, A. Romero, A.M. Borreguero, M. Carmona, P. Sánchez, Microencapsulation of PCMs with a styrene-methyl methacrylate copolymer shell by suspension-like polymerisation, Chem. Eng. J. 157 (1) (2010) 216–222, doi:10.1016/j.cej.2009.12.013.
[158] A. Jamekhorshid, S.M. Sadrameli, A.R. Bahramian, Process optimization and modeling of microencapsulated phase change material using response surface methodology, Appl. Therm. Eng. 70 (1) (2014) 183–189, doi:10.1016/j.applthermaleng.2014.05.011.
[159] C.C. Chang, Y.L. Tsai, J.J. Chiu, H. Chen, Preparation of phase change materials microcapsules by using PMMA network-silica hybrid shell via sol-gel process, J. Appl. Polym. Sci. 112 (3) (2009) 1850–1857, doi:10.1002/app.29742.
[160] R. Al-Shannaq, J. Kurdi, S. Al-Muhtaseb, M. Dickinson, M. Farid, Supercooling elimination of phase change materials (PCMs) microcapsules, Energy 87 (2015) 654–662, doi:10.1016/j.energy.2015.05.033.
[161] S. Lashgari, H. Arabi, A.R. Mahdavian, V. Ambrogi, Thermal and morphological studies on novel PCM microcapsules containing n-hexadecane as the core in a flexible shell, Appl. Energy 190 (2017) 612–622, doi:10.1016/j.apenergy.2016.12.158.
[162] S. Parvate, J. Singh, P. Dixit, J.R. Vennapusa, T.K. Maiti, S. Chattopadhyay, Titanium dioxide nanoparticle-decorated polymer microcapsules enclosing phase change material for thermal energy storage and photocatalysis, ACS Appl. Polym. Mater. 3 (4) (2021) 1866–1879, doi:10.1021/acsapm.0c01410.
[163] K. Zhang, J. Wang, L. Xu, H. Xie, Z. Guo, Preparation and thermal characterization of n-octadecane/pentafluorostyrene nanocapsules for phase-change energy storage, J. Energy Storage 35 (2021) 102327, doi:10.1016/j.est.2021.102327.
[164] O.M. Maithya, X. Li, X. Feng, X. Sui, B. Wang, Microencapsulated phase change material via Pickering emulsion stabilized by graphene oxide for photothermal conversion, J. Mater. Sci. 55 (18) (2020) 7731–7742, doi:10.1007/s10853-020-04499-5.
[165] B. Oktay, E. Baştürk, M.V. Kahraman, N.K. Apohan, Designing coconut oil encapsulated poly(stearyl methacrylate-co-hydroxylethyl metacrylate) based microcapsule for phase change materials, ChemistrySelect 4 (17) (2019) 5110–5115, doi:10.1002/slct.201900340.
[166] C. Rulison, Two-component surface energy characterization as a predictor of wettability and dispersability, Krüss Technical Note # 213, no. 213, pp. 1–22, 2000.
[167] S. Torza, S.G. Mason, Three-phase interactions in shear and electrical fields, J. Colloid Interface Sci. 33 (1) (1970) 67–83 /05/01/1970, doi:10.1016/0021-9797(70)90073-1.
[168] J. Zhao, et al., Microencapsulated phase change materials with TiO2-doped PMMA shell for thermal energy storage and UV-shielding, Sol. Energy Mater. Sol. Cells 168 (2017) 62–68 /08/01/2017, doi:10.1016/j.solmat.2017.04.014.
[169] S. Parvate, J. Singh, J.R. Vennapusa, P. Dixit, S. Chattopadhyay, Copper nanoparticles interlocked phase-change microcapsules for thermal buffering in packaging application, J. Ind. Eng. Chem. 102 (2021) 69–85 /10/25/2021, doi:10.1016/j.jiec.2021.06.029.
[170] A. Jamekhorshid, S.M. Sadrameli, M. Farid, A review of microencapsulation methods of phase change materials (PCMs) as a thermal energy storage (TES) medium, Renew. Sustain. Energy Rev. 31 (2014) 531–542, doi:10.1016/j.rser.2013.12.033.
[171] R. Arshady, Suspension, emulsion, and dispersion polymerization: a methodological survey, Colloid Polym. Sci. 270 (8) (1992) 717–732.
[172] A. Sarı, C. Alkan, A. Karaipekli, O. Uzun, Microencapsulated n-octacosane as phase change material for thermal energy storage, Sol. Energy 83 (10) (2009) 1757–1763, doi:10.1016/j.solener.2009.05.008.
[173] A. Sarı, C. Alkan, A. Karaipekli, Preparation, characterization and thermal properties of PMMA/n-heptadecane microcapsules as novel solid–liquid microPCM for thermal energy storage, Appl. Energy 87 (5) (2010) 1529–1534, doi:10.1016/j.apenergy.2009.10.011.
[174] S. Alay, F. Göde, C. Alkan, Synthesis and thermal properties of poly(n-butyl acrylate)/n-hexadecane microcapsules using different cross-linkers and their application to textile fabrics, J. Appl. Polym. Sci. 120 (5) (2011) 2821–2829, doi:10.1002/app.33266.
[175] A. Sarı, C. Alkan, C. Bilgin, Micro/nano encapsulation of some paraffin eutectic mixtures with poly(methyl methacrylate) shell: Preparation, characterization and latent heat thermal energy storage properties, Appl. Energy 136 (2014) 217–227, doi:10.1016/j.apenergy.2014.09.047.
[176] X. Jiang, R. Luo, F. Peng, Y. Fang, T. Akiyama, S. Wang, Synthesis, characterization and thermal properties of paraffin microcapsules modified with nano-Al_2O_3, Appl. Energy 137 (2015) 731–737 /01/01/2015, doi:10.1016/j.apenergy.2014.09.028.
[177] G. Abdeali, M. Abdollahi, A.R. Bahramian, Synthesis and characterization of paraffin wax nanocapsules with polyurethane shell (PU/PW); the droplet size distribution: a key factor for thermal performance, Renew. Energy 163 (2021) 720–731 /01/01/2021, doi:10.1016/j.renene.2020.09.013.
[178] J. Singh, S. Parvate, P. Dixit, S. Chattopadhyay, Facile synthesis of microencapsulated 1-dodecanol (PCM) for thermal energy storage and thermal buffering ability in embedded PVC film, Energy Fuels 34 (7) (2020) 8919–8930, doi:10.1021/acs.energyfuels.0c01019.
[179] M. Zhao, M. Li, L. Wang, X. Zhang, X. Kong, Preparation and characterization of paraffin@CLPS/MS phase change microcapsules for thermal energy storage, ChemistrySelect 5 (24) (2020) 7190–7196, doi:10.1002/slct.202001263.
[180] Y. Wang, et al., Lignin assisted pickering emulsion polymerization to microencapsulate 1-tetradecanol for thermal management, Int. J. Biol. Macromol. 146 (2020) 1–8, doi:10.1016/j.ijbiomac.2019.12.175.
[181] N. Şahan, H. Paksoy, Designing behenic acid microcapsules as novel phase change material for thermal energy storage applications at medium temperature, Int. J. Energy Res. 44 (5) (2020) 3922–3933, doi:10.1002/er.5193.
[182] J. Zhou, J. Zhao, Y. Cui, W. Cheng, Synthesis of bifunctional nanoencapsulated phase change materials with nano-TiO 2 modified polyacrylate shell for thermal energy storage and ultraviolet absorption, Polym. Int. 69 (2) (2020) 140–148, doi:10.1002/pi.5924.

[183] Z. Li, J. Yuan, Phase change microcapsules with high encapsulation efficiency using Janus silica particles as stabilizers and their application in cement, Constr. Build. Mater. 307 (2021) 124971 /11/08/2021, doi:10.1016/j.conbuildmat.2021.124971.
[184] Y. Luo, T.T.Y. Wang, Z. Teng, P. Chen, J. Sun, Q. Wang, Encapsulation of indole-3-carbinol and 3,3′-diindolylmethane in zein/carboxymethyl chitosan nanoparticles with controlled release property and improved stability, Food Chem. 139 (1) (2013) 224–230 /08/15/2013, doi:10.1016/j.foodchem.2013.01.113.
[185] Y. Yeo, N. Baek, K. Park, Microencapsulation methods for delivery of protein drugs, Biotechnol. Bioprocess Eng. 6 (4) (2001) 213–230.
[186] H.J. Huang, W.K. Yuan, X.D. Chen, Microencapsulation based on emulsification for producing pharmaceutical products: a literature review, Dev. Chem. Eng. Miner. Process. 14 (3-4) (2006) 515–544.
[187] B. Németh, Á.S. Németh, J. Tóth, A. Fodor-Kardos, J. Gyenis, T. Feczkó, Consolidated microcapsules with double alginate shell containing paraffin for latent heat storage, Sol. Energy Mater. Sol. Cells 143 (2015) 397–405 /12/01/2015, doi:10.1016/j.solmat.2015.07.029.
[188] R. Miloudi, D. Zerrouki, Encapsulation of phase change materials with alginate modified by nanostructured sodium carbonate and silicate, Iran. Polym. J. 29 (7) (2020) 543–550, doi:10.1007/s13726-020-00819-3.
[189] G. Ozkan, P. Franco, I. De Marco, J. Xiao, E. Capanoglu, A review of microencapsulation methods for food antioxidants: Principles, advantages, drawbacks and applications, Food Chem. 272 (2019) 494–506.
[190] M.N.A. Hawlader, M.S. Uddin, H.J. Zhu, Encapsulated phase change materials for thermal energy storage: experiments and simulation, Int. J. Energy Res. 26 (2) (2002) 159–171, doi:10.1002/er.773.
[191] E. Onder, N. Sarier, E. Cimen, Encapsulation of phase change materials by complex coacervation to improve thermal performances of woven fabrics, Thermochim. Acta 467 (1) (2008) 63–72 /01/30/2008, doi:10.1016/j.tca.2007.11.007.
[192] S.S. Deveci, G. Basal, Preparation of PCM microcapsules by complex coacervation of silk fibroin and chitosan, Colloid Polym. Sci. 287 (12) (2009) 1455–1467, doi:10.1007/s00396-009-2115-z.
[193] G. Basal, S. Sirin Deveci, D. Yalcin, O. Bayraktar, Properties of n-eicosane-loaded silk fibroin-chitosan microcapsules, J. Appl. Polym. Sci. 121 (4) (2011) 1885–1889, doi:10.1002/app.33651.
[194] S. Demirbağ, S.A. Aksoy, Encapsulation of phase change materials by complex coacervation to improve thermal performances and flame retardant properties of the cotton fabrics, Fibers Polym. 17 (3) (2016) 408–417, doi:10.1007/s12221-016-5113-z.
[195] J.C. Roy, S. Giraud, A. Ferri, R. Mossotti, J. Guan, F. Salaün, Influence of process parameters on microcapsule formation from chitosan-type B gelatin complex coacervates, Carbohydr. Polym. 198 (2018) 281–293, doi:10.1016/j.carbpol.2018.06.087.
[196] B. Wu, L. Shi, Q. Zhang, W.J. Wang, Microencapsulation of 1-hexadecanol as a phase change material with reversible thermochromic properties, RSC Adv. 7 (67) (2017) 42129–42137, doi:10.1039/c7ra06764j.
[197] X. Geng, Y. Gao, N. Wang, N. Han, X. Zhang, W. Li, Intelligent adjustment of light-to-thermal energy conversion efficiency of thermo-regulated fabric containing reversible thermochromic MicroPCMs, Chem. Eng. J. 408 (2021) 127276 /03/15/2021, doi:10.1016/j.cej.2020.127276.
[198] Y. Konuklu, H.O. Paksoy, The Preparation and Characterization of Chitosan-Gelatin microcapsules and microcomposites with fatty acids as thermal energy storage materials, Energy Technol. 3 (5) (2015) 503–508, doi:10.1002/ente.201402178.
[199] Y. Konuklu, M. Unal, H.O. Paksoy, Microencapsulation of caprylic acid with different wall materials as phase change material for thermal energy storage, Sol. Energy Mater. Sol. Cells 120 (2014) 536–542.
[200] Z. Ma, Q. Jiang, W. Lv, Z. Song, Novel phase separation method for the microencapsulation of oxalic acid dihydrate/boric acid eutectic system in a hybrid polymer shell for thermal energy storage, Colloids Surf. A 628 (2021) 127369 /11/05/2021, doi:10.1016/j.colsurfa.2021.127369.
[201] M. Ahmadzadeh, S. Chini, A. Sadeghi, Size and shape tailored sol-gel synthesis and characterization of lanthanum phosphate (LaPO4) nanoparticles, Mater. Des. 181 (2019) 108058.
[202] L.Y. Wang, P.S. Tsai, Y.M. Yang, Preparation of silica microspheres encapsulating phase-change material by sol-gel method in O/W emulsion, J. Microencapsul. 23 (1) (2006) 3–14, doi:10.1080/02652040500286045.
[203] H. Zhang, X. Wang, D. Wu, Silica encapsulation of n-octadecane via sol–gel process: A novel microencapsulated phase-change material with enhanced thermal conductivity and performance, J. Colloid Interface Sci. 343 (1) (2010) 246–255 /03/01/2010, doi:10.1016/j.jcis.2009.11.036.
[204] S. Tahan Latibari, M. Mehrali, M. Mehrali, T.M. Indra Mahlia, H.S. Cornelis Metselaar, Synthesis, characterization and thermal properties of nanoencapsulated phase change materials via sol–gel method, Energy 61 (2013) 664–672 /11/01/2013, doi:10.1016/j.energy.2013.09.012.
[205] J. Luan, et al., Influence of acid and alkali reaction system on the morphology and thermal properties of paraffin@SiO_2 phase change microcapsules for heat storage, J. Renew. Sustain. Energy 14 (4) (2022) 044102 2022/07/01, doi:10.1063/5.0098752.
[206] F. He, X. Wang, D. Wu, New approach for sol–gel synthesis of microencapsulated n-octadecane phase change material with silica wall using sodium silicate precursor, Energy 67 (2014) 223–233 /04/01/2014, doi:10.1016/j.energy.2013.11.088.
[207] L. Chai, X. Wang, D. Wu, Development of bifunctional microencapsulated phase change materials with crystalline titanium dioxide shell for latent-heat storage and photocatalytic effectiveness, Appl. Energy 138 (2015) 661–674 /01/15/2015, doi:10.1016/j.apenergy.2014.11.006.
[208] S. Mo, B. Mo, F. Wu, L. Jia, Y. Chen, Preparation and thermal performance of ternary carbonates/silica microcomposites as phase change materials, J. Sol-Gel Sci. Technol. 99 (1) (2021) 220–229, doi:10.1007/s10971-021-05563-5.
[209] B. Srinivasaraonaik, S. Sinha, L.P. Singh, Synthesis of encapsulation of binary mixture by silica and its performance in pure cementitious system, Energy Storage (2021), doi:10.1002/est2.229.
[210] J. Lee, B. Jo, Surfactant-free synthesis protocol of robust and sustainable molten salt microcapsules for solar thermal energy storage, Sol. Energy Mater. Sol. Cells 222 (2021) 110954, doi:10.1016/j.solmat.2020.110954.
[211] A. Subramanian, Synthesis, characterization and thermal analysis of microencapsulated alumina–myristic acid phase change material for thermal energy storage, Appl. Phys. A 126 (11) (2020), doi:10.1007/s00339-020-04098-w.
[212] S. Ishak, S. Mandal, H.S. Lee, J.K. Singh, Microencapsulation of stearic acid with SiO2 shell as phase change material for potential energy storage, Sci. Rep. 10 (1) (2020), doi:10.1038/s41598-020-71940-9.
[213] A. Subramanian, S. Appukuttan, Sol-gel synthesis and characterization of microencapsulated strontium titanate-myristic acid phase change material for thermal energy storage, J. Sol-Gel Sci. Technol. 94 (3) (2020) 573–581, doi:10.1007/s10971-019-05084-2.
[214] I.S. Hussain, A. Ameelia Roseline, S. Kalaiselvam, Bifunctional nanoencapsulated eutectic phase change material core with SiO_2/SnO_2 nanosphere shell for thermal and electrical energy storage, Mater. Des. 154 (2018) 291–301 /09/15/2018, doi:10.1016/j.matdes.2018.05.046.
[215] S. Ishak, S. Mandal, H.S. Lee, J.K. Singh, pH-controlled synthesis of sustainable lauric acid/SiO_2 phase change material for scalable thermal energy storage, Sci. Rep. 11 (1) (2021) 15012 2021/07/22, doi:10.1038/s41598-021-94571-0.
[216] Y.E. Milian, S. Ushak, Influence of monomers and solvents in the direct sol-gel synthesis of $LiNO_3$ shape stabilized phase change materials, Mater. Chem. Phys. 273 (2021) 125089 /11/15/2021, doi:10.1016/j.matchemphys.2021.125089.
[217] Z. Cheng, G. Chang, B. Xue, L. Xie, Q. Zheng, Hierarchical Ni-plated melamine sponge and MXene film synergistically supported phase change materials towards integrated shape stability, thermal management and electromagnetic interference shielding, J. Mater. Sci. Technol. 132 (2023) 132–143 /01/01/2023, doi:10.1016/j.jmst.2022.05.049.
[218] R. Dorati, I. Genta, T. Modena, B. Conti, Microencapsulation of a hydrophilic model molecule through vibration nozzle and emulsion phase inversion technologies, J. Microencapsul. 30 (6) (2013) 559–570, doi:10.3109/02652048.2013.764938.
[219] S.K. Ghosh, Functional Coatings: By Polymer Microencapsulation, Wiley-VCH, Weinheim, 2006.
[220] A. Elgafy, K. Lafdi, Effect of carbon nanofiber additives on thermal behavior of phase change materials, Carbon 43 (15) (2005) 3067–3074 /12/01/2005, doi:10.1016/j.carbon.2005.06.042.
[221] M. Rai, R. Pandit, S. Gaikwad, A. Yadav, A. Gade, Potential applications of curcumin and curcumin nanoparticles: from traditional therapeutics to modern nanomedicine, Nanotechnol. Rev. 4 (2) (2015) 161–172 (Berlin), doi:10.1515/ntrev-2015-0001.
[222] C. Cárdenas-Ramírez, F. Jaramillo, M. Gómez, Systematic review of encapsulation and shape-stabilization of phase change materials, J. Energy Storage 30 (2020) 101495 /08/01/2020, doi:10.1016/j.est.2020.101495.
[223] Y. Ma, et al., Synthesis and characterization of thermal energy storage microencapsulated n-dodecanol with acrylic polymer shell, Energy 87 (2015) 86–94, doi:10.1016/j.energy.2015.04.096.